Cristina Isabel Pereira Correia

Captura de CO₂ usando líquidos iónicos

CO₂ capture using ionic liquids

Universidade de Aveiro 2020

Departamento de Química

Cristina Isabel Pereira Correia

Captura de CO$_2$ usando líquidos iónicos

CO$_2$ capture using ionic liquids

Dissertação apresentada à Universidade de Aveiro para cumprimento dos requisitos necessários à obtenção do grau de Mestre em Engenharia Química, realizada sob a orientação científica do Doutor Pedro Jorge Marques de Carvalho, Equiparado a Investigador Auxiliar do Departamento de Química da Universidade de Aveiro e coorientação da Doutora Mónia Andreia Rodrigues Martins, estagiária de pós-doutoramento do Departamento de Química da Universidade de Aveiro.

Dedico este trabalho aos meus pais.

o júri

presidente   Doutora Maria Inês Purcell de Portugal Branco
Professora Auxiliar do Departamento de Química da Universidade de Aveiro

Doutor Abel Gomes Martins Ferreira
Professor Assistente do Departamento de Engenharia Química da Universidade de Coimbra

Doutora Mónia Andreia Rodrigues Martins
Estagiária de Pós-Doutoramento do Departamento de Química da Universidade de Aveiro

palavras-chave   Líquidos Iónicos Próticos, Dióxido de Carbono, Densidade, Solubilidade, Modelação

resumo   A emissão de gases de efeito de estufa para a atmosfera, em particular o dióxido de carbono (CO_2), tem vindo a tornar-se cada vez mais preocupante devido às alterações climáticas. Para combater este problema, muitos investigadores têm focado as suas atividades no desenvolvimento de novos processos e metodologias que permitam mitigar os gases do efeito estufa. Dentro das alternativas, as tecnologias de captura e armazenamento de carbono desempenham um papel fundamental na mitigação do CO_2. Dentro do leque de solventes propostos como inovadores e com elevado potencial para a captura de CO_2, os líquidos iónicos (LIs) oferecem propriedades únicas, sendo uma alternativa promissora na substituição de solventes críticos comumente usados na sorção física deste gás. Apesar do potencial dos LIs ser evidente na captura de CO_2, a aplicação destes solventes a processos à escala industrial está numa fase muito inicial. Isto deve-se em parte ao escasso conhecimento das propriedades termofísicas dos LIs, como a densidade e solubilidade, que limitam o desenvolvimento de modelos robustos essenciais no desenvolvimento de processos. Assim, nesta tese, LIs à base de carboxilatos são avaliados como potenciais solventes na captura de CO_2. Para estudar a viabilidade desta alternativa, dados de equilíbrio líquido-vapor são necessários. Além disso, o conhecimento e a descrição das propriedades termofísicas por equações de estado adequadas são essenciais para o design e desempenho do processo industrial.

Os dados de solubilidade – diagrama *pVT* – foram obtidos usando uma célula isocórica, na gama de temperaturas e pressões de 303 a 343 K e 0.1 a 0.5 MPa. Os dados de densidade foram medidos usando uma célula de medição a alta pressão – diagrama *ρpT* – na gama de temperaturas e pressões de 283 a 363 K e 0.1 a 95 MPa. Estes foram modelados utilizando equações de estado baseadas na mecânica estatística, PC-SAFT e *Soft*-SAFT.

Os LIs analisados neste trabalho mostram elevada capacidade de absorção física de CO_2 demonstrando que o composto com maior capacidade de absorção é o [DEEA][Prop]|$_{1.5:1}$ obtido um valor de solubilidade de x_{CO2}=0.10 e molalidade m_{CO2}=0.49 mol$_{CO2}$·kg$_{IL}^{-1}$ a 0.5 MPa e 303 K. A densidade e as propriedades derivadas, nomeadamente compressibilidade isotérmica e expansividade térmica isobárica, foram modelados usando a PC-SAFT e a Soft-SAFT. A EoS PC-SAFT apresenta dificuldade na descrição dos dados experimentais, sendo o parâmetro de volume de associação muito próximo de zero, o que não possui significado físico uma vez que os compostos possuem grupos funcionais que interagem entre si. Já a *Soft*-SAFT providencia uma melhor descrição dos dados experimentais com parâmetros com significado físico válido.

De acordo com os resultados obtidos neste trabalho, são necessários mais estudos de caracterização termofísica de diferentes líquidos iónicos de forma a criar uma base sólida de dados que permita a sua aplicação a nível industrial.

abstract

The emission of greenhouse gases into the atmosphere, in particular carbon dioxide (CO_2), has become problematic due to climate change. To combat this problem, many researchers have focused their activities on the development of new processes and methodologies to mitigate greenhouse gases. Among the alternatives, carbon capture and storage technologies play a key role in mitigating CO_2. Within the range of solvents proposed as innovative and with a high potential for CO_2 capture, ionic liquids (ILs) offer unique properties, being a promising alternative in the replacement of critical solvents commonly used in the physical sorption of this gas. Although the potential of ILs is evident in CO_2 capture, the application of these solvents to industrial-scale processes is still at a very early stage. This is partly due to the little knowledge of thermophysical properties of ILs, such as density and solubility, that limit the development of robust models essential in the development of processes. Thus, in this thesis, ILs based on carboxylates are evaluated as potential solvents for CO_2 capture.

To study the viability of this alternative, liquid-vapor equilibrium data are necessary. In addition, the description of thermophysical properties by equations of state (EoS) are essential for the design of industrial process.

The solubility data - pVT diagram - were obtained using an isochoric cell, in the range of temperatures and pressures from 303 to 343 K and 0.1 to 0.5 MPa. The density data were measured using a high-pressure measuring cell - diagram ρpT - in the temperature and pressure range from 283 to 363 K and 0.1 to 95 MPa. These were modeled using EoS based on statistical mechanics, PC-SAFT and soft-SAFT.

The ILs analyzed in this work show a high capacity for the physical absorption of CO_2. The compound with the highest absorption capacity is [DEEA][Prop] $\vert$ 1.5:1 with a solubility value of x_{CO2}=0.10 and molality m_{CO2}=0.49 $mol_{CO2} \cdot kg_{IL}^{-1}$ at 0.5 MPa and 303 K. The density and derived properties, namely isothermal compressibility and isobaric thermal expansion, were modeled using PC-SAFT and soft-SAFT EoS. The EoS PC-SAFT demonstrated difficulty in describing the experimental data, with the association volume parameter very close to zero, which has no physical significance, since the compounds have functional groups that interact with each other. soft-SAFT provides a better description of the experimental data, with parameters with valid physical meaning.

According to the results obtained in this work, further studies of thermophysical characterization of different ionic liquids are necessary to create a solid database that allows its application at an industrial level.

Contents

List of Tables

List of Figures

Nomenclature

List of symbols

f	Fugacity	
K_H	Henry's Constant	bar
m	Number of segments	
m^0_{CO2}	Molality	$mol_{CO2} \cdot kg_{IL}^{-1}$
M_w	Molecular weight	$g\ mol^{-1}$
n	Number of moles	mol
p	System pressure	bar
T	System temperature	ºC
R^2	Correlation coefficient	
V	Total volume	mL
V_m	Molar volume	$cm^3 \cdot mol^{-1}$
x	Mole fraction	

Superscripts

assoc	Helmholtz energy contribution due to association
disp	Helmholtz energy contribution due to dispersive interactions
HB	Hydrogen Bonding
hc	Helmholtz energy contribution due to hard chain formation
id	Ideal
L	Liquid phase
res	Residual

Subscripts

CO_2	Carbon dioxide
i	Component i
IL	Ionic Liquid
j	Component j

Greek letters

ε	Depth of the square-well potential for dispersive interactions	K
ε^{HB}	Depth of the square-well potential of the interaction between associative sites	K
η	Association parameter for volume	
k^{HB}	Width of the square-well potential of the interaction between associative sites	
ρ	Density	g mL^{-1}
ξ	Association parameter for energy	
σ	Segment diameter	m

List of Abbreviations

AAD	Absolute Average Deviation
Ace	Acetate
AAIL	Amino Acid Ionic Liquids
But	Butanoate
^{13}C	Carbon 13

¹H	Hydrogen 1
CCS	Carbon Capture and Storage
DEEA	*N*,*N*-diethylethanolammonium
EoS	Equation of State
GHG	Greenhouse Gases
Hex	Hexanoate
IL	Ionic Liquid
NMR	Nuclear Magnetic Ressonance
Pent	Pentanoate
PIL	Protic Ionic Liquid
Prop	Propanoate
SAFT	Statistical Associating Fluid Theory
VLE	Vapor-Liquid Equilibrium
VOCs	Volatile Organic Compounds

1   Introduction

1.1 Motivation – Greenhouse gases (GHG) and climate changes

The fast-economic growth has contributed to today's ever-increasing demand for energy. An evident consequence of this is an increase in the use of fuels, particularly fossil fuels (*i.e.* coal, oil and natural gas) that have become key energy sources since the industrial revolution.[1],[2] However, the excessive use of fossil fuels has become problematic due to their negative impact on the environment. Since the industrial revolution, the greenhouse gases like water vapor, carbon dioxide (CO_2), methane, nitrous oxide and ozone, have been reflecting infrared radiation emitted by the Earth's surface, blocking part of it from being lost to space, and consequently inducing an increase of temperature in the surface of the troposphere.[3] The rise in global average temperature has then been attributed to the emission of volatile organic compounds (VOCs) and GHG, being carbon dioxide the most critical one.[4] For a long period, the balance was maintained, since CO_2 was removed by the existing natural agents, being its concentration in atmosphere around 280 ppm.[3] However, between 1970 and 2004, global annual CO_2 emissions increased by 80% due to the Industrial Revolution that caused an increase in the burning of fossil fuels.[5] **Figure 1** represents the global average concentrations of CO_2 in the atmosphere since 1500.[6] In the last decades, the situation is getting worse with the concentration exceeding 400 ppm.
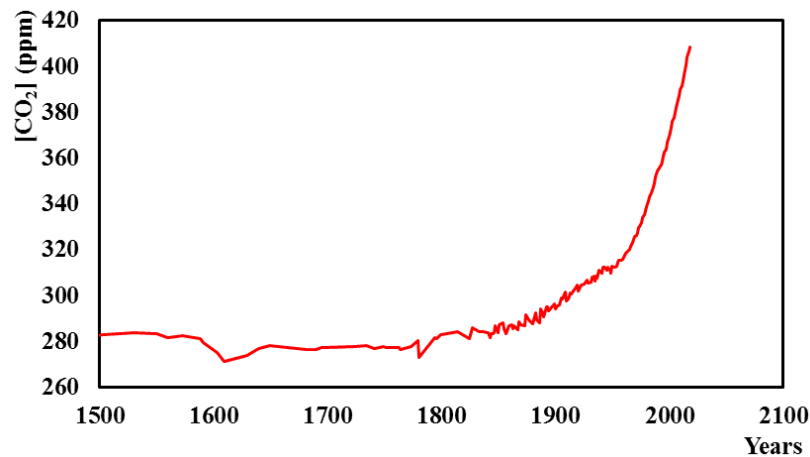
Figure 1. Global average long-term atmospheric concentration of CO_2, measured in parts per million (ppm) [adapted from reference [6]].

According to the fifth evaluation report (5th Evaluation Report - AR5) of *The Intergovernmental Panel on Climate Change* (IPCC) of 2014, the period between 1983 and 2012 was the warmest in the last years in the Northern Hemisphere. To reduce the serious effects of global warming, in that report it was decided that it is essential to keep the average

increase in global temperature below 2 °C compared to pre-industrial levels (1.5 °C). Thus, it is necessary to reduce the release of greenhouse gases between 40 and 70% by 2050, compared to 2010 levels, and maintain the expectation of reaching zero emissions by 2100.[7] However, according to International Energy Agency (IEA) the 2015[8], global demand for energy will grow 25% by 2040 with 75% to 80% of primary energy still coming from fossil fuels.[9] Taking these factors into account, the average global temperature in the long term would increase by 3.6 °C, which is not in line with the IPCC target.[10] To overcome this obstacle, the European Union adopted the Strategic Energy Technology plan to achieve sustainable growth through the development of low-carbon technologies. Among these, carbon capture and storage (CCS) plays a central role in mitigating CO_2 emissions.[11]

1.2 Carbon dioxide Capture and Sequestration

CCS from anthropogenic sources stand as the most promising option to reduce CO_2 emissions and decrease the global warming.[4],[12] CCS allows the reduction of CO_2 emissions from industrial processes involving three basic steps: capture, transport, and storage of CO_2 in an appropriate locations. This technology is mainly applied to industries with a high emission of pollutants, particularly fossil fuel plants to produce electricity, but special attention is also given to large industrial facilities, including the production of oil, gas, chemicals, steel, and cement. A plant containing the CCS technologies can reduce CO_2 emissions to the atmosphere in a range of 80 to 90%. Currently, it is predicted that by 2050 the potential for capture, transport and storage will be 236 billion tons of CO_2.[2],[4],[12] The main challenge in the implementation of this process is the development of technologies that allow, in an effective and sustainable way, a low environmental and economic impact.[4],[13] Carbon capture can be achieved through the following technologies: pre-combustion, oxyfuel combustion and post-combustion.[14]

Pre-Combustion Capture: In coal plants, when coal reacts with oxygen and steam at high temperatures and pressures, it produces gas or syngas, composed mainly of CO (carbon monoxide) and hydrogen with trace amounts of water vapor and hydrogen sulphide (H_2S), in a process called gasification, see **Figure 2**. After the gasification step, syngas reacts with steam in a water – gas – shift reactor, which converts CO to CO_2, resulting in a mixture of CO_2 and H_2.[2] The flue gas (400 °C) originated has high concentrations of CO_2 (20-40%) that need to be removed before combustion. [15] The pre-combustion process involves the

3

capture of CO_2 (40ºC) and the H_2 present in it is later use to produce energy (electricity and heat). This process produces a mixture of gases with high partial pressures of CO_2, favouring it separation. This type of plant is called an integrated gasification combined cycle (IGCC) plant that uses fuel (coal, biomass, oil, etc.) for energy production of energy.[4],[14],[16]

Oxy-fuel Combustion Capture: The oxy-combustion process is quite promising however it is still under development. In this process, air is injected in a separation unit where nitrogen is separated from O_2, the fuel is burned with almost pure oxygen (> 95%) in a boiler, so that the final product contains only CO_2, water (H_2O), particulates and dioxide sulphur (SO_2), resulting in a high concentration of CO_2 in the output stream (80-98%), depending on the fuel used, see **Figure 2**. The high-pressure steam generated passes through a steam turbine generating electricity. As this process uses pure O_2 in combustion, there is a reduction in the amount of nitrogen in the gas in the outlet stream. The substantial reduction in thermal NO_x is one of the great advantages of this technology.[4],[16] Water is removed by condensation.

Oxyfuel is the CO_2 capture technology most similar to post-combustion, once the fuel is burned with pure oxygen instead of air, obtaining an output current with a CO_2 concentration above 80%. An advantage associated with this process is the elimination of NO_x formation, due to the absence of nitrogen, promoting low gas volume and, therefore, reduced equipment size. However, a major disadvantage associated with oxy-fuel combustion is the need for high amounts of energy, due to the separation of O_2, complex unit processes are required that cause high operating costs, causing a negative impact on the efficiency of the plant. In addition, the high concentration of SO_2 in the fuel stream can create corrosion problems in the equipment.[4] Another challenge to take into account is the high gas flow, therefore, large amounts of flue gas in the boiler must be recycled in order to maintain high operating temperatures.[17] Despite the advantages, this process is still considered very complex and economically unfeasible, which makes investment in research unattractive.

Post-Combustion Capture (PCC): Within the capture options, the most promising approach to tackle GHG emissions is post-combustion. It consists in the separation of CO_2 from the flue gas after combustion, as shown in **Figure 2**. In this process, the fuel is burned with excess air, where the CO_2 concentration in the flue gas stream varies with the type of fuel used, 12-15 v/v% for combustion of coal and 4 - 11 v/v% for natural gas burning.[18]

4

The high pressure steam generated in the combustion phase is used to generate electricity through a turbine and the flue gas containing CO_2, N_2 and H_2O is subjected to absorption separation units using a solvent, separating CO_2 from N_2 and H_2O. Subsequently, the captured CO_2 is dehydrated and compressed so that it can be transported and stored in an appropriate place. However, the removal of SO_2 is required in current PCC technologies prior to the separation unit. Thus, the removal of SO_2 and particles from the combustion stream will allow less impact of the impurities in the solvent sorption, increase the selectivity of the solvent for CO_2, as well as the reduction of problems associated with corrosion and incrustation in the equipment.[14]
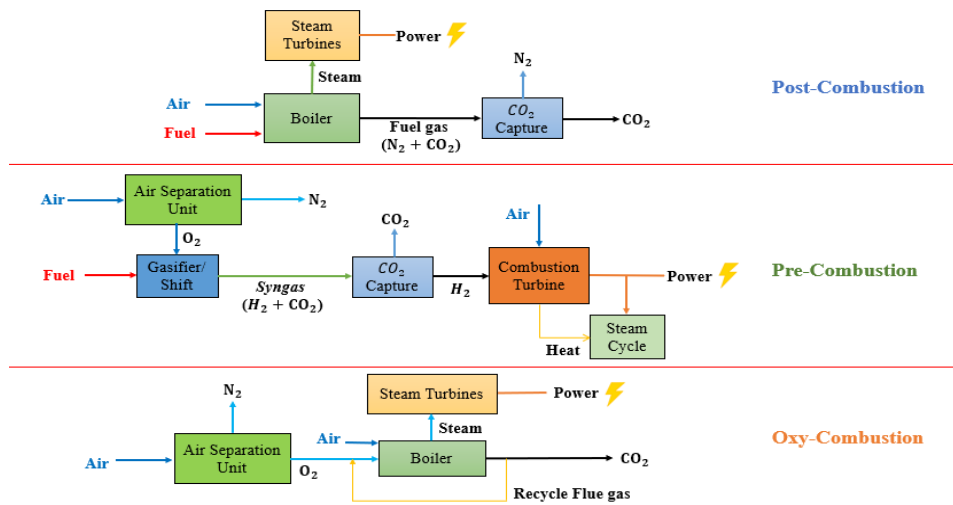
Figure 2. Illustration of different CO_2 capture pathways [adapted from reference [5]].

Post-combustion is easy and simple to implement in existing plants, not requiring a complete remodelling of the facilities, compared to the other technologies. In pre-combustion and oxy-fuel, the CO_2 capture process needs to be planned and integrated into the process from the beginning. In addition, post-combustion is flexible, as maintenance does not interrupt the plant's operation. Therefore, even if the pre-combustion and oxy-fuel processes offer greater efficiency compared to the post-combustion, it will still be better to introduce post-combustion CO_2 capture to existing installations (power plants).[4],[19],[20]

1.2.1   Carbon capture in post-combustion

There are a variety of commercially available separation technologies to separate CO_2 from mixtures of gases from post-combustion streams, such as physical and chemical absorption, selective adsorption, cryogenic separation, membrane separation and bio-fixation microalgae – **Figure 3**.[21],[22]
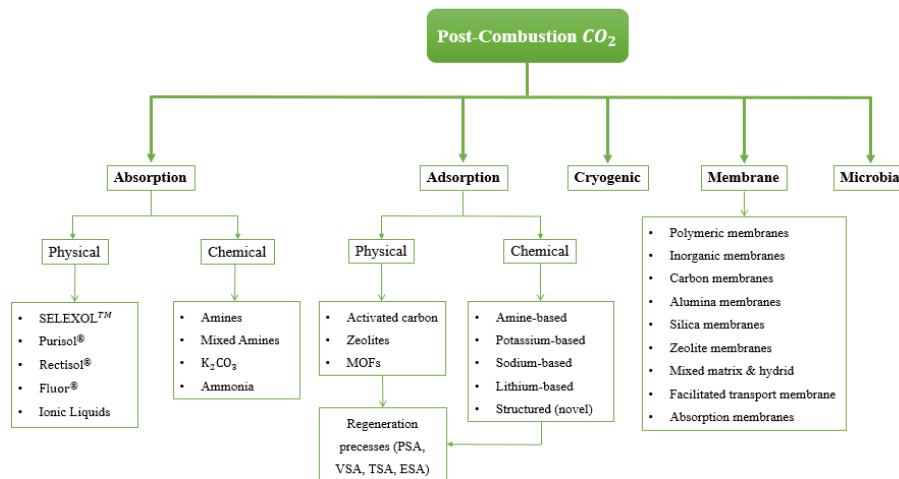
Figure 3. Main carbon capture methods in post-combustion.[21]

Absorption: In absorption processes, carbon dioxide is absorbed or incorporated into an absorbent solution and the sorbent is subsequently removed, in a regeneration process. Depending on the type of bond formed between the sorbent and the gas molecules, this process can be divided into two types: chemical absorption, if the bond is molecular, or physical absorption, if the sorbent occupies the free space present between the molecules of solvent, establishing intermolecular forces. Chemical absorption by means of amine solution is the most mature technology for capturing post-combustion CO_2. However, there are problems associated with this technology, such as the low partial pressure of CO_2 in the flue gas, which implies the need for large volumes of solvent and thus, large separation units.

Adsorption: Adsorption is a separation process where ions, atoms or molecules of a fluid or gas adhere to a solid surface. The adhesion created between the molecule (adsorbate), in this case, CO_2, and the solid surface (adsorbent) is based on intermolecular forces. Based on the type of forces involved during adsorption, it is divided into two classes: physical adsorption when weak Van der Waals forces (physi-sorption) occur and chemical adsorption that occurs when covalent bonds (chemi-sorption) prevail. As the adsorption process occurs on the absorbent surface, the amount of material adsorbed is related to the contact area available for adsorption, therefore, the development of future adsorbents should privilege the maximization of the solid surface area.[23]–[25]

Cryogenic: Cryogenic separation consists in the separation of CO_2 from the remaining gases present in the combustion stream by cooling and condensation. This technique is only used commercially for flows with high concentrations of CO_2 (> 90%), due to the high capital to be invested, and has been implemented for the production of oxygen in the combustion of

oxy-fuel.[15] This process is useful for the separation of CO_2 since it does not use solvents, however, large amounts of energy are required for cooling. In addition, to avoid blockages in the system, water must be removed from the combustion stream before cooling.[24]

Membranes: Membranes are porous materials that act as permeable and selective barriers in the separation of CO_2 from the combustion stream. The gas is fed to the tangential chamber ("cross flow filtration") where there is a selective membrane for a certain compound (in this case, CO_2). Then, due to the pressure difference across the membrane (driving force), the CO_2 passes through the membrane producing a flow of CO_2-rich gas (permeate) and a flow rich in compounds retained by the membrane (retentate). The disadvantages associated with this type of processes comprise the low permeate gas flow, which may block ("fouling") the membrane due to impurities present in the supply stream.[17] There are three types of membrane, ceramic (inorganic), polymeric (organic) and hybrid. Polymeric membranes have been the subject of study for gas separation, they offer numerous advantages, such as small equipment dimensions, reduced environmental impact, low operating cost, low energy consumption, high thermal stability, simple manufacturing, reduced environmental impact, easy implementation and high mechanical resistance compared to ceramic membranes.[22],[26] Although polymer membranes have achieved high importance in separation processes, development of new materials aims to design membranes with greater selectivity and permeability to CO_2, improving separation efficiency.

Microbial: The bio fixation of microalgae consists of the use of photosynthetic unicellular organisms to capture CO_2. Although aquatic microalgae crops are expensive, they have high potential since they have higher carbon fixation rates than terrestrial plants for the same purpose. At the same time, microalgae can also be used for the production of biofuels from biomass, as well as other added value compounds (hydrogen, food products, pharmaceuticals and cosmetics).[24],[27]

Among these techniques, absorption is more popular, being widely applied in industrial plants to capture post-combustion CO_2. However, the selection of the technology to use depends on the purity requested for the product flow and on the conditions of the gas flow being treated, such as the partial pressure of CO_2, temperature and type and concentration of trace species or impurities.[4],[21],[28] When capturing CO_2 from acidic gases, for example, the main factor to take into account for choosing the technology to be used is the partial pressure of CO_2 present in the gas. Chemical absorption is more suitable for gases

with low partial CO_2 pressure, between 5 and 8 bar, while for medium and high CO_2 partial pressures the membranes have a better performance.[29] For higher CO_2 partial pressures, above 15 bar, physical absorption is the most suitable. For very high partial pressures of CO_2, cryogenic distillation is the most suitable for producing liquid CO_2 at high pressure, making it easier to transport.[11],[30]

The selection of the solvent is the most important factor in an absorption process. It must have a high absorption capacity, low solvent loss and low energy consumption in the regeneration stage. The most used solvents in the chemical industry for CO_2 capture by chemical absorption are based on alkanolamines (1st Generation), due to the high absorption rate, low solvent cost, high resistance to thermal degradation, low molecular weight and low hydrocarbon solubility. However, aqueous alkanolamines have intrinsic disadvantages, such as the need for large amounts of energy in the regeneration stage, oxidation degradation, losses to the gas flow or to the environment due to their high volatility and high viscosity. In addition, these solvents can cause operational problems, such as corrosion, foaming and fouling in process equipment.[15],[31]–[33] Thus, in order to circumvent the adversities associated with this type of solvents, the study of new alternatives has been investigated, such as functionalized solvents (2nd Generation), formed by the addition of chemical groups to the traditional solvent to change the molecular structure and the molecule geometry.[34] These solvents, sterically hindered amines, form weak CO_2-amine bonds when compared to primary and secondary amines, decreasing regeneration energy.[10] Another new technique is the combination of different amines, allowing a better performance of the absorption process compared to the individual solvent. Piperazine has been widely used to promote the performance of aqueous monoethanolamine solutions.[35],[36]

In physical absorption processes, the CO_2 removed depends on the solubility of CO_2 in physical solvents, and in turn, the solubility of CO_2 in solvents depends on the partial pressure and temperature of the feed gas. The increase in CO_2 solubility in the solvent is favored by the low temperature and partial pressure of CO_2.[11] The most mature and important physical absorption technologies applied to CO_2 capture include: Selexol process, which uses a solvent based on a dimethyl ethers of polyethylene glycol; Rectisol process, based on low methanol temperature absorption (cold methanol); Fluor process, that uses propylene carbonate; and Purisol process, that uses *N*-methyl-2-pyrrolidone.[2],[15],[17] The physical solvents mentioned above are favorites in capturing CO_2, as they require little

8

energy in the regeneration step due to the weak connections established between CO_2 and the solvent used, when compared to chemical solvents. This process is not economically viable for gas flows with partial CO_2 pressures below 15 v/v%. One of the disadvantages associated with physical solvents is the need to cool the flow of synthesis gas before capturing CO_2, as these solvents have higher solubility at lower temperatures.

Other interesting classes of compounds that have been increasingly prominent in gas physi-separation processes, namely the physical absorption of CO_2, are the ionic liquids - whose unique properties and enhanced solubility will be further discussed in the next section,[33] and deep eutectic solvents (DES) - eutectic mixture of two or more compounds. DES are formed by strong and complex hydrogen bonds between a hydrogen bond acceptor and a hydrogen bond donor, that allow to obtain lower eutectic temperatures than the ones predicted for an ideal liquid phase. The strong interactions between DES components may give rise to stable liquids at low temperatures with interesting properties, such as low vapor pressure, good physical and chemical stability, low toxicity and simple and economic synthesis using biodegradable materials (depending on the starting materials used).[37]–[41] This class of solvents can also be considered designer solvents due to the numerous possibilities of combining the constituents for a given application. In general, deep eutectic solvents are considered a promising and economical alternative to conventional solvents.[42]

In all techniques presented, the high need for energy in the process of absorbing CO_2 from flue gases is one of the biggest obstacles in industrial scale applications, and the development of technologically and economically efficient technologies in capturing CO_2 is crucial.[17],[24] Currently, new technologies are being investigated, such as zeolites[43],[44], metal organic-frameworks[24], carbon nanotubes[45], membranes[46],[47], supported ionic liquid membranes[48],[49], encapsulated ionic liquids[50],[51] and gas-liquid membrane contactors[52],[53].

1.3 Ionic Liquids

ILs are salts made up of large organic cations and organic or inorganic anions of variable nature, which cannot form an ordered crystalline network and, therefore, unlike common salts such as sodium chloride (NaCl), remain liquid over a wide range of temperatures, by general definition, below 373 K (100 ºC).[54] The ionic nature of these compounds results in a unique combination of intrinsic physical properties, such as high thermal and chemical stability, non-flammable, high solvation capacity, high conductivity,

and negligible vapor pressures.[55]–[58] Since the physical and chemical properties of ILs, such as viscosity, density, sorption capacity, thermal decomposition temperatures or surface tension, are dependent on the chemical structures of the constituent ions, the wide possibility of combining different cations and anions, represent an important and complementary advantage of ILs, giving them the designation "*designer solvents*". This "tunability" allows for the design of solvents with high process performance for specific tasks.[12],[59],[60]

Among the wide variety of ILs that can be synthesized, the most studied cations are nitrogen-based, such as pyrrolidinium-, imidazolium-, piperidinium-, pyridinium- and ammonium-based ILs. Regarding the most common anions used in ILs, these include simple halogenates, such as Cl⁻, Br⁻ and I⁻, and more complex organic structures, such as tosylates, acetates and fluorides, namely $[BF_4]^-$, $[BF_6]^-$ and $[NTf_2]^-$. **Figure 4** shows the most common chemical structures of anions and cations used in ILs synthesis.

Due to their unique characteristics, ILs become useful in several fields such as synthesis and catalysis, biotechnology, pharmaceuticals, cleaning and purification operations, gas separations, electrolytes, lubricants and heat transfer fluids; being the most interesting research area related with the substitution of VOCs in gas separation.[61]–[64]
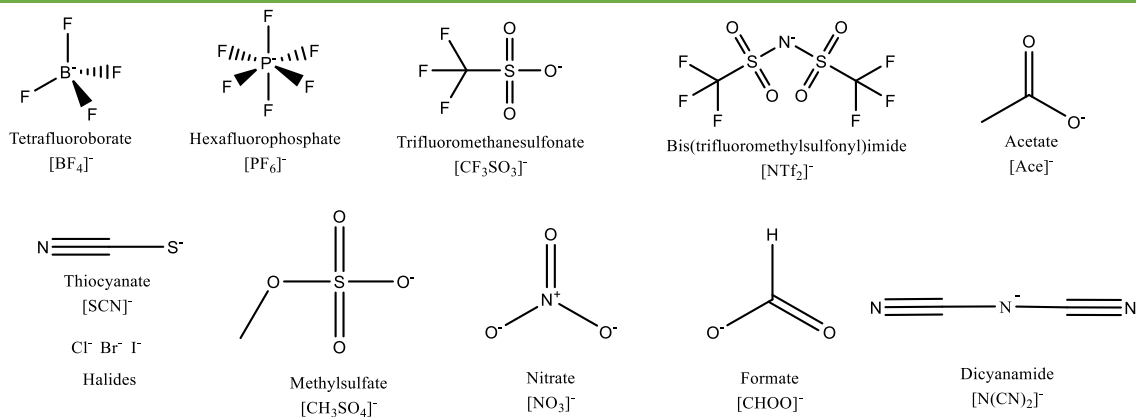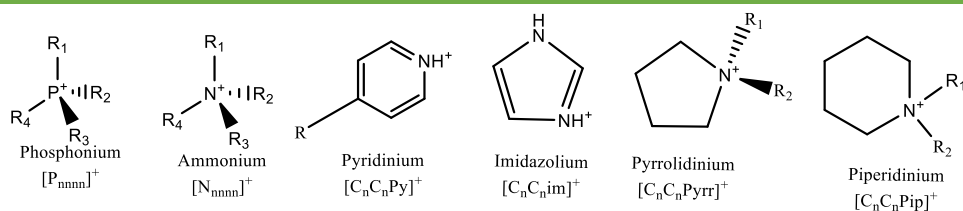
Figure 4. Chemical structures of some IL ions.[54]

ILs are neoteric solvents with unique and interesting characteristics for CO_2 capture, mainly due to the low vapor pressure and high selectivity for CO_2 when compared to other gases in combustion currents.[65] In the absorption process of post-combustion, the type of interactions established between CO_2-IL can be chemical or physical. Regarding chemical solvents, recent studies analyze the CO_2 absorption capacity using amino functionalized ILs, such as Amino Acid Ionic Liquids (AAILs). Structural changes as fluorination, oxygenation, or the introduction of the anion $[B(CN)_4]$ have been analyzed to maximize the CO_2 capture capacity. Bates et al.[66] showed the first example of chemical absorption by ILs in CO_2 capture, demonstrating that the CO_2 absorption capacity using amino functionalized ILs was three times more than ILs used in physical absorption. In this new strategy, the study of the solubility of CO_2 in the amino-functionalized IL 1-propylamide-3-butylimidazolium tetrafluoroborate ([apbim][BF_4]) was carried out, leading to capture 0.074 g_{CO2}/g_{IL} at room temperature and pressure. Further works with amino-functionalized ILs were carried out, including amine-based ILs and amino acids.[67],[68] As a subcategory of amine functionalized ILs, AAILs are particularly interesting due to their availability, low cost, and the non-toxic biodegradability of amino acids. In addition, AAILs have a fast reaction kinetics, good thermal and chemical stability and low environmental impact making them promising solvents for CO_2 capture.[69] Although AAILS have a high absorption capacity, this type of solvent has low mass transfer coefficients due to the high viscosity, which limits their application in the treatment of combustion currents on an industrial scale.[70] The most studied and analyzed IL in the chemical absorption process is 1-butyl-3-methylimidazolium Acetate, [C_4C_1im][Ace], that shows the formation of a reversible molecular complex.[71]–[73]

Unlike chemical solvents, physical solvents capture CO_2 present in the gas stream without a chemical reaction taking place, obeying Henry's Law. In this mechanism, CO_2 occupies the "free spaces" (free volume) between the molecular structures of the solvent, with an interaction of the solvent and CO_2 mainly through Van der Waals forces. The typical behavior of physical solvents is observed by increasing the pressure and, consequently, increasing the concentration of CO_2 present in the liquid phase. As mentioned earlier, the more mature physical absorption technologies applied to CO_2 capture include the Selexol, Retisol, Fluor, and Purisol processes.[2],[15],[17] However, LIs stand out in this field due to the presence of certain groups present in the structure, the most investigated chemical modifications are fluorination, oxygenation and anion introduction $[B(CN)_4]$.

According to several authors[2],[74]–[80], the fluorination of the IL anion or cation can increase CO_2 solubility. The introduction of fluorine in the IL favors the weakening of the interactions between functional groups of the cation-anion, increasing the interactions between CO_2 and ionic pairs, decreasing the surface tension and, thus, favoring the formation of cavities between structures. Another modification analyzed in several reviews is oxygenation, which consists of the introduction of ether, ester or carbonyl groups in the alkyl chain of the cation.[71] The effect of oxygenation is quite interesting since two successful processes in sweetening combustion currents, Rectisol and Selexol, use oxygenated solvents, methanol and polyester, respectively. Pensado et al.[81] and Deng et al[82] found that no significant increase in solubility was observed, that is, the introduction of functional oxygen groups does not significantly affect the solvation of the gas. However, studies of CO_2 solubility in glymes, glycols and polymers have revealed high CO_2 solubilities compared to ILs without oxygen groups.[71] Cyan-based ionic liquids demonstrated high efficiency in capturing CO_2, Mota-Martinez et al.[83] and Makino et al.[84] studied the solubility of CO_2 at high pressure using the IL 1-hexyl-3-methylimidazolium tetracyanoborate, $[C_6C_1im][B(CN)_4]$, verifying greater CO_2 absorption capacity, as well as rapid kinetics (lower viscosity). Mahurin et al.[85], for ILs based on anion $[B(CN)_4]$ are particularly interesting due to their high CO_2 absorption capacity and low viscosity, promoting high mass transfer, when compared to other ILs. Regardless of the ILs analyzed for CO_2 capture, Kazarian et al.[86] revealed for the first time that the strength of anion-CO_2 interactions is not solely responsible for gas solubility, stating that the contribution of free volume in ILs is significant in determining CO_2 solubility. Aki et al.[87], Bogel-Łukasik et al.[88],[89] and Baiker et al.[90],[91], state that one should not only consider the enthalpy effects (strength of the interactions between gas and IL), but also entropic effects (organization of molecular structures in bulk).

The mechanism that governs gas solubility in ILs is still under discussion, however, there is general agreement about the influence of anion-cation, CO_2-anion, and CO_2-CO_2 interactions on solubility, but a disagreement regarding the relative importance and weight of each interaction.[90],[92],[93] Babarao et al.[94] demonstrated that the cation-anion interaction is weaker for $[C_2C_1im][B(CN)_4]$ than for 1-ethyl-3-methylimidazolium tetrafluoroborate, $[C_2C_1im][BF_4]$, 1-ethyl-3-methylimidazolium hexafluoroborate, $[C_2C_1im][PF_6]$, or 1-ethyl-3-methylimidazolium bis(trifluoromethylsulfonyl)imide, $[C_2C_1im][NTf_2]$, leading to greater

structure flexibility, rearrangement capacity, CO_2-anion interaction, leading to greater solubility. Recently, Gupta[95] evaluated the impact of the cation on CO_2 solubility in ILs based on $[B(CN)_4]$ using molecular simulations. The author proposes that CO_2 is captured due to the low electrostatic cation-anion interactions observed in this type of LIs. However, the CO_2 solubility database using other cyan-based anions is quite limited, and further studies are needed to develop new functionalized ILs with a high CO_2 absorption capacity.

ILs can be divided in two main types: aprotic ionic liquids (AILs) and protic ionic liquids (PILs). PILs can be easily synthetized through the simple neutralization reaction of a Brønsted acid and a base.[33] According to a study by Peric et al.[96], when compared to AILs, PILs have less cytoxicity and have been shown to be less harmful to aquatic organisms. In addition, PILs are more economical, making the CO_2 capture process more promising, efficient and more "greener" than conventional solvents.[97] Due to the diversity of organic super-bases and weak proton donors, the properties of PILs can be easily adjustable to the desired separation process. In this sense, Wang et al.[70] developed a new strategy using anion-functionalized PILs, using a very strong base (super-base) that easily captures weak proton donors (weak acids), such as imidazoles, fluorinated alcohols, pyrrolidinones and phenols, obtaining extremely high values in the reversible CO_2 capture ($>1mol_{CO2}/mol_{PIL}$). Wang et al. [70] demonstrated the importance of basicity in PILs for the rapid and reversible absorption of CO_2, with a small loss of capacity after several cycles of regeneration. PILs based on tetramethylguanidine, have been widely used in the absorption of acid gases.[98] Thus, Li et al. [33] synthesized tetramethylguanidine-based PILs with three weak bases, imidazoles, phenol and pyrrolidinones, analyzing then their performance in the absorption of CO_2, the anion effect and solvent regeneration. According to the authors[33], the synthesized PILs, tetramethylguanidine imidazole, tetramethylguanidine phenol, and tetramethylguanidine pyrrolidinone have much lower viscosity values than most conventional ILs, facilitating the diffusion of CO_2 in the solvent during the absorption process.[99] Regarding the CO_2 absorption capacity, tetramethylguanidine imidazole and tetramethylguanidine pyrrolidinone, presented high values, 0.154 and 0.159 g_{CO2}/g_{PIL}, respectively, the 40ºC at atmospheric pressure, tetramethylguanidine imidazole was the one with the fastest CO_2 absorption rate. As expected, the anion imidazole with the highest pKa (in this case, $pKa=23$) had greater CO_2 absorption capacity, resulting from its greater reactivity with CO_2.[100] However, the same authors state that, despite the ions of the

compound *N*-ethyl-2-hydroxyethylammonium butanoate ([e-2HEA][But]) have a higher volume than the others, there is no increase in CO_2 solubility, as suggested by the literature trend. tetramethylguanidine imidazole shows high capacity for absorption, high absorption rate, and excellent regeneration capacity, making it a very interesting solvent to capture CO_2.

As already mentioned throughout this thesis, the energy required in the regeneration stage is one of the biggest problems associated with this type of separation processes. Wang et al. [100] demonstrated that it is possible to project ILs with low absorption enthalpy, where stability, absorption enthalpy, and CO_2 absorption capacity vary with the basicity of PILs. The study showed that the stability of ILs increased with the decrease in the *pKa* value and that there is a linear dependence between the enthalpy of absorption and the *pKa* value, indicating the adjustment of absorption enthalpy by adjusting the basicity of the PILs. Still in the study of the alkalinity of PILs, Xu et al.[101] investigated the case of CO_2 absorption using azole-based PILs, verifying that the value of the thermal expansion coefficient, α_P, can be used to evaluate the free volume present in ILs. According to the literature,[102] in physical absorption processes, the CO_2 can be captured in the free spaces (free volume) of the bulky PIL structure. According to Xu et al.,[101] α_P is affected by the type of anion used, in this case, the free volume of PIL with [pyr]⁻ is greater than PILs with [im]⁻. Therefore, azole-based PILs are a viable alternative to capture CO_2, since the PIL with [pyr]⁻ demonstrated a high basicity and free volume, resulting in high CO_2 capture capacity.

Alcantara et al.[103] proposed another approach to evaluate the performance of the CO_2 absorption, through the neutralization reaction of three ethanolamines and butanoic acid. The results show that the growth of the alkyl chain of the cation promoted an increase in CO_2 solubility but only at high pressures. It is verified that the increase in the alkyl chain in ILs leads to an increase in free volume between ions, increasing the solubility of CO_2 in the PIL.[104] In addition, the results indicated that 2-hydroxyethylammonium butanoate, [2HEA][But], and *N*-methyl-2-hydroxyethylammonium butanoate, [m-2HEA][But], have higher CO_2 absorption capacity than most of the analyzed conventional ILs in literature. However, they also claim that despite the ions of the compound *N*-ethyl-2-hydroxyethylammonium butanoate, [e-2HEA][But], have a higher volume than the others, this did not led to an increase in the CO_2 solubility, as suggested by the trend in literature.[105]

As reported in previous studies, the increase in the number of carbon atoms in the alkyl chain in the cation increases solubility, however the selectivity for CO_2 decreases in

relation to other gases present in the combustion chain.[106],[107] Thus, in an absorption process, the design and optimization must consider solubility and selectivity as main parameters in order to obtain the IL mass and the number of stages required for a given operation. Several studies have been proposing mixtures of low viscosity ILs as separation agents that enhance the solubility and selectivity of CO_2.[108] In this sense, the mixing of ILs opens a new "range" of opportunities in the application of this new method in the capture of CO_2. Recently, Martins et al. [109], based on the analysis of excess volume of IL mixtures, demonstrated that mixtures of 1-butyl-3-methylimidazolium dimethylphosphate, [C_4C_1im][DMP], with carboxylate based protic ILs can present good results in capturing CO_2 post-combustion. In addition, the mixtures of these compounds have low viscosities, facilitating the mass transfer coefficient. However, these mixtures of ILs require further investigation due to the limited data available in the literature and the divergence between different authors.[71]

From the point of view of process engineering, the design and optimization of industrial processes and new solvents based on ILs for CO_2 capture, should not only focus on the carbon absorption capacity, but also on the knowledge of thermophysical and transport properties (Henry coefficient, viscosity, density, heat capacity, thermal conductivity, surface tension). As previously mentioned, ILs offer unique properties in the CO_2 capture process, however, application of this type of solvent in the industry has always been restricted due to the high viscosity, as well as the need for large amounts of energy in the regeneration of ILs. Recently, new technologies have been proposed to be coupled with the ILs, aiming at taking advantage of both technologies properties, and ultimately making the CO_2 absorption process viable. Among these technologies, membrane technology stands out as one of the most promising ones.[110] Supported ionic liquid membranes is a new technology that combines the best properties of ILs with the advantages of polymeric membranes. Within this technology, several materials have been analyzed in order to obtain high selectivity, permeability and mechanical resistance, such as supported ionic liquid membranes[111], phosphonium-based magnetic ionic liquid membranes[112], supported ionic liquid membranes using enzymes[113]. Regarding the ILs used in this technology, it is worth mentioning cholinium carboxylate ILs[111], ILs functionalized with amine[114],[115], ILs based on dicarboxylate[116] and protic ILs based on diamine monocarboxylate[117].

Unfortunately, due to the enormous number of possible ILs, their thermophysical characterization is still scarce. Is thus necessary to continue measuring the physical and chemical properties of these solvents, not only for the process and product design, but also for the development of tools that allow the consistent and robust forecast of equations of state (EoS), activity coefficient models and/or correlations.[118] A promising equation of state that successfully predicts the VLE of complex fluids such as ILs, is the theory of statistical association of fluids (SAFT).[103],[119] Thus, the combination of promising design tools with the adjustable capacity of the ILs, will allow a better design and performance of the process, essential in the area of chemical engineering. Taking into account the research on PILs available in the literature related to CO_2 capture, namely the work of Martins et al.[109], the present thesis will focus on the study of CO_2 solubilities and in the presentation of reliable density data of a series of protic ILs based on carboxylates. Additionally, the properties dependence on temperature and pressure will be evaluated, which can be used to infer in the use of these PILs as promising solvents in carbon capture by physical absorption.

1.4 Scope and Objectives

Ionic Liquids are neoteric solvents with a very high potential for the sustainable capture of CO_2, compared to conventional solvents. However, before the development and optimization of a new technology involving these compounds, it is necessary to know the thermophysical properties and the phase behaviour of the fluids involved in the process, in order to obtain a rigorous design, simulation and evaluation of the viability of the industrial process. In this way, density is the key property in the modelling of PILs using advanced molecular based EoSs, SAFT, which allows for the development of thermodynamic models capable of describing this type of fluids with simplicity. In addition, the CO_2 absorption capacity is studied by obtaining phase balance systems that allow the analysis of the behaviour of the compounds.

The methodology used in the synthesis of PILs, solubility and density measurements and the procedure used in PC-SAFT and soft-SAFT modelling are described in **Chapter 2**. **Chapter 3** presents the experimental results obtained and the modelling of the thermophysical properties using PC-SAFT and soft-SAFT EoSs. In addition, the binary CO_2+PIL systems for the four different PILs were analysed and discussed, regarding the kinetics, sorption, and desorption capacity of the studied compounds. To conclude, in **Chapter 4** the final conclusions are addressed and future works proposed.

16

2 Experimental

2.1 **Chemicals**

In this work five protic ionic liquids based on the *N,N*-diethylethanolammonium ([DEEA]⁺) cation and the anions: Acetate ([Ace]⁻), Propanoate ([Prop]⁻), Butanoate ([But]⁻), Pentanoate ([Pent]⁻) or Hexanoate ([Hex]⁻) were synthetized and investigated. Information on these compounds is summarized in Table 1, namely their chemical structure, acid:base proportion, molecular weight, average water content and purity. The water mass fraction of the ionic liquids was determined by coulometric Karl Fischer titration (Metrohm, model 831) and it was verified to be always less than 0.08 *wt*% - **Table 1**. Ultra-pure water used in the high-pressure measurements was double-distilled, underwent a reverse osmosis system and was treated with a Milli-Q plus 185 water purification device. 1 - butanol and dichloromethane were purchased from AnalaR NORMAPUR, with a mass fraction purity greater than 99.9%. *N,N*-Diethylethanolamine, Acetic Acid, Propionic Acid, Butyric Acid, Pentanoic Acid and Hexanoic Acid, used for the synthesis of the ILs, were acquired from Acros Organics, Sigma-Aldrich, Acros Organics, Prolabo, Riedel-de Haen, and Aldrich, respectively, with mass fraction purities greater than 99%.

2.1.1 **Synthesis and Purification of the PILs**

The protic ILs were prepared using *N,N*-diethylethanolamine and acetic, propionic, butyric, pentanoic or hexanoic acid. The precursors were used as received from the supplier without further purification.

The synthesis of the carboxylate-based protic ILs was based on the Brønsted acid - base neutralization method, as reported by Sharma et al.[120] and Chennuri et al.[121], in which the acid is added dropwise to an equimolar quantity of base. *N,N*-Diethylethanolamine was placed in a three necked round bottom flask equipped with a reflux condenser and two ampoules where the acid and a flow of nitrogen was added, respectively. Methanol was added to both the base and the acid to mitigate the heat release from the exothermic reaction and avoid the formation of fumes upon mixing. As the reaction is exothermic an ice bath was used to keep the reaction at low temperatures (0-5 °C). After the amine addition the mixture was vigorous mixed during 2 hours in a nitrogen atmosphere at room temperature. To remove the excess of methanol, the reaction mixture obtained was dried in a rotary evaporator (Rotavapor BUCHI R-210 with Heating Bath B-4910). The resulting IL was then dried under vacuum (10^{-3} mbar) for at least 48 h at room temperature. Compounds were then

stored in the glove box to avoid moisture absorption. The structure of all compounds synthesized was evaluated and confirmed by ^{1}H and ^{13}C NMR spectroscopy (**Appendix A**), showing a high purity level – **Table 1.**

Table 1. Name, abbreviation, acid:base proportion, chemical structure, molecular weight, purity and water content of the compounds synthetized.

Compound	Acid	Base
[DEEA][Ace] *N,N*-diethylethanolammonium acetate **1.5:1** *Mw*=207.76 g·mol^{-1}; mol%>97^a; *wt*%=0.04^b		
[DEEA][Prop] *N,N*-diethylethanolammonium propanoate **1.5:1** *Mw*=228.81 g·mol^{-1}; mol%>98^a; *wt*%=0.03^b		
[DEEA][But] *N,N*-diethylethanolammonium butanoate **1:1** *Mw*=205.30 g·mol^{-1}; mol%>96^a; *wt*%=0.08^b **2:1** *Mw*=293.40 g·mol^{-1}; mol%>98^a; *wt*%=0.03^b		
[DEEA][Pent] *N,N*-diethylethanolammonium pentanoate **1:1** *Mw*=219.33 g·mol^{-1}; mol%>97^a; *wt*%=0.08^b **2:1** *Mw*=321.45 g·mol^{-1}; mol%>98^a; *wt*%=0.05^b		
[DEEA][Hex] *N,N*-diethylethanolammonium hexanoate **2:1** *Mw*=349.51 g·mol^{-1}; mol%>96^a; *wt*%=0.08^b		

^{a}Molar percentage purity measured by NMR; ^{b}Mass percentage of water measured by Karl-Fisher titration.

2.1.2 **Acid-base proportions**

As already mentioned, PILs are a subclass of ILs synthesized through the stoichiometric acid neutralization reaction to a Brønsted base. And, unlike protic ILs that have measurable or non-existent vapor pressures,[122],[123] PILs can distil as reported by Angell et al.[124] in 2003. In accordance, analysing the spectra obtained by ^{1}H NMR spectroscopy **- Appendix A -** it is possible to observe that the synthesized ILs do not always present the expected acid:base ratio (1:1). This is the result of the drying process in the

vacuum line performed to reduce the presence of water and methanol from the synthesis. The acid: base ratio other than 1:1 is due to the ability of the carboxylic acids to form hydrogen bonds with the protic ionic liquid ion pair leading to an acid-rich azeotropic composition.[56],[124],[125] Thus, depending on the distillation (purification) extension (time), the system may not reach the azeotrope, allowing to obtain different acid:base ratios; here acid:base ratios of 2:1 or 1.5:1 were achieved – **Table 1**.

An example of the analysis performed is shown in **Figure 5** for [DEEA][Ace]|1.5:1. Using the Software MestreNOVA 6.0.3 it was possible to calculate, from the ^{1}H NMR spectrum, the area under the peaks. The ratio of the areas under the peaks corresponds to the ratio of the numbers of hydrogen atoms in each chemical environment. Thus, assigning 3 protons to the methyl group of the acid (number 1) the area of, per example, number 4 should be 2, since it corresponds to two protons. Instead it is around 1.25, leading thus to an acid:base proportion of 1.5:1. The remaining analysis are reported in **Appendix A.**
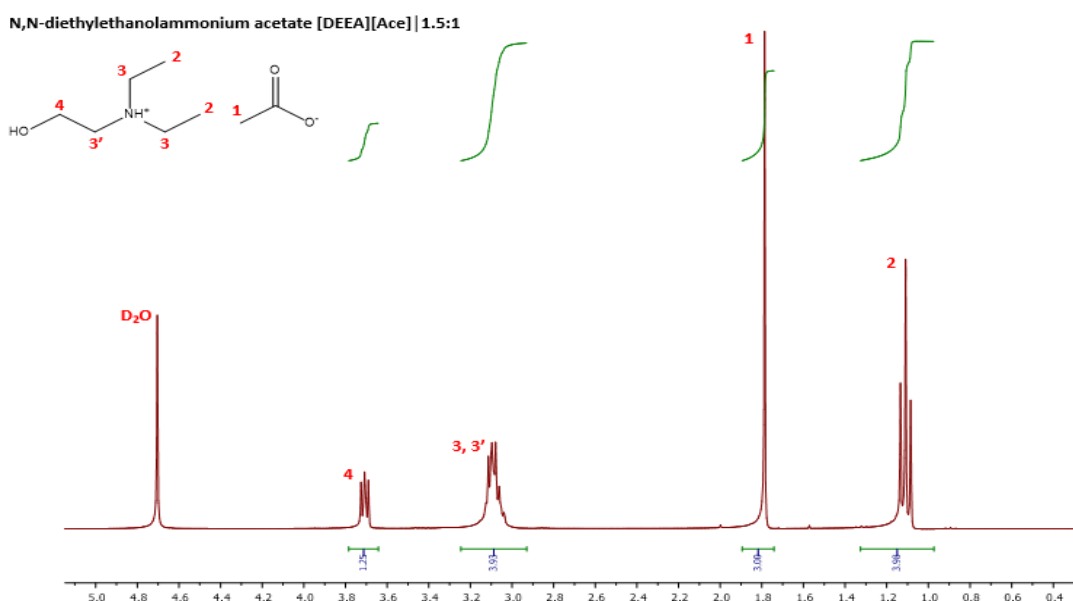
Figure 5. ^{1}H NMR spectrum of [DEEA][Ace]|1.5:1.

2.2   **High-Pressure Density**

Densities of the synthetized PILs were measured in the (283-363) K and (0.1 - 95) MPa temperature and pressure ranges, respectively, using an Anton Paar high pressure density meter (DMA-HPD) coupled to an mPDS 5 unit. The density standard uncertainty was found to be $5 \cdot 10^{-4}$ g cm^{-3}, as reported in previous publications.[126],[127] The

density cell was thermostatized by circulating of a thermoregulated heat transfer fluid (distilled water), with the aid of a thermostat bath circulator (Julabo MC), which has a temperature standard uncertainty of 0.1 K. The pressure was measured with a piezoresistive silicon pressure transducer (Kulite HEM 375) with an accuracy of 0.2%. The transducer was fixed directly in the ¼" stainless stainless-steel line to reduce dead volumes, and placed between the DMA - HPM measuring cell and a movable piston.[126],[128],[129] The schematic representation of the equipment used is displayed in **Figure 6**.
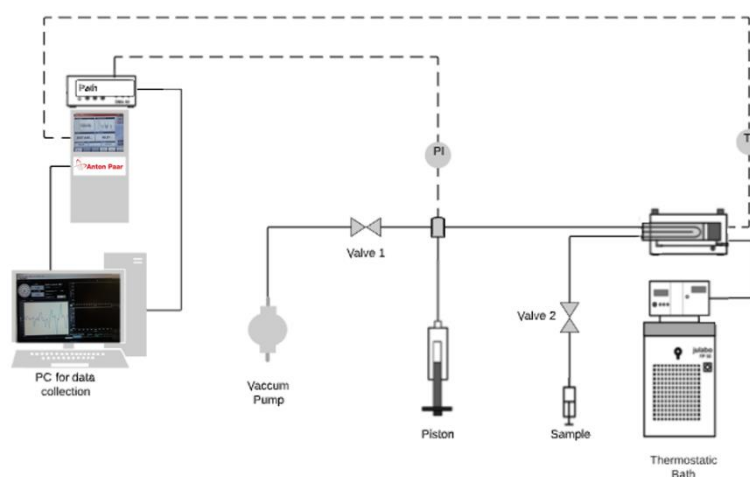
Figure 6. Schematic diagram of the high-pressure density experimental setup.

The densimeter was initially calibrated with ultra-pure water, 1-butanol, and dichloromethane in the pressure ranges of (0.1-95) MPa. The calibration validation for the solvents mentioned above was performed within the temperature range (293-343) K. The data and the linear regression obtained are in **Appendix B**. The density standard uncertainty was found to be $5 \cdot 10^{-4}$ g cm^{-3}, as reported in previous publications.[126],[127] The measurement methodology for this type of equipment is relatively simple. When the sample is inside the system, the operator starts measurements at the lowest stipulated pressure (0.1 MPa). The pressure exerted on the sample is controlled with the movement of the piston. The operator adjusts the piston until the desired pressure is reached, the temperature and oscillation period are monitored until all properties denote stability; that is, when the temperature, pressure and oscillation period do not change within 0.1 K, 0.1 MPa and 0.001 mS for 5 min. Once equilibrium is reached all the conditions and variables are recorded. The same procedure is carried out for the remaining pressures and temperatures. After the measurements, the setup is cleaned by removing the compound under measurement by means of compressed air,

solvent cleaning, and vacuum. Finally, acetone is circulated through the setup to ensure the solvent (usually water and ethanol) removal and an easier clean of the setup by applying vacuum. With the setup under vacuum a new sample is placed in a syringe connected to the setup inlet, **Valve 2,** and allowed to fill the setup liquid line. To ensure enough liquid volume to apply pressure to the system the piston is moved back, allowing more liquid to flow in. Once the entire sample is in the system, **Valve 2** is closed and the system ready for measurement.

Density values, ρ, were calculated from the obtained oscillation period through a polynomial equation suggested by the manufacturer:

$$\rho = A_1 + A_2 \cdot T + A_3 \cdot p + A_4 \cdot T^2 + A_5 \cdot p^2 + (A_6 + A_7 \cdot T + A_8 \cdot p + A_9 \cdot T^2 + A_{10} \cdot p^2) \cdot period^2 + A_{11} \cdot period^4 \tag{1}$$

where T is the temperature, p the pressure, $period$ the oscillation period and A_i (where $i=1$, …, 11) the polynomial coefficients. The values of the polynomial coefficients used are reported in **Appendix C**, and the values of density as a function of temperature and pressure for each compound are reported in **Appendix D**.

2.3   Solubility measurements

CO_2 solubility was measured using a constant temperature-volume equilibrium cell made of stainless steel, as shown in **Figure 6**. The setup can be divided in two section: a section V_1, of known volume, composed by a stainless steel cylinder and a pressure transducer (Swagelow S model), able to measure the pressure up to 1 MPa with an uncertainty of 0.2 %; and section V_2, also of know volume, composed by the measuring cell and a temperature probe. These two sections are isolated from each other and from the gas inlet by stainless steel valves. The experimental configuration, except the pressure transducer, is placed inside an oven with temperature stability of 0.5 K. The pressure transducer is accommodated outside the interior of the oven to ensure that the temperature do not influence the pressure uncertainty. An exact mass of solvent is introduced into the cell, the mass of which is determined using a high-weight/high-precision balance (Sartorius LA200P) with an accuracy of 1 mg. The sample is then kept under vacuum at a temperature of 353 K overnight, to remove atmospheric gases and moisture absorbed during manipulation. The gas is introduced into V1 section (area highlighted in yellow in **Figure 7** until the desired pressure is reached. Section V_1 volume was previously calibrated, and once

temperature stabilization is reached, the number of moles of gas is determined using Peng-Robinson EoS, knowing the gas volume, pressure, and temperature of the system. Knowing the exact mass, temperature and density of the compound placed in the measuring cell one is able to determine the compound volume and thus, determine the available volume for the gas phase and consequently, the total volume of the gas phase on the entire setup. Then, **Valve 1** is open allowing the contact between the gas and the solvent. The system pressure is then monitored over time and the vapor-liquid equilibrium evaluated. The VLE is identified by evaluating the pressure dependency with time – once no pressure variation, within 0.1 bar, is observed the system is considered at equilibrium. Once the equilibrium data is determined, the temperature is decrease, allowing for additional gas to dissolve into the liquid, and a new VLE point determined. The methodology is repeated for all the intended temperatures. The gas cylinder has a larger volume, compared to the cell volume, to avoid a large pressure drop on opening **Valve 1** and to ensure enough gas moles to allow good resolution on the pressure measurements. At each VLE point the number of moles absorbed by the liquid phase is determined. The number of moles absorbed in the compound is determined by the difference between the final number of moles and the number of moles initially added to the system. After determining the equilibrium pressure for the six defined temperatures, the PIL is regenerated by subjecting the system to low pressure (1 Pa) and moderate temperature (353 K) for a period never smaller than ten hours – time determined to be sufficient to regenerate the IL. Once PIL regeneration is achieved, the absorption procedure is then repeated with an initial pressure different from that set in previous measurements (thus, different initial moles of gas), to determine additional equilibrium points and to better describe the system's phase diagram. The determined equilibrium points were measured three times, to minimize, identify, and eliminate measurement and manipulation errors. Regarding the sorption/desorption cycles, after each pressure balance is reached, the system is degassed at 1 Pa and 353 K for two hours, and the absorption methodology described above is repeated for four cycles.

The LabView program was used to monitor and record the data measured over the course of the experiments. In addition, it provides the monitoring of configuration signals over time through graphs, allowing the recorded results to be better analysed. In addition, it allows monitoring the evolution of the system, providing an easy perception of errors or failures in the system, as well as simpler and more critical monitoring by the user.
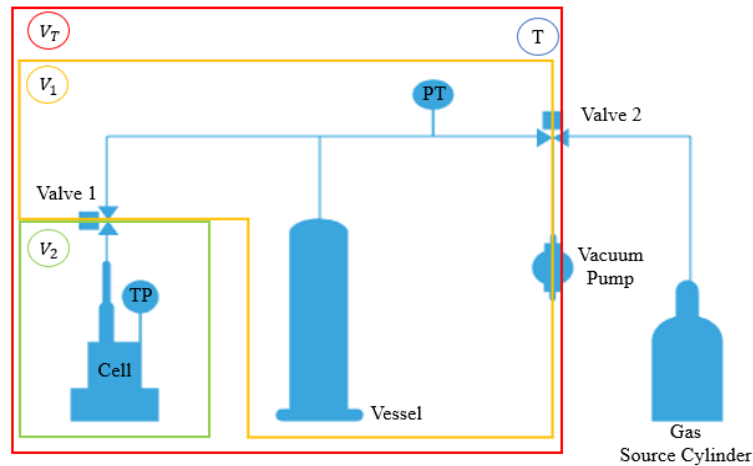
Figure 7. Schematic diagram of the isochoric cell: V_1 represents the volume of the gas line, V_2 represents the volume of the measuring cell and V_T represents the total volume (V_1+V_2) at constant temperature.

2.4 PC-SAFT and soft-SAFT Modelling

In industry, the development and optimization of processes are based on process simulators, using correlations and EoS.[126],[130] The main limitation associated with classic cubic EoS is their inability to describe interactions between molecules, considering the molecule as a "whole". Then, an EoS was developed based on the theory of perturbations of quantum mechanics, SAFT EoS, introducing an associative term that allows defining which sites where the molecule can create interactions with molecules present in the system, allowing the prediction of the behavior of fluids.[130]

Chapman et al.[131],[132] was the first to propose an EoS based on the perturbation theory, SAFT (Statistical Statistics of Associated Fluids). It considers a fluid made up of homonuclear chains composed of hard spheres (segments or monomers), covalently bonded to each other, of fixed size, energy and volume, with interactions and repulsions, linked together in specific places in the chain.[133]–[135] However, specific short range linkage sites between chains may or may not exist, making modeling difficult for associative interactions.[136] The accuracy of the results obtained with SAFT type EoS depends on the meticulous development of association models capable of describing the physical and energetic behavior of the fluid.

The expression for SAFT equations, **Equation (2),** is given in terms of Helmholtz residual free energy, A^{res}, for a mixture of components associating chains of monomers. The Helmholtz residual free energy is usually expressed as the sum of different contributions for

24

a specific effect: a term of reference, A^{ref}, that represents the contribution due to the monomer-monomer physical interactions (either attractive and repulsive), a chain term, A^{chain}, that represents chain formation and an association term, A^{assoc}, that represents due to the strong and highly associating forces, for example, hydrogen-bonding.[126],[130] Regarding polar molecules, an additional term can be considered (A^{polar}).[137]

$$A^{res} = A^{total} - A^{ideal} = A^{ref} + A^{chain} + A^{assoc} + A^{polar} \tag{2}$$

From the original version of SAFT, many modifications were proposed. The PC-SAFT EoS proposed by Gross and Sadowski[138],[139] is the most applied extension of SAFT-type equations.[140] This has attracted a lot of attention due to the good modelling results on long chain molecules, such as ILs.[141]–[143] PC-SAFT, in contrast to the original SAFT, considers the rigid chain as a reference fluid instead of hard spheres, consisting of several segments of monomers with free articulation. The model is described as the sum of different terms of Helmholtz residual energy (A^{res}), defined as the difference between Helmholtz's molar energy and that of an ideal gas at the same temperature and density. PC-SAFT accounts for repulsive interactions (A^{hc}), while dispersive interactions are recorded in a separate term (A^{disp}):

$$A^{res} = A^{total} - A^{ideal} = A^{hc} + A^{disp} + A^{assoc} \tag{3}$$

For non-associating compounds PC-SAFT is characterized by only three parameters: number of segments (m), the segment diameter (σ), and depth of the energy well (ε). For association compounds there are two additional parameters related to the energy (ε^{HB}) and volume (k^{HB}) of the association sites.

Although the selection of reasonable properties for the EoS parameters is still controversial, the use of density as a function of temperature and pressure is the most significant.[126],[140] To obtain the PC-SAFT EoS molecular parameters the Multiflash software[144] was used. These parameters were determined by regressing the parameters of the pure PILs and the experimental density data and their respective derivative properties, using as objective function (OF) the following equation.

$$OF = a \cdot \frac{1}{N} \left[\sum_{i=1}^{N} \frac{\rho_{exp} - \rho_{calc}}{\rho_{exp}} \right] + b \cdot \frac{1}{N} \left[\sum_{i=1}^{N} \frac{(\alpha_P)_{exp} - (\alpha_P)_{calc}}{(\alpha_P)_{exp}} \right] + c \cdot \frac{1}{N} \left[\sum_{i=1}^{N} \frac{(k_T)_{exp} - (k_T)_{calc}}{(k_T)_{exp}} \right] +$$

$$d \cdot \left| \frac{1}{N} \left[\sum_{i=1}^{N} \frac{\rho_{exp} - \rho_{calc}}{\rho_{exp}} \right] \right| \Big|_{P=0.1\ MPa} \tag{4}$$

where a, b, c and d are the weights of each property on the OF, N is the number of experimental data, ρ_{calc}, ρ_{exp}, $(\alpha_P)_{calc}$, $(\alpha_P)_{exp}$, $(k_T)_{calc}$, $(k_T)_{exp}$ correspond to the density (ρ), isobaric thermal expansion (α_P) and isothermal compressibility (k_T). The subscripts *calc* and *exp* stand for calculated and experimental data, respectively. For the model to better describe the experimental data at lower pressures (0.1 MPa), the *OF* considers explicit the density error at atmospheric pressure. Regarding the derived properties, the smallest (283 K) and the highest (363 K) isotherm were considered to maintain the predictive character of the EoS.

The characterization of a system using the PC-SAFT equation also requires the definition of an appropriate association scheme for each molecule. Therefore, the use of this type of EoS requires an appropriate choice of association sites to accurately represent the number and type of association sites present in the molecule and how they can interact within the system.[145] The association sites are of two types: positive site (represented by the letter A), which represents the proton donor and the negative pole (represented by the letter B), which represents the proton receptor. Over the years, several articles on the modeling of pure ionic liquids and mixtures of IL-IL have been published.[146]–[152] Recently, Alcantara et al. [103] modelled the thermophysical properties, using EoS PC-SAFT, of three PILs with structures and functional groups very similar to those analysed in this work. The authors treated these ILs as molecules with associative behaviour using a 2B association scheme, where each molecule was assigned two association sites (cation and anion, respectively) and association interactions were allowed only between different sites. According to the author, the modelling allowed the correct description of the density at high pressure and the properties of the derivatives.

Initially, two associative schemes for the studied PILs were considered (**Figure 8**), scheme **a)** which considers five sites and scheme **b)** which considers four possible sites in the structure of the molecule more favorable to establishing interactions with other molecules. Thus, analyzing the two association schemes, there was a slight discrepancy in the modeling, as reported in **Appendix E**, however, we opted for the 2/3 association scheme (**Figure 8. (a)**), where there is the contribution of one more group, with two pairs of unpaired electrons, which can establish interactions with other molecules, allowing a better modeling of these compounds in more complex mixtures.

In this work, the associative parameters (ε^{HB} and k^{HB}) were adopted from literature,[103],[136],[142] and the non-associative parameters (m, σ and ε) were optimized here

by minimizing the objective function (*OF)* described in **Equation (4)**. To minimize the *OF*, the solver optimization routine available in the MS Excel was used.
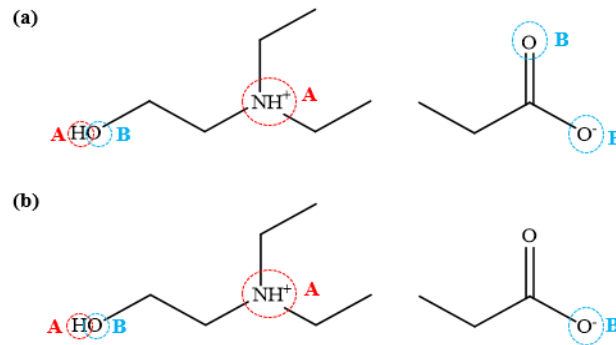
Figure 8. Example of the PILs associative scheme used, exemplified for [DEEA][Prop]│₁.₅:₁. (a) Association scheme 3/2 and (b) Association scheme 2/2.

Table 2. PC-SAFT EoS *m* and k^{HB} molecular parameters and *OF* values.

[DEEA][Prop] │ 1.5:1			[DEEA][But] │ 2:1		
m	k^{HB}	*OF*/%	*m*	k^{HB}	*OF*/%
12.0531	$1.00 \cdot 10^{-2}$	29.2016	12.6363	$1.00 \cdot 10^{-2}$	23.6448
15.0535	$1.00 \cdot 10^{-3}$	24.7001	17.5053	$1.00 \cdot 10^{-2}$	19.7583
16.0534	$1.00 \cdot 10^{-4}$	21.4041	20.7744	$1.00 \cdot 10^{-3}$	17.2877
15.5532	$1.00 \cdot 10^{-5}$	18.5819	15.6363	$1.00 \cdot 10^{-4}$	15.4760
12.5539	$1.00 \cdot 10^{-7}$	15.2114	16.8228	$1.00 \cdot 10^{-4}$	14.8587

The process of optimization of the molecular parameters of the PC-SAFT EoS showed an error in the description of the studied properties while maintaining the physical meaning of the EoS molecular parameters.– As reported in **Table 2** minimizing the error of the *OF* the values of the k^{HB} energy parameter tends to zero, losing its physical meaning. Furthermore, restricting this parameter value, in the optimization rotine, to values reported in the literature leads to a poor description of the property by the EoS, as reported in **Appendix C**. Thus, it was decided to apply another extension of the SAFT-type EoS, the soft-SAFT. This EoS was developed by Blas and Vegas[153] and it considers Lennard-Jones (LJ) intermolecular potential as a term of reference. The LJ term considers repulsive and attractive interactions between chain monomers in a single contribution. This extension stands out for successfully describing the thermodynamic behavior of several different

solvent families, including ILs.[137] Following the same method used in PC-SAFT EoS, the experimental data were modeled using soft-SAFT EoS.

As the reference term is used for a pure LJ fluid, the analysis of mixtures is done using the Van der Waals fluid theory, with size and energy parameters obtained through the modified Lorentz-Berthelot (LB) mixing rules represented by **Equations (5)** and **(6)**.[154]

$$\sigma_{ij} = \eta_{ij} \left(\frac{\sigma_{ii} + \sigma_{jj}}{2} \right) \tag{5}$$

$$\varepsilon_{ij} = \xi_{ij} \sqrt{\varepsilon_{ii} \cdot \varepsilon_{jj}} \tag{6}$$

where, η_{ij} and ξ_{ij} are the binary adjustable parameters of size and energy among the species i and j. Thus, when adjusted to the mixture, these binary parameters are responsible for the differences in size and/or energy of the monomers that make up the different compounds in the mixture. When the binary parameters are defined for the unit, the model becomes predictive, that is, the model can be used for the calculation of multicomponent mixtures without requiring the adjustment of other mixture data.

For associate molecules, two additional parameters are required, the energy ($\varepsilon_{ii}^{HB}/k_B$) and binding volume ($k_{ii}^{HB}$) of the association sites. Thus, the same association scheme used in the PC-SAFT modeling was considered, which guarantees the closest description of reality in this type of systems. Thus, the general extension for mixtures requires the evaluation of the assessment of cross-association of energy and volume, represented by **Equations (7)** and **(8)**, respectively.

$$\varepsilon_{ij}^{HB} = \sqrt{\varepsilon_{ii}^{HB} \cdot \varepsilon_{jj}^{HB}} \tag{7}$$

$$K_{ij}^{HB} = \left(\frac{\sqrt[3]{K_{ii}^{HB}} + \sqrt[3]{K_{jj}^{HB}}}{2} \right)^3 \tag{8}$$

28

3 Results and discussion

The development of new technologies and optimization of existing processes require precise data on the thermophysical and thermodynamic properties of pure compounds or mixtures over a wide range of temperatures and pressures. In this work, an experimental and modelling study was carried out using the SAFT-type EoS and densities and CO_2 solubilities measured experimentally. The choice of the compounds herein investigated was based on the work of Martins et al.[56], where mixtures involving carboxylate-based protic ILs and APILs were identified as good candidates for CO_2 capture. Using the COSMO-RS software, authors[56] identified mixtures with excess positive enthalpies, that is, large positive excess volumes, favouring the capture of CO_2. From the results obtained, the pure PILs with the best results were selected and are here analysed for the capture of CO_2. These ILs are characterized by economic synthesis, require low energy for the regeneration, and have large molecular structures allowing a greater capture of CO_2.[33],[103],[155]

3.1 High-pressure Density

The density of the synthetized PILs as a function of temperature (283-363) K and pressure (0.1-95) MPa was measured using a high-pressure cell and results are shown in **Figure 9** and listed in **Appendix D**. When analysing **Figure 9**, a clear dependence of the density of each compound with pressure and temperature is observed: density increases with increasing pressure and with decreasing temperature, as observed for other ILs families.[156]–[159] As far as is known, there is no literature data on densities available for the PILs studied.

From the experimental density, molar volumes, V_m, were calculated using the following expression:

$$V_m = \frac{M_w}{\rho} \tag{9}$$

where M_w and ρ are the molar mass and density of the PIL studied, respectively. The V_m of the different PILs were calculated as a function of temperature and pressure and are represented in **Figure 10**. The tabulated data can be found in **Appendix E**.

Molar volume is inversely proportional to density and directly proportional to molecular mass as represented in **Equation (9)**. The increase in the molecular mass of the compounds will imply an increase in the molar volume, as would be expected, since V_m is considered an additive property. The molecular volumes of the studied PILs, in the range of pressures (0.1-95) MPa and temperatures (283-363) K, increase with increasing molecular

mass in the order: [DEEA][Ace]$\big|$ $_{1.5:1}$ < [DEEA][Prop]$\big|$ $_{1.5:1}$ < [DEEA][But]$\big|$ $_{2:1}$ <[DEEA][Pent]$\big|$ $_{2:1}$ < [DEEA][Hex]$\big|$ $_{2:1}$, while density values have the opposite behavior: [DEEA][Hex]$\big|$ $_{2:1}$ < [DEEA][Pent]$\big|$ $_{2:1}$ < [DEEA][But]$\big|$ $_{2:1}$ < [DEEA][Prop]$\big|$ $_{1.5:1}$ < [DEEA][Ace]$\big|$ $_{1.5:1}$. This behavior is related to the increase in molecular mass leading to more bulky molecules, occupying larger molar volumes per mole of component and, therefore, lower densities. Observing at **Figures 10 a)** and **b)**, the PILs studied have small dependence on temperature and pressure, with a small increase in V_m with temperature and a decrease with pressure. In addition, it is possible to observe the impact of pressure and temperature on the V_m with the increase of the molecular mass.

The derivative properties, isothermal compressibility (k_T) and isobaric thermal expansion (α_P), were obtained from the following expressions:

$$k_T = \frac{1}{\rho}\left(\frac{d(\rho)}{d(P)}\right)_T = \left(\frac{d\ln(\rho)}{d(P)}\right)_T \tag{10}$$

$$\alpha_P = -\frac{1}{\rho}\left(\frac{d(\rho)}{d(T)}\right)_P = -\left(\frac{d\ln(\rho)}{d(T)}\right)_P \tag{11}$$

Isothermal compressibility is a measure of the variation in the volume of the PILs due to the change in pressure, at constant temperature, while the isobaric thermal expansiveness is a measure of the variation in the volume of the PILs due to the change in temperature, at constant pressure. The derived properties, k_T and α_P are shown in **Figures 11** and **12**, respectively, observing that the increase in pressure and temperature have a similar impact on k_T and α_P. The k_T values range from $2.72 \cdot 10^{-4}$ to $8.07 \cdot 10^{-4}$ MPa^{-1}, which are in the same order of magnitude as those reported for other IL families.[160]–[162] Analyzing the behavior of k_T with temperature and pressure, it can be seen that in **Figure 11 a)**, **b)** and **c)**, k_T has a higher temperature dependence at low pressures, with a decrease in temperature dependence at higher pressures. The α_P values vary in the range $5.56 \cdot 10^{-4}$ to $10.7 \cdot 10^{-4}$ K^{-1}, which are in the same order of magnitude as those reported for other IL families.[159],[163],[164] Analyzing **Figure 12 a)**, **b)** and **e)** it is possible to verify the decrease in temperature dependence with the increase in pressure for the experimental data. **Figure 12 a)** and **b)** shows a temperature dependence that soft-SAFT overestimates over the entire pressure range. In relation to **Figure 12 c)** the experimental data show a greater dependence on temperature when compared to the other compounds.
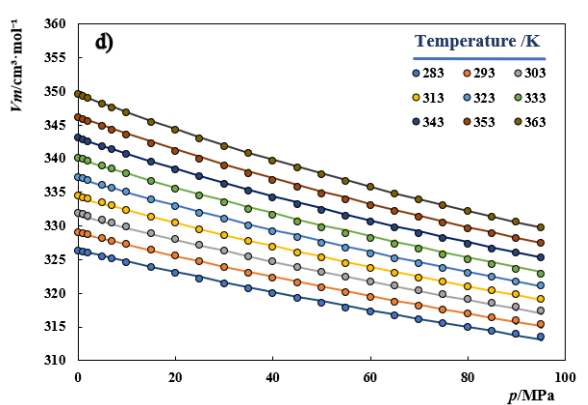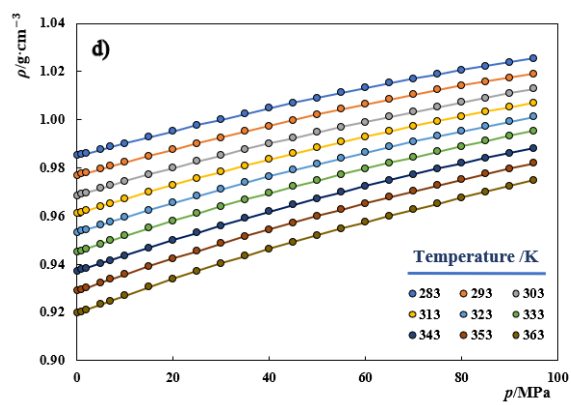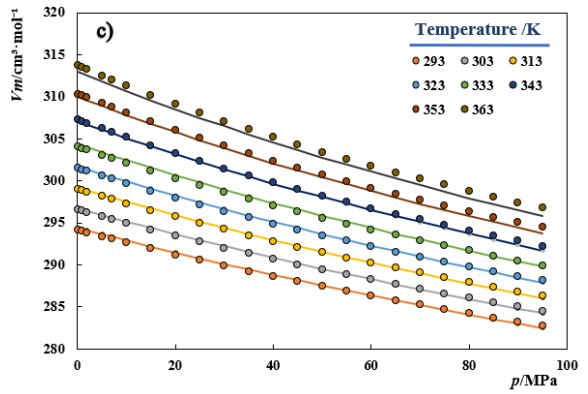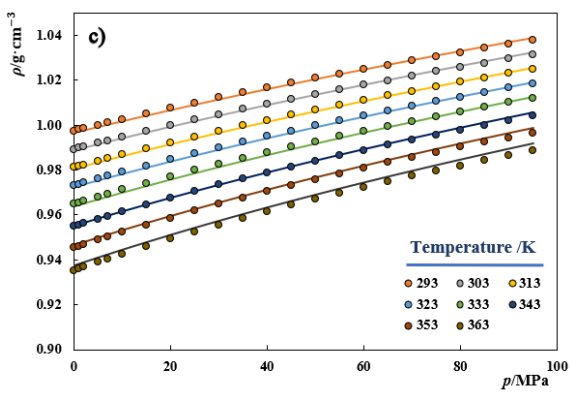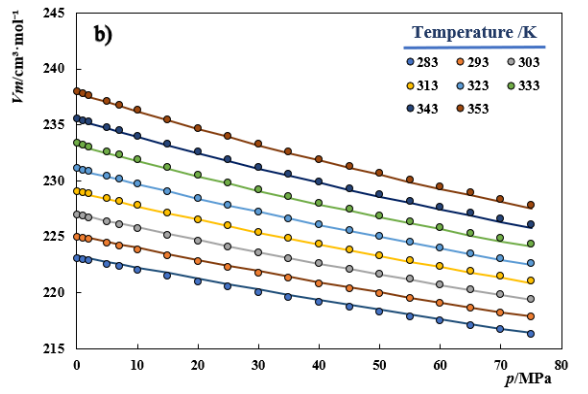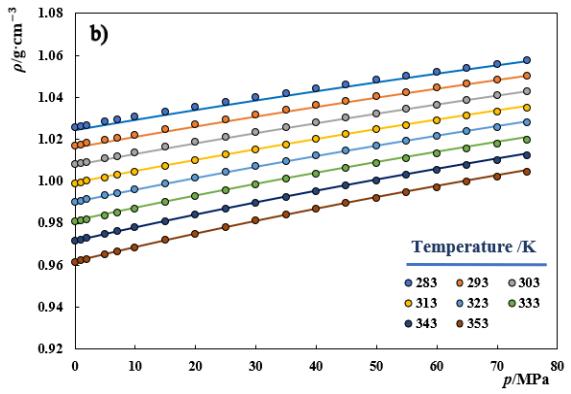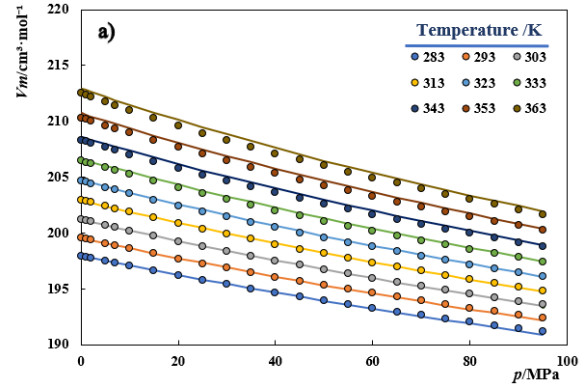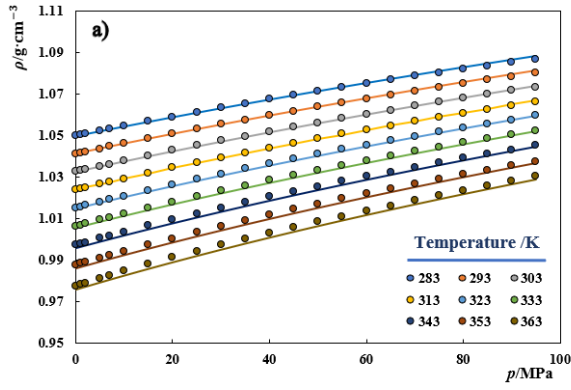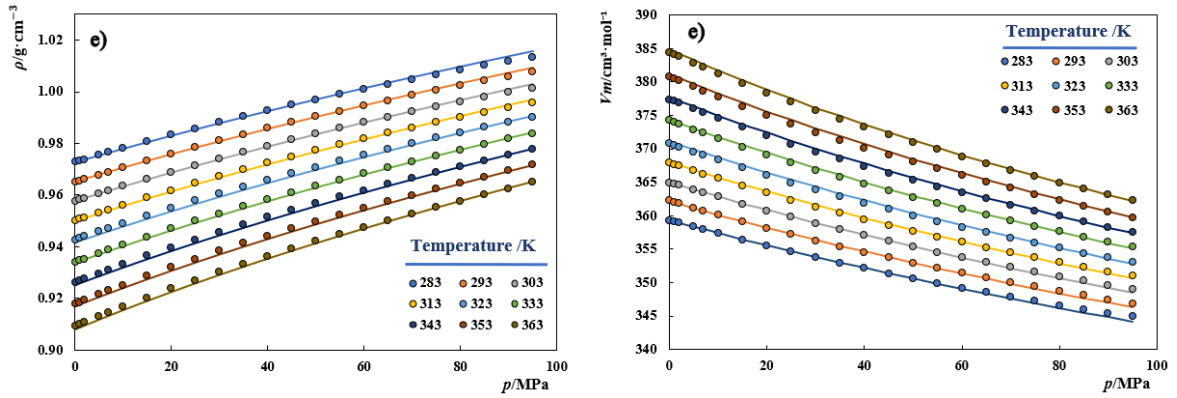
Figure 10. Experimental diagrams *pTρ* (left column) and *pTVm* (right column) for the studied systems. The symbols represent the experimental data and the lines are the results of soft - SAFT modelling: a) [DEEA][Ace] │ 1.5:1, b) [DEEA][Prop] │ 1.5:1, c) [DEEA][But] │ 2:1, d) [DEEA][Pent] │ 2:1 and e) [DEEA][Hex] │ 2:1.
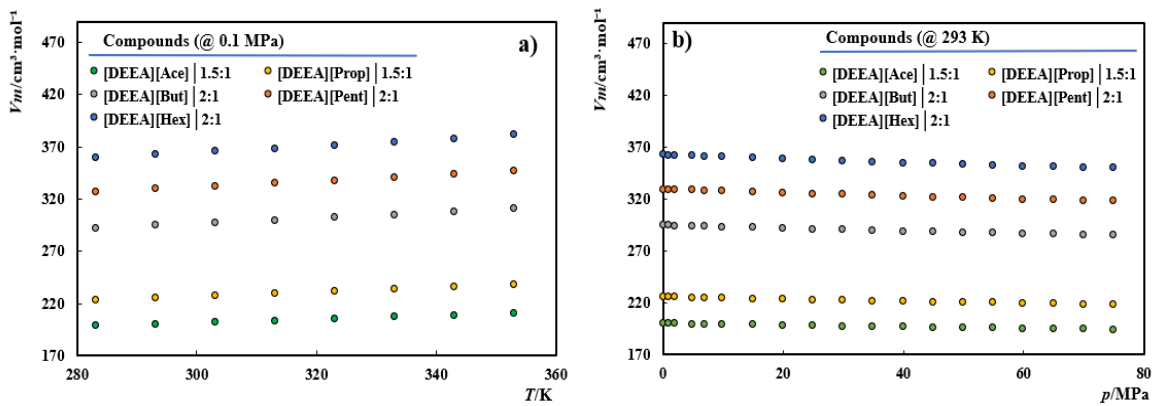
Figure 9. a) Molar volume as a function of temperature at a pressure of 0.1 MPa. b) Molar volume as a function of pressure at a temperature of 293 K.

Before the development and optimization of any new technology, it is essential to know the thermophysical properties and phase behaviour of the fluids involved in the process, to obtain a rigorous design of the industrial process. A promising equation of state for more complex compounds is the soft-SAFT EoS, which allows for a physical interpretation of the system and the reduction of phase equilibrium in complex fluids and mixtures, such as ILs and their subclasses, PILs.[103],[119] Although the discussion about the most reliable properties to be used on the determination of these EoS molecular parameters is still under debate, the simultaneous regression of density and its derivative properties stand as a good approach for systems containing non-volatile compounds like the ILs.[165]

The description of the liquid density as well as the derivative properties is evaluated

by the percentage average absolute deviation (*%AAD*), defined as the difference between the experimental data and the results provided by the soft-SAFT EoS.

$$\%AAD_Z = \left| \frac{1}{N} \sum_{i=1}^{N} \frac{z^{exp} - z^{calc}}{z^{exp}} \right| \times 100 \qquad (12)$$

where *N* stands for the number of points considered and the subscript *exp* and *calc*, are the experimental and calculated values by the model, respectively, for the studies property, *Z*. The tabulated values of *%AAD* for each property studied in the four systems are shown in **Appendix G**.

Soft-SAFT EoS was applied to the density data measured and, as can be observed in **Figure 9**, it provides an excellent representation of the data, with *%ADD* values in the range [$8.90 \cdot 10^{-2}\%$;4.98%], however, the model has some difficulty in modelling k_T with *%ADD* values in the range [2.78%;4.98%], and α_P with *%ADD* values in the range [1.68%;5.49%] - **Figures 11** and **12**. Comparing the values of the absolute average deviations for each property, α_P and k_T, α_P has a slightly larger deviation, which is somewhat contradictory, since the temperature effect is generally easier to describe than the effect of pressure. In addition, soft-SAFT EoS overestimates the values of k_T at higher pressures for all compounds studied, as can be seen from **Figure 11**. Regarding α_P modelling, **Figure 12 a)**, **b)** and **e)** show the decrease in dependence on temperature with increasing pressure, both for experimental data and for data obtained from soft-SAFT. **Figure 12 a)**, **b)** and **c)** shows a temperature dependence that the soft-SAFT overestimates over the entire pressure range. In relation to **Figure 12 c)** the experimental data show a greater dependence on temperature when compared to the other compounds, with anomalies in the description of the data, and consequently the loss of the soft-SAFT EoS modeling capacity. That is, the experimental data obtained show that the compound [DEEA][But]│₂:₁ has a volume variation so dependent on the temperature that soft-SAFT was unable to predict this dependence.

The soft-SAFT parameters obtained for each pure compound are shown in **Table 3** where it is possible to verify the increase of the associative parameters with the increase of the ILs molecular mass.[126] However, the volume and the energy of association remained constant and equal to 515 and 3400, respectively, for all protic ionic liquids adjusted in this work. The k^{HB} and ε^{HB} parameters have constant values due to the existence of association interactions between equivalent chains, only allowing one type of connection.[126] Thus,

there is a reduction in the number of parameters required in the adjustment procedure without loss of precision.
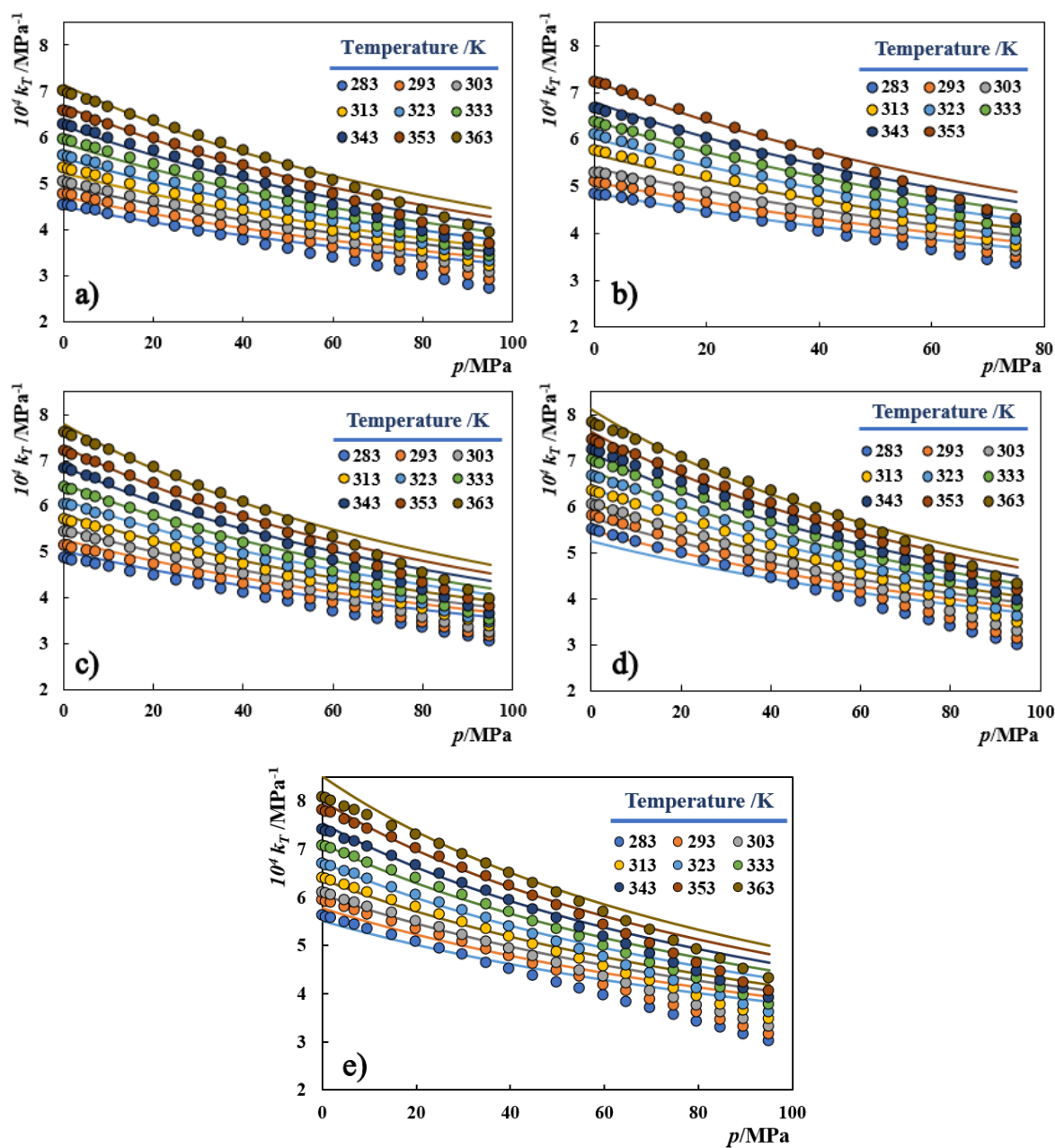
Figure 11. Isothermal compressibility, k_T, as a function of pressure for the PILs studied at different temperatures: symbols represent experimental data and lines are the soft-SAFT modelling results: a) [DEEA][Ace]│1.5:1, b) [DEEA][Prop]│1.5:1, c) [DEEA][But]│2:1, d) [DEEA][Pent]│2:1 and e) [DEEA][Hex]│2:1.
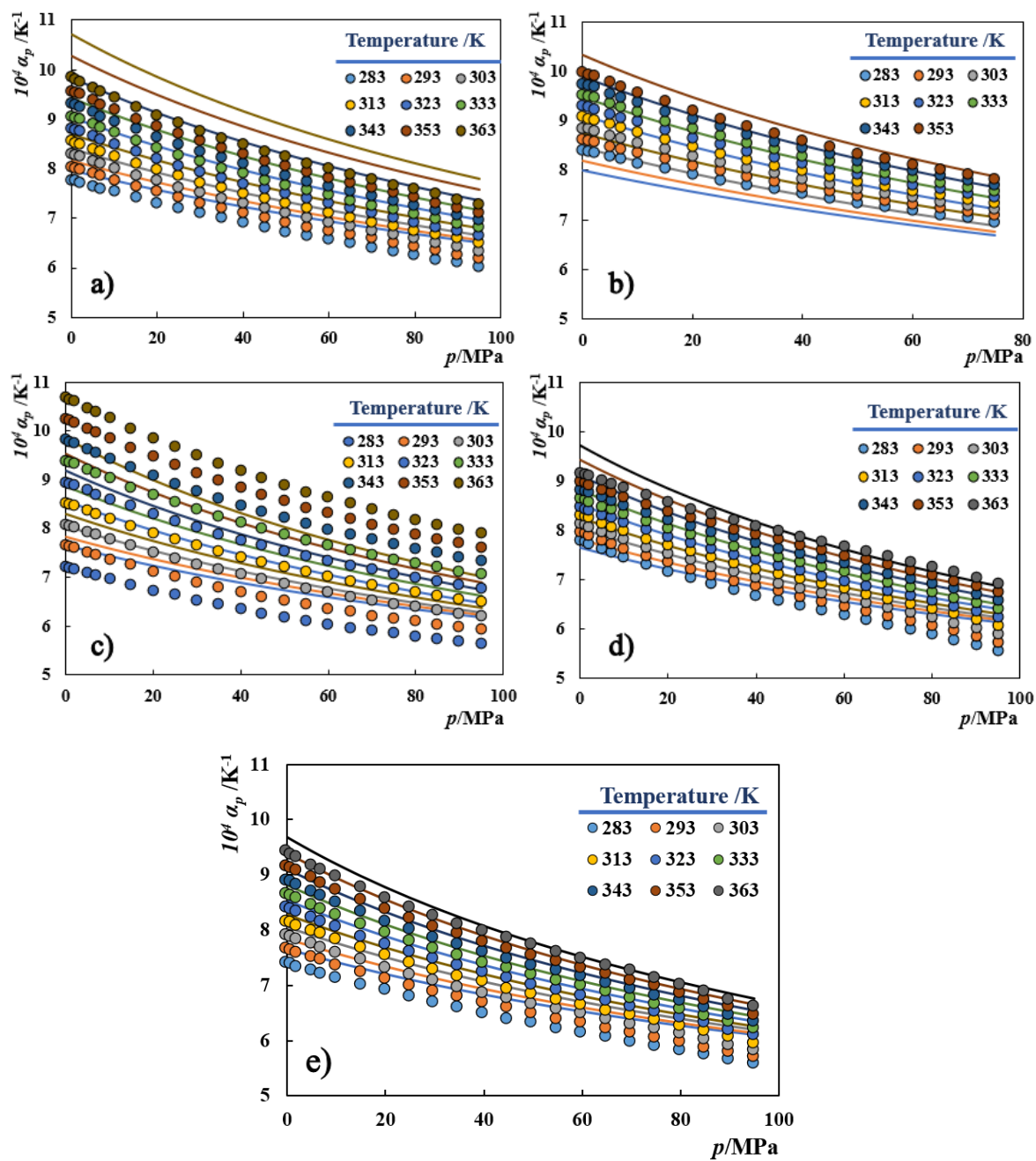
Figure 122. Isobaric thermal expansivity, α_P, as a function of pressure for PILs studied at different temperatures: symbols represent experimental data and lines are the soft-SAFT modeling results: a) [DEEA][Ace]│1.5:1, b) [DEEA][Prop]│1.5:1, c) [DEEA][But]│2:1, d) [DEEA][Pent]│2:1 and e) [DEEA][Hex]│2:1.

Table 3. Soft-SAFT molecular parameters for the compounds studied.

	M_W (g·mol^{-1})	m	$\sigma(\text{Å})$	$\varepsilon(K)$	k^{HB}	ε^{HB}
[DEEA][Ace] $\vert$ 1.5:1	207.76	7.845	3.3594	268.56	515	3400
[DEEA][Prop] $\vert$ 1.5:1	228.81	8.079	3.4642	270.87	515	3400
[DEEA][But] $\vert$ 2:1	293.40	8.698	3.7167	296.84	515	3400
[DEEA][Pent] $\vert$ 2:1	321.45	9.032	3.8120	302.28	515	3400
[DEEA][Hex] $\vert$ 2:1	349.51	9.345	3.8930	305.28	515	3400
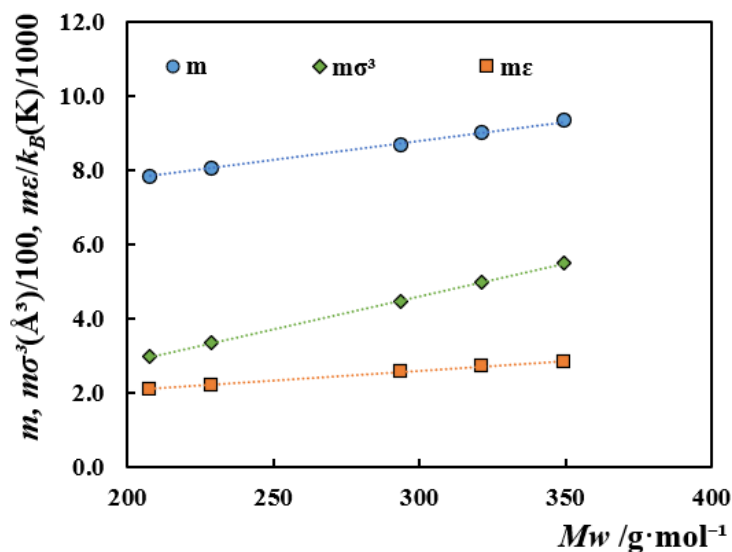
Figure 13. Soft-SAFT parameters as function of the compound molecular mass, for the studied PILs.

One of the main advantages of SAFT type EoS is the physical meaning of the parameters, which allows to create a physical trend within the same chemical family.[166],[167] Thus, for a set of protic ionic liquids in which the length of the alkyl chain increases and, consequently, the increase in molecular mass is expected, it is assumed that the non-associated parameters can often show a linear trend with the molecular mass within a series. Therefore, as observed in previous works[168],[169], the three non-associative molecular parameters of the PILs are linearly correlated ($R^2 > 0.99$) with the molecular mass, as shown in **Figure 13**, the following expressions were obtained:

$$m = 1.04 \cdot 10^{-2} \, M_w(g/mol) + 5.6723 \ (R^2 = 0.9986) \tag{13}$$

$$m\sigma^3 = 1.78 \cdot 10^{-2} \, M_w(g/mol) - 0.7319 \ (R^2 = 0.9997) \tag{14}$$

$$m\varepsilon = 5.50 \cdot 10^{-3}\, M_w(g/mol) + 0.9625 \;\; (R^2 = 0.9967) \hspace{2cm} (15)$$

Equations (13), **(14)** and **(15)** demonstrate that, as expected, the increase of the anion's alkyl chain length, and consequently, the increase of the molecular mass, is reflected in the soft-SAFT parameters by an increase in the parameters values, as well as dispersive energy. The physical meaning of the soft-SAFT parameters allows to present correlations that can predict the thermodynamic behavior of other similar compounds.

The modeling of the experimental data using the PC-SAFT was based on the alteration of the five characteristic parameters (m, σ, ε, ε^{HB} and k^{HB}) of this type of EoS, to obtain an optimization routine to minimize the *OF*. Initially, several optimization routines to the *OF* were performed changing the five parameters of the model, however, in all the performed optimization, values of parameters without physical significance were verified, obtaining high m values and k^{HB} values very close to zero. Since the PILs analysed have functional groups, with a certain volume of association, k^{HB}, it does not make sense that PC-SAFT EoS considers this parameter to be approximately zero. In addition, comparing the parameters m and k^{HB} with the parameters obtained in the literature, shown in **Table 5**, it appears that the values of m and k^{HB} are not in the same order of magnitude as the values present in the literature. The compounds shown in **Table 5** have functional groups like the ILs analysed, as well as the same type of interaction between molecules (hydrogen bonds). Therefore, to improve the fit of the properties, restrictions were applied, where m would be a fixed value and the energy of the association could not assume values less than $1 \cdot 10^{-02}$ ($k^{HB} \geq 0.01$) and $1 \cdot 10^{-04}$ ($k^{HB} \geq 0.0001$), the graphs and respective values of the obtained parameters are shown in **Table 4**. As seen in **Table 4**, the imposition of restrictions on *OF* optimization resulted in m values is very high and the α_P adjustment is not is suitable for experimental data, verifying a "compression" of the isotherms in the graph α_P vs. p. However, the decrease in the k^{HB} value ($k^{HB} = 0.0001$) provided an improved adjustment of α_P when compared to higher k^{HB} values ($k^{HB} = 0.01$), but such a low k^{HB} value is not acceptable. **Appendix F** demonstrates other attempts at modeling experimental data using PC-SAFT, with the respective restrictions. In addition, the mean absolute deviation associated with α_P is greater when compared to the mean absolute deviation of k_T, which is unusual, since in this type of EoS the effect of temperature is generally easier to describe than the effect of pressure.

Table 4. PC-SAFT modeling results with the constraint $k^{HB} \geq 0.01$ (left column) and constraint: $k^{HB} \geq 0.0001$ (right column), for compound [DEEA][But] $\big|_{2:1}$.

m	**17.5053**	m	**16.8228**
$\sigma(\text{Å})$	2.8712	$\sigma(\text{Å})$	2.9127
$\varepsilon(K)$	213.35	$\varepsilon(K)$	217.63
$\varepsilon^{HB}(K)$	2579.5	$\varepsilon^{HB}(K)$	3975.6
k^{HB}	**0.01**	k^{HB}	**0.0001**
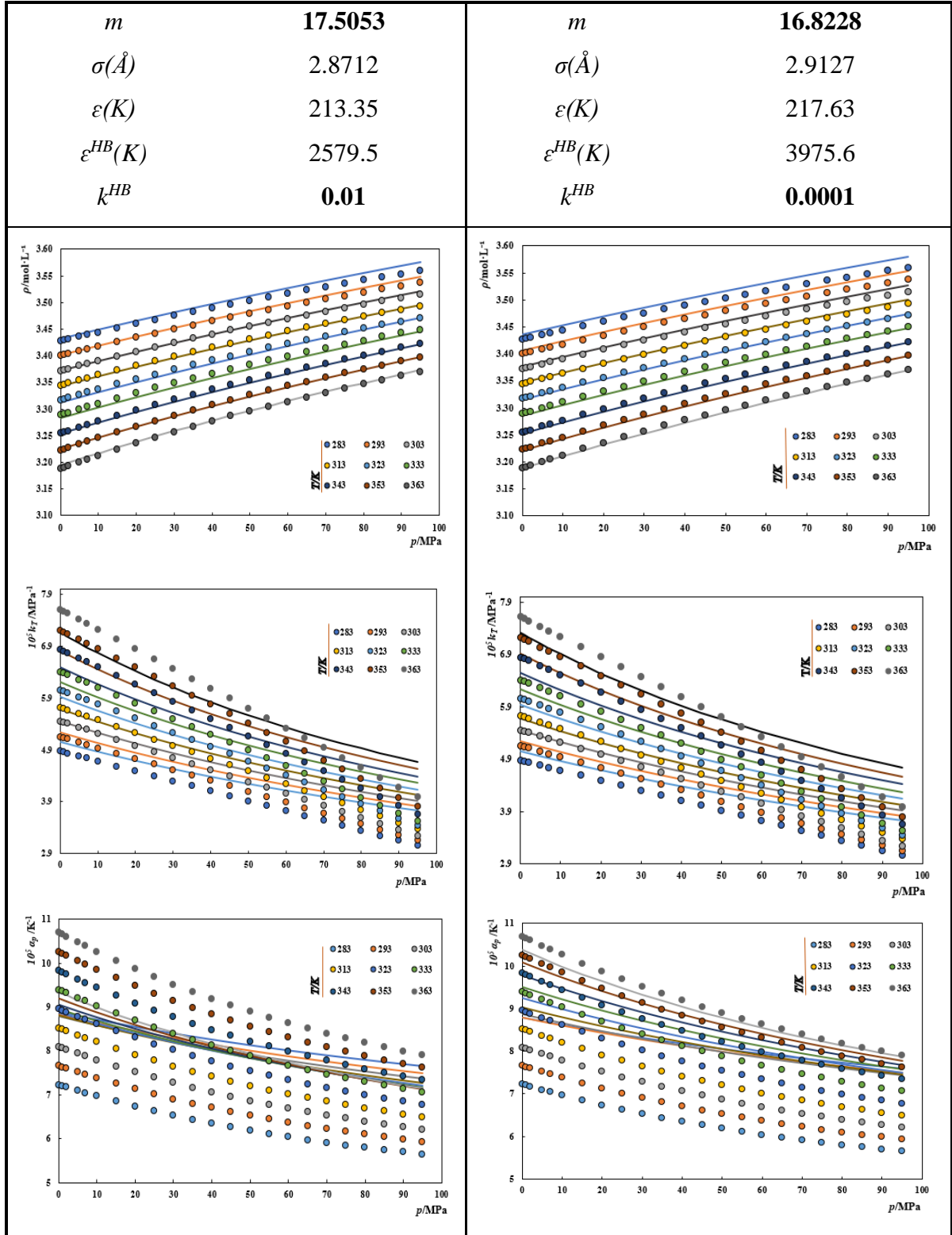
Table 5. PC-SAFT molecular parameters for compounds with functional groups similar, as well as the type of interactions (hydrogen bonding) between molecules with to the investigated PILs.

	Compound	M_W/g·mol^{-1}	m	k^{HB}	Ref.
Acids	Myristic	228.37	7.4126	0.04399	[170]
	Palmitic	256.42	7.5599	0.02000	[170]
ILs	[2HEA][Bu]	149.19	11.76	0.00416	[103]
	[m-2HEA][Bu]	163.21	13.22	0.00193	[103]
	[e-2HEA][Bu]	177.24	14.016	0.00189	[103]

3.2   CO$_2$ solubility

The CO$_2$ solubility in carboxylate-based PILs was measured using an isochoric cell in the temperature (303 to 343) K and pressures (0.1 to 0.5) MPa ranges – **Figure 13**. The values obtained for solubilities are shown in **Appendix D**. The analysis of the data presented in **Figure 13** shows a linear relationship between CO$_2$ solubility and pressure. Solubility follows a typical behavior, it decreases with temperature and increases with pressure, as previously reported for other ILs.[61],[171]–[173] Analyzing **Figure 13**, physical absorption dominates the pressure range analyzed.[174],[175]

According to the literature, the solubility of CO$_2$ in ILs depends on the free volume between solvent molecules, however, the interactions and rearrangement of the ion pair may or may not increase the free volume between solvent molecules.[66,68,155–158] According to shown in **Figure 13**, the length of the anion's alkyl chain influences CO$_2$ solubility, indicating that an entropic effect is present. [87] However, the increase in the alkyl chain of the compounds [DEEA][But]|$_{1:1}$ and [DEEA][Pent]|$_{1:1}$ does not result in greater CO$_2$ solubilities. This fact can be explained due to the rearrangement of ionic pairs in the bulk, thus giving a smaller free volume between IL molecules. Therefore, although the available data demonstrate an increase in solubility with the increase in the alkyl chain and, consequently, a greater free volume, this increase in the chain can alter the rearrangement of ionic pairs in order to disadvantage the increase in the free volume of the system.

Most of the gas solubility data in ionic liquids are represented in molar fraction, however, for process design it is not the most adequate, since the sorption performance of a solvent based on molar fractions depends of the molecular mass of the solvent, as represented

in **Figure 13**. Knowing that ionic liquids have high molecular weights, the increase in molecular mass is quite relevant in this type of analysis, since the physical sorption of CO_2 increases with the molecular mass of the solvent when the concentration is represented in molar fraction.[93],[181] Thus, on an engineering perspective one should represent the solubility on a scale able to minimize the effect of the species different molecular masses and sizes, like molality. That is, analyzing the solubility in molality it is possible to analyze the solubilities without the influence of the size difference between molecules, in this case, CO_2 and PIL, because the comparison of solubilities is in relation to the number of moles of CO_2 per kg of IL, regardless how many moles of IL are present in a kg of solvent. Therefore, for the project design, the molality provides a quantitative perspective regarding the mass of solvent required to remove a certain number of moles of CO_2 from the combustion stream. Analyzing **Figure 13**, it is possible to verify that the molar fraction and molality increase, for all systems analyzed, with decreasing temperature and increasing pressure. Based on the values obtained for the solubilities and molalities of the four systems studied, the compound [DEEA][Prop]│$_{1.5:1}$ obtained the highest CO_2 capacity value observed with a solubility of $x_{CO2} = 0.10$ and a molality value of $m_{CO2} = 0.49$ $mol_{CO2} \cdot kg_{IL}^{-1}$ at 0.5 MPa and 303 K.

Henry's law relates the amount of a gas, in this case CO_2, dissolved in each volume of liquid, at a constant temperature and pressure, to the fugacity of that gas, as described by **Equation (15)**:[61],[180]

$$K_H(T,p) = \lim_{x_{CO_2} \to 0} \frac{f_{CO_2}{}^{L}}{x_{CO_2}} \tag{15}$$

$$p = K_H \cdot x_{CO_2} \tag{16}$$

where $K_H(T,p)$ is the Henry's constant, x_{CO2} is the mole fraction of gas dissolved in the liquid phase, $f_{CO2}{}^{L}$ is the fugacity of gas in the liquid phase and, p represents pressure. As represented in **Equation (15)** Henry's law is strictly valid in the diluted region.
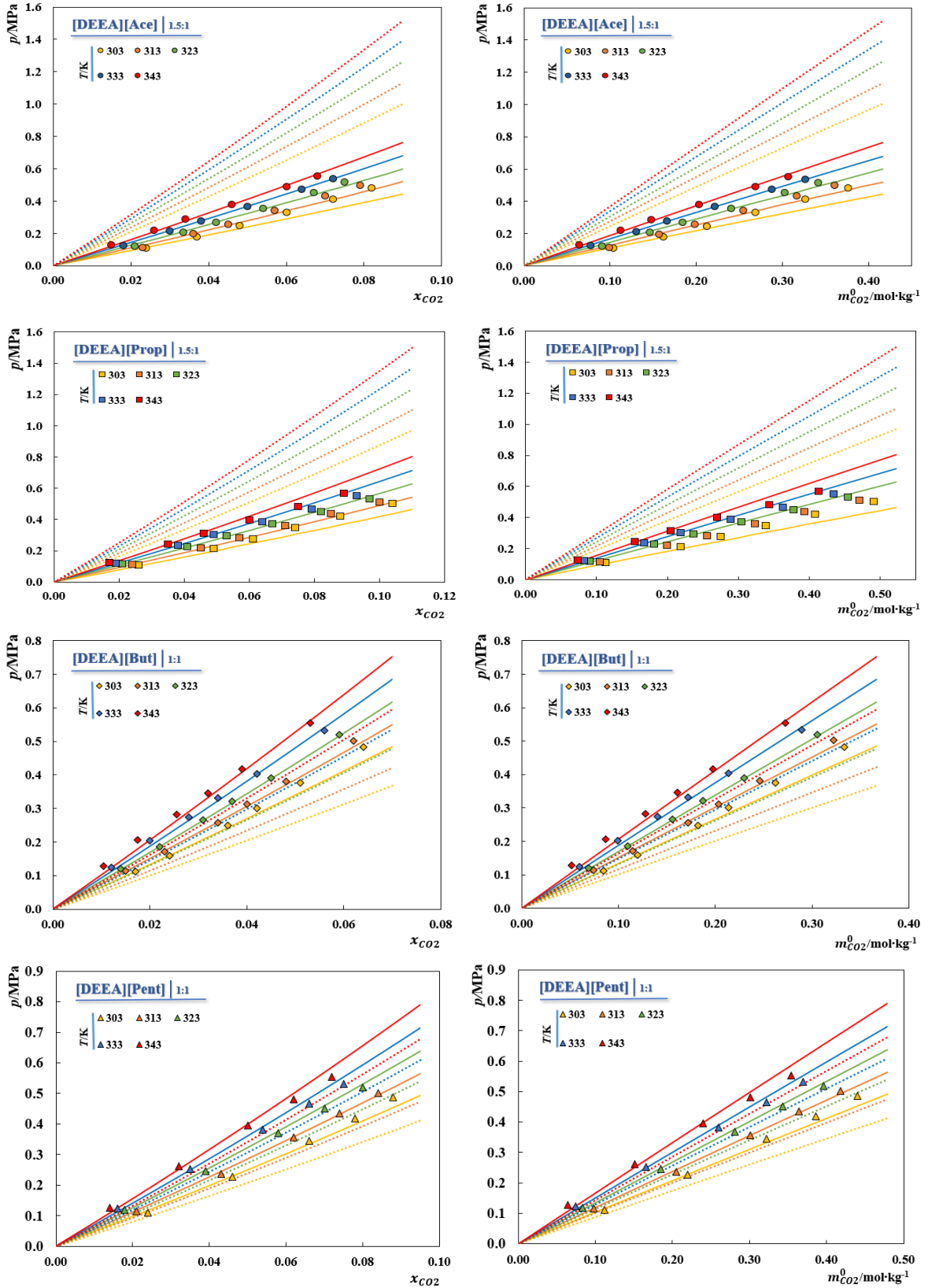
Figure 14. Experimental pTx (left column) and $pTm_{CO_2}^0$ (right column) phase diagrams for the studied systems. The dashed lines represent the soft-SAFT EoS predictive description of

the VLE (ξ_{ij}=1) and the solids lines represent the soft-SAFT EoS VLE description using temperature independent binary interaction parameters.

Henry's constants for CO_2 in the investigated PILs were determined by adjusting the isotherms represented in **Figure 13** using **Equation (16)**, since the pressure is linearly dependent on the solubility of the gas in the liquid. The values obtained for Henry's constants are shown in **Table 6**. According to the analysis of Henry's constants, the compound [DEEA][Prop]│1.5:1 obtained the lowest value at 303 K, resulting in the highest solubility. Comparing the values obtained for the Henry constants of the PILs analysed with those in the literature, the K_H values of the PILs studied here are always higher than other ILs previously analysed in the literature, as can be seen in **Table 7**.[61],[80],[103]

Table 6. Henry's law constants as function of temperature for the PILs + CO_2.

PILs	Henry's law constant, $K_H \pm \sigma^*$ (bar)				
	303 K	**313 K**	**323 K**	**333K**	**343 K**
[DEEA][Ace]│1.5:1	53.7 ± 1.3	56.5 ± 0.8	65.1 ± 0.6	73.8 ± 0.2	82.3 ± 0.5
[DEEA][Prop]│1.5:1	47.6 ± 0.2	50.3 ± 0.4	55.5 ± 0.2	59.4 ± 0.7	67.7 ± 0.7
[DEEA][But]│1:1	72.9 ± 0.7	78.7 ± 0.5	86.2 ± 0.4	96.9 ± 0.5	108.0 ± 0.9
[DEEA][Pent]│1:1	51.3 ± 0.8	58.1 ± 0.5	63.3 ± 0.3	70.8 ± 0.1	77.6 ± 0.4
* Standard deviation					

Using the soft-SAFT EoS parameters obtained for the pure compounds, in the previous section, it was possible to model the solubilities of the four PIL-CO_2 systems studied – **Figure 13**. The tabulated data are reported in **Appendix E**. In **Table 8** are represented the values of the binary interaction parameters for the four PILs studied, as well as the mean absolute deviation for soft-SAFT modeling in non-predictive and predictive modes (ξ_{ij}=1). By analyzing **Figure 13** and **Table 8**, the soft-SAFT model in predictive mode cannot describe the experimental data related to solubility, obtaining values of *%AAD* below 45.53%. Thus, parameters of binary interaction are necessary to obtain a good description of the experimental data. The introduction of the binary parameter for the volume, ξ_{ij}, offered a more correct description of the experimental data. However, values were found very close to the unit, denoting the need for a small correction to the EoS description of VLE, there are two situations: the compounds [DEEA][Ace]│1.5:1 and [DEEA][Prop]│1.5:1 have ξ_{ij} values

higher than the unit, that is, the Lorentz rule underestimates gas/PIL interactions and CO_2 solubility, the opposite is true for the compounds [DEEA][But] | 1:1 and [DEEA][Pent] | 1:1, which have ξ_{ij} values lower than the unit, verifying that the Lorentz rule overestimates gas/PIL interactions than predicted by the ideal case (Lorentz-Berthelot rule with $\xi_{ij}=1$). Using the association parameter for energy in the description of the experimental data, it was found that the *%AAD* was less than 4.82%, demonstrating a good description of the experimental data.

Table 7. Henry's law constants as a function of temperature for ILs + CO_2 systems in the literature.

ILs	Henry's law constant, K_H (bar)						
	303 K	**313 K**	**323 K**	**333 K**	**343 K**	**353K**	**Ref.**
[2HEA][But]	-	0.1	3.3	6.1	12.7	20.5	[103]
[m-2HEA][But]	-	0.7	9.7	28.7	69.9	87.4	[103]
[e-2HEA][But]	-	71.1	83.3	91.7	109.4	-	[103]
HEA	12.1	15.3	19.6	-	-	-	[182]
HEAA	8.2	9.8	11.6	-	-	-	[182]

Abbreviations: [2HEA][But]: 2-hydroxyethylammonium butanoate; [m-2HEA][But]: N-methyl-2- hydroxyethylammonium butanoate; [e-2HEA][But]: N-ethyl-2- hydroxyethylammonium butanoate; HEA: 2-hydroxy ethylammonium acetate; HEAA: 2-(2-hydroxy ethyl)-ammonium acetate;

Table 8. Binary interaction parameters used in the soft-SAFT calculation and respective average absolute deviations from the experimental data using soft-SAFT in non-predictive and predictive mode($\xi_{ij}=1$).

CO_2 +	η_{ij}	ξ_{ij}	*%AAD*	*%AAD* ($\xi_{ij}=1$)
[DEEA][Ace] | 1.5:1		1.085	4.80	45.53
[DEEA][Prop] | 1.5:1	1.000	1.080	4.82	43.10
[DEEA][But] | 1:1		0.970	3.13	24.54
[DEEA][Pent] | 1:1		0.980	4.42	11.36

Kinetic analysis is essential in controlling mass transfer,[183],[184] since, in many cases, ILs are viscous.[185] Thus, it is important to include kinetic mass transfer criteria in the selection of ILs[186], due to the impact on industrial scale operations, such as energy consumption and the operational conditions.[187],[188] As shown in **Figure 14.A**, equilibrium

was achieved after four hours for all measurements, with slow kinetics, which results in slow mass and heat transfer and, consequently, big separation units and high operational cost. A promising approach to avoid these limitations is the use of encapsulated ionic liquids, referred earlier in **Chapter 1**. According to Silva et al.[189] this gas-liquid separation technique demonstrates a high solvent absorption capacity with a high CO_2 sorption rate, regardless of the use of physical or chemical solvents in the separation process gases, keeping the gas sorption capacity intact and increasing the sorption kinetics of the system.[190],[191]

To guarantee application on an industrial scale, a study of the impact of regeneration cycles on the sorption capacity of [DEEA][Ace]│1.5:1, [DEEA][Prop]│1.5:1, [DEEA][But]│1:1, [DEEA][Pent]│1:1 or [DEEA][Hex]│2:1 in the capture of CO_2 was carried out during four sorption-desorption cycles. As shown in **Figure 14.B**, the regeneration of the PILs shows no loss of sorption capability after four regeneration cycles. However, a small loss of solvent is observed in each cycle, obtaining a maximum regeneration yield of 93.04%. Compared with previous works,[192] this fact can be explained by the ease of the studied PILs to distill when pressure is applied to the system.
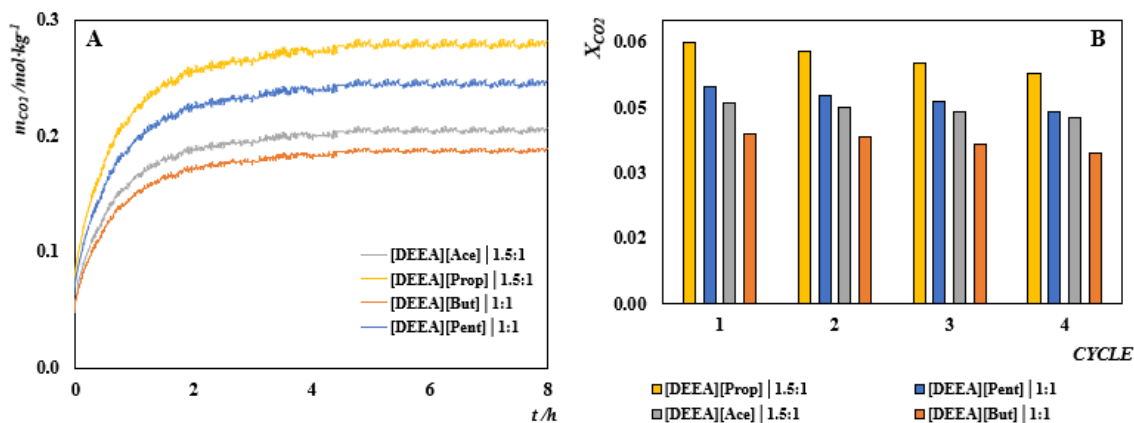
Figure 15. A) Kinects of the solubility measurement for all systems of PILs and B) sorption (333 K and 0.4 MPa) and desorption (343 K and 1 Pa) cycles.

4 Conclusions and Future Remarks

The main objective of this thesis was to study the thermodynamic modeling and absorption capacity of carboxylate-based protic ionic liquids in CO_2 capture processes. To develop a model capable of describing complex thermodynamic behaviors, density data was determined over a wide range of temperatures (283-363) K and pressures (0.1-95) MPa, using a high-pressure density measuring cell. Its derivative properties, namely, isothermal compressibility and isobaric thermal expansiveness, were then calculated and modeled using equations of state based on statistical mechanics, PC-SAFT and soft-SAFT. For both SAFT EoSs, the associative scheme chosen was the 3/2 scheme, which considers five possible sites in the structure of the molecule more favorable to the establishment of interactions with other molecules. The modeling using PC-SAFT was not successful due to the obtention of parameters without physical significance ($k^{HB} \to 0$), regardless of the restrictions used in the optimization routine of the objective function. The modeling with soft-SAFT obtained quite satisfactory results since the model was able to describe the density and its derived properties, obtaining *%AAD* below 5.49% when compared to experimental data. In addition, these properties had the same order of magnitude reported for other ILs families, allowing to verify the veracity of the model description to the experimental data for other ILs families. The parameters obtained for the soft-SAFT showed physical significance, allowing correlations that predict the thermodynamic behavior of compounds with structures such as those analyzed.

The solubility of CO_2 in carboxylate-based protic ionic liquids, namely [DEEA][Ace]│$_{1.5:1}$, [DEEA][Prop]│$_{1.5:1}$, [DEEA][But]│$_{1:1}$ and [DEEA][Pent]│$_{1:1}$, was determined using an isochoric cell, in the temperature and pressure ranges (303-343) K and (0.1-0.5) MPa, respectively. Based on the values obtained for the solubilities and molalities of the four systems studied, the greatest capacity of CO_2 belongs to the compound [DEEA][Prop]│$_{1.5:1}$ obtaining a solubility of x_{CO2}=0.10 and a molality value of m_{CO2}=0.49 $mol_{CO2} \cdot kg_{IL}^{-1}$ at 0.5 MPa and 303 K. That is, in these same conditions the compound [DEEA][Prop]│$_{1.5:1}$ allows to capture 21.56 $kg_{CO2} \cdot ton_{IL}^{-1}$, which from an industrial point of view may not be the most viable, since a large amount of solvent is needed to capture a small amount of CO_2. Analyzing the Henry constants, the compound [DEEA][Prop]│$_{1.5:1}$ presents the lowest value in the studied temperature range, *i.e.*, a higher CO_2 solubility. In addition, comparing the Henry constants obtained with values reported in the literature for CO_2 capture, it was found that the studied PILs have lower CO_2 solubilities.

In addition, the phase balance description has been well described using soft - SAFT EoS, with molecular parameters and using binary interaction parameters. The model successfully describes the behavior of the mixtures under study, allowing to have a notion of the type of interactions between PILs and CO_2, assisting in the engineering design of CO_2 capture systems.

In this study it was found that the kinetics of the studied PILs is very slow, causing problems in the mass and heat transfer of the system and, consequently, high operational cost. In addition, the regeneration capacity test confirmed the thermal stability of the compounds, however, a small loss of mass due to the ease of these PILs to distill when subjected to high pressures was observed.

After the synthesis of the PILs, an acid:base ratio different from the expected 1:1 was obtained, due to the formation of an azeotrope during the distillation process. As future work, a study of the characterization of this type of phase diagram and the determination of the azeotropic point is proposed. Additionally, it will be interesting to measure the solubility of carbon dioxide in the mixtures of the studied PILs and $[C_4C_1im][DMP]$, that offer high free volumes between ILs according to the work of Martins et al.[109], and have low viscosity, favoring mass transfer and, consequently, faster diffusion of CO_2 in the solvent

5 Bibliography

[1] Shakerian, Kim, Szulejko, Park. A Comparative Review between Amines and Ammonia as Sorptive Media for Post-Combustion CO_2 Capture. *Appl. Energy* **2015**, *148*, 10–22.

[2] Ramdin, De Loos, Vlugt. State-of-the-Art of CO_2 Capture with Ionic Liquids. *Ind. Eng. Chem. Res.* **2012**, *51*, 8149–8177.

[3] Laricia, Almeida. Captura e Conversão Química de CO_2 Em Materiais Porfirínicos, Master's thesis, University of Coimbra, 2015.

[4] Leung, Caramanna, Maroto-Valer. An Overview of Current Status of Carbon Dioxide Capture and Storage Technologies. *Renew. Sustain. Energy Rev.* **2014**, *39*, 426–443.

[5] D'Alessandro, Smit, Long. Carbon Dioxide Capture: Prospects for New Materials. *Angew. Chemie Int. Ed.* **2010**, *49*, 6058–6082.

[6] Hannah Ritchie. CO_2 and Greenhouse Gas Emissions https://ourworldindata.org/co2-and-other-greenhouse-gas-emissions#citation (accessed Feb 22, 2020).

[7] Allen, Barros, Burton, Campbell-Lendrum. Summary for Policymakers. In *Managing the Risks of Extreme Events and Disasters to Advance Climate Change Adaptation*; Cambridge University Press: Cambridge, 2012.

[8] International Energy Agency. *Energy and Climate Change*; 2015.

[9] International Energy Agency. Global CO_2 emissions in 2019 https://www.iea.org/articles/global-co2-emissions-in-2019 (accessed Feb 2, 2020).

[10] Vega, Baena-Moreno, Gallego Fernández, Portillo, Navarrete, Zhang. Current Status of CO_2 Chemical Absorption Research Applied to CCS: Towards Full Deployment at Industrial Scale. *Appl. Energy* **2020**, *260*, 114–313.

[11] Ofélia de Queiroz Fernandes Araújo. Carbon Capture and Storage Technologies: Present Scenario and Drivers of Innovation. *Curr. Opin. Chem. Eng.* **2017**, *17*, 22–34.

[12] Torralba-Calleja, Skinner, Gutiérrez-Tauste. CO_2 Capture in Ionic Liquids: A Review of Solubilities and Experimental Methods. *J. Chem.* **2013**, *2013*, 1–16.

[13] Working Group III of the Intergovernmental Panel on Climate Change. *Carbon Dioxide Capture and Storage*; Bert Metz, Ogunlade Davidson, Heleen de Coninck, Manuela Loos, L. M., Ed.; Cambridge University Press: New York, 2005.

[14] Asif, Suleman, Haq, Jamal. Post-Combustion CO_2 Capture with Chemical Absorption and Hybrid System: Current Status and Challenges. *Greenh. Gases Sci. Technol.* **2018**, *8*, 998–1031.

[15] Kenarsari, Yang, Jiang, Zhang, Wang, Russell, Wei, Fan. Review of Recent Advances in Carbon Dioxide Separation and Capture. *RSC Adv.* **2013**, *3*, 22739–22773.

[16] Plasynski, Litynski, McIlvried, Srivastava. Progress and New Developments in Carbon Capture and Storage. *CRC. Crit. Rev. Plant Sci.* **2009**, *28*, 123–138.

[17] Zaman, Lee. Carbon Capture from Stationary Power Generation Sources: A Review of the Current Status of the Technologies. *Korean J. Chem. Eng.* **2013**, *30*, 1497–1526.

[18] Asif, Suleman, Haq, Jamal. Post-Combustion CO 2 Capture with Chemical Absorption and Hybrid System: Current Status and Challenges. *Greenh. Gases Sci. Technol.* **2018**, *8*, 998–1031.

[19] Arshad. CO_2 Capture Using Ionic Liquids, University of Denmark, 2009.

[20] Olajire. CO_2 Capture and Separation Technologies for End-of-Pipe Applications – A Review. *Energy* **2010**, *35*, 2610–2628.

[21] Aghaie, Rezaei, Zendehboudi. A Systematic Review on CO_2 Capture with Ionic Liquids: Current Status and Future Prospects. *Renew. Sustain. Energy Rev.* **2018**, *96*, 502–525.

[22] Wang, Zhao, Otto, Robinius, Stolten. A Review of Post-Combustion CO_2 Capture

Technologies from Coal-Fired Power Plants. *Energy Procedia* **2017**, *114*, 650–665.

[23] Venkatesan. Adsorption. In *Separation and Purification Technologies in Biorefineries*; John Wiley & Sons, Ltd: Chichester, UK, 2013.

[24] Ben-Mansour, Habib, Bamidele, Basha, Qasem, Peedikakkal, Laoui, Ali. Carbon Capture by Physical Adsorption: Materials, Experimental Investigations and Numerical Modeling and Simulations - A Review. *Appl. Energy* **2016**, *161*, 225–255.

[25] Yu, Huang, Tan. A Review of CO_2 Capture by Absorption and Adsorption. *Aerosol Air Qual. Res.* **2012**, *12*, 745–769.

[26] Richard W. Baker. Overview of membrane science and technology. *Membrane Technology And Applications*; John Wiley & Sons, Ed.; Chichester, England, 2004.

[27] Cruz, Leonett, Chenard Díaz, Carliz, Rossa, Galindo, Aranda, Oliveira. Biofixação de CO_2 Pela Microalga Monoraphidium Sp. *Acta Sci. Tech.* **2018**, *6*, 13–20.

[28] Badiei, Asim, Yarmo, Jahim, Sopian. Overview of Carbon Dioxide Separation Technology. *Power Energy Syst. Appl.* **2012**, 146–151.

[29] Barbosa. Análise de Tecnologias Para Separação de CO_2 Em Plataforma Offshore: Absorção Física Por Líquidos Iônicos, Absorção Química Por Aminas e Permeação Por Membranas, Tese de Mestrado, Universidade Federal do Rio de Janeiro, 2018.

[30] Barbosa. Análise de Tecnologias Para Separação de CO_2 Em Plataforma Offshore: Absorção Física Por Líquidos Iônicos, Absorção Química Por Aminas e Permeação Por Membranas. **2018**.

[31] Vega, Baena-Moreno, Gallego Fernández, Portillo, Navarrete, Zhang. Current Status of CO_2 Chemical Absorption Research Applied to CCS: Towards Full Deployment at Industrial Scale. *Appl. Energy* **2020**, *260*, 114313.

[32] Sang Sefidi, Luis. Advanced Amino Acid-Based Technologies for CO_2 Capture: A Review. *Ind. Eng. Chem. Res.* **2019**, *58*, 20181–20194.

[33] Li, Bai, Zeng, Liang, Wang, Huo, Zhang. Protic Ionic Liquids with Low Viscosity for Efficient and Reversible Capture of Carbon Dioxide. *Int.J.Greenh.Ga Control* **2019**, *90*, 102801.

[34] Koronaki, Prentza, Papaefthimiou. Modeling of CO_2 Capture via Chemical Absorption Processes − An Extensive Literature Review. *Renew. Sustain. Energy Rev.* **2015**, *50*, 547–566.

[35] Freeman, Bhown. Assessment of the Technology Readiness of Post-Combustion CO_2 Capture Technologies. *Energy Procedia* **2011**, *4*, 1791–1796.

[36] Rubin, Mantripragada, Marks, Versteeg, Kitchin. The Outlook for Improved Carbon Capture Technology. *Prog. Energy Combust. Sci.* **2012**, *38*, 630–671.

[37] Abranches, Martins, Silva, Schaeffer, Pinho, Coutinho. Phenolic Hydrogen Bond Donors in the Formation of Non-Ionic Deep Eutectic Solvents: The Quest for Type V DES. *Chem. Commun.* **2019**, *55*, 10253–10256.

[38] Crespo, Silva, Lloret, Carvalho, Vega, Llovell, Coutinho. A Methodology to Parameterize SAFT-Type Equations of State for Solid Precursors of Deep Eutectic Solvents: The Example of Cholinium Chloride. *Phys. Chem. Chem. Phys.* **2019**, *21*, 15046–15061.

[39] Crespo, Silva, Martins, Bülow, Ferreira, Sadowski, Held, Pinho, Coutinho. The Role of Polyfunctionality in the Formation of [Ch]Cl-Carboxylic Acid-Based Deep Eutectic Solvents. *Ind. Eng. Chem. Res.* **2018**, *57*, 11195–11209.

[40] Crespo, Silva, Martins, Fernandez, Ortega, Ferreira, Sadowski, Held, Pinho, Coutinho. Characterization and Modeling of the Liquid Phase of Deep Eutectic Solvents Based on Fatty

Acids/Alcohols and Choline Chloride. *Ind. Eng. Chem. Res.* **2017**, *56*, 12192–12202.

[41] Silva, Fernandez, Conceição, Martins, Sosa, Ortega, Pinho, Coutinho. Design and Characterization of Sugar-Based Deep Eutectic Solvents Using Conductor-like Screening Model for Real Solvents. *ACS Sustain. Chem. Eng.* **2018**, *6*, 10724–10734.

[42] Schuur, Brouwer, Smink, Sprakel. Green Solvents for Sustainable Separation Processes. *Curr. Opin. Green Sustain. Chem.* **2019**, *18*, 57–65.

[43] Hernandez, Pestryakov, Portillo, Salgado, Rojas, Rubio, Ruiz, Petranovskii. CO_2 Sequestration by Natural Zeolite for Greenhouse Effect Control. *ProcediaChem.***2015**,*15*,33–41.

[44] Phan, Doonan, Uribe-Romo, Knobler, O'Keeffe, Yaghi. Synthesis, Structure, and Carbon Dioxide Capture Properties of Zeolitic Imidazolate Frameworks. *Acc.Chem.Res.***2010**,*43*,58–67.

[45] Dillon, Crouse, Barron. Synthesis, Characterization, and Carbon Dioxide Adsorption of Covalently Attached Polyethyleneimine-Functionalized Single-Wall Carbon Nanotubes. *ACS Nano* **2008**, *2*, 156–164.

[46] Bernardo, Drioli, Golemme. Membrane Gas Separation: A Review/State of the Art. *Ind. Eng. Chem. Res.* **2009**, *48*, 4638–4663.

[47] Chen, Mu, Hardacre, Fan. Integration of Membrane Separation with Nonthermal Plasma Catalysis: A Proof-of-Concept for CO_2 Capture and Utilization. *Ind. Eng. Chem. Res.* **2020**, *59*, 8202–8211.

[48] Martínez-Palou, Likhanova, Olivares-Xometl. Supported Ionic Liquid Membranes for Separations of Gases and Liquids: An Overview. *Pet. Chem.* **2014**, *54*, 595–607.

[49] Liu, Xu, Wang, Zhu, Yin. Preparation of Supported Ionic Liquid Membranes Using a Supercritical Fluid Deposition Method and Study of the Capillary Phase Transition of Ionic Liquids in Supercritical CO_2. *Ind. Eng. Chem. Res.* **2019**, *58*, 19189–19196.

[50] Palomar, Lemus, Alonso-Morales, Bedia, Gilarranz, Rodriguez. Encapsulated Ionic Liquids (ENILs): From Continuous to Discrete Liquid Phase. *Chem. Commun.* **2012**, *48*, 10046–10048.

[51] Moya, Alonso-Morales, de Riva, Morales-Collazo, Brennecke, Palomar. Encapsulation of Ionic Liquids with an Aprotic Heterocyclic Anion (AHA-IL) for CO_2 Capture: Preserving the Favorable Thermodynamics and Enhancing the Kinetics of Absorption. *J. Phys. Chem. B* **2018**, *122*, 2616–2626.

[52] Zhao, Feron, Deng, Favre, Chabanon, Yan, Hou, Chen, Qi. Status and Progress of Membrane Contactors in Post-Combustion Carbon Capture: A State-of-the-Art Review of New Developments. *J. Memb. Sci.* **2016**, *511*, 180–206.

[53] Chuah, Kim, Lee, Koh, Bae. CO 2 Absorption Using Membrane Contactors: Recent Progress and Future Perspective. *Ind. Eng. Chem. Res.* **2020**, *59*, 6773–6794.

[54] Hayes, Warr, Atkin. Structure and Nanostructure in Ionic Liquids. *Chem. Rev.* **2015**, *115*, 6357–6426.

[55] Haider, Saeed, Qyyum, Kazmi, Ahmad, Muhammad, Lee. Simultaneous Capture of Acid Gases from Natural Gas Adopting Ionic Liquids: Challenges, Recent Developments, and Prospects. *Renew. Sustain. Energy Rev.* **2020**, *123*, 109771.

[56] Martins, Sharma, Pinho, Gardas, Coutinho, Carvalho. Selection and Characterization of Non-Ideal Ionic Liquids Mixtures to Be Used in CO_2 Capture.*Fluid Phase Equilib.***2020**, 112621.

[57] Yethiraj. Structure of Room Temperature Ionic Liquids. *J. Phys. Condens. Matter* **2016**, *28*, 414020–4140026.

[58] Rogers. Chemistry: Ionic Liquids--Solvents of the Future? *Science.* **2003**, *302*, 792–793.

[59] Hasib-ur-Rahman, Siaj, Larachi. Ionic Liquids for CO_2 Capture-Development and Progress. *Chem. Eng. Process. Process Intensif.* **2010**, *49*, 313–322.

[60] Cevasco, Chiappe. Are Ionic Liquids a Proper Solution to Current Environmental Challenges? *Green Chem.* **2014**, *16*, 2375–2385.

[61] Carvalho, Álvarez, Machado, Pauly, Daridon, Marrucho, Aznar, Coutinho. High Pressure Phase Behavior of Carbon Dioxide in 1-Alkyl-3-Methylimidazolium Bis(Trifluoromethylsulfonyl)Imide Ionic Liquids. *J. Supercrit. Fluids* **2009**, *48*, 99–107.

[62] Stracke, Migliorini, Lissner, Schrekker, Dupont, Gonçalves. Imidazolium Ionic Liquids as Electrolytes for Manganese Dioxide Free Leclanché Batteries. *Appl. Energy.* **2009**, *86*, 1512–1516.

[63] Dias, Petrin, H. B. Sosa, da Costa Lopes, Coutinho, da Costa. Investigation of Kraft Lignin Solubility in Protic Ionic Liquids and Their Aqueous Solutions. *Ind. Eng. Chem. Res.* **2020**, *59*, 18193–18202.

[64] Dong, Lin, Liu, Li. Synthesis of ZrO_2 Nanowires by Ionic-Liquid Route. *J. Colloid Interface Sci.* **2009**, *333*, 734–740.

[65] Moya, Gonzalez-Miquel, Rodriguez, Soto, Rodriguez, Palomar. Non-Ideal Behavior of Ionic Liquid Mixtures to Enhance CO_2 Capture. *Fluid Phase Equilib.* **2017**, *450*, 175–183.

[66] Bates, Mayton, Ntai, Davis. CO_2 Capture by a Task-Specific Ionic Liquid. *J. Am. Chem. Soc.* **2002**, *124*, 926–927.

[67] Hu, Li, Xia, Li, Liao, Fan. Research on Influencing Factors and Mechanism of CO_2 Absorption by Poly-Amino-Based Ionic Liquids. *Int. J. Greenh. Gas Control* **2014**, *31*, 33–40.

[68] Lv, Xia, Shi, Liu, Li, Li. A Novel Hydrophilic Amino Acid Ionic Liquid [C_2OHmim][Gly] as Aqueous Sorbent for CO_2 Capture. *Int. J. Greenh. Gas Control* **2016**, *46*, 1–6.

[69] Chen, Huang, Fan, Tao. Chemical Solvent in Chemical Solvent: A Class of Hybrid Materials for Effective Capture of CO_2. *AIChE J.* **2018**, *64*, 632–639.

[70] Wang, Luo, Jiang, Li, Dai. Carbon Dioxide Capture by Superbase-Derived Protic Ionic Liquids. *Angew. Chemie - Int. Ed.* **2010**, *49*, 5978–5981.

[71] Carvalho, Kurnia, Coutinho. Dispelling Some Myths about the CO_2 Solubility in Ionic Liquids. *Phys. Chem. Chem. Phys.* **2016**, *18*, 14757–14771.

[72] Cabaço, Besnard, Danten, Coutinho. Carbon Dioxide in 1-Butyl-3-Methylimidazolium Acetate. I. Unusual Solubility Investigated by Raman Spectroscopy and DFT Calculations. *J. Phys. Chem. A.* **2012**, *116*, 1605–1620.

[73] Besnard, Cabaço, Vaca Chávez, Pinaud, Sebastião, Coutinho, Mascetti, Danten. CO_2 in 1-Butyl-3-Methylimidazolium Acetate. 2. NMR Investigation of Chemical Reactions. *J. Phys. Chem. A* **2012**, *116*, 4890–4901.

[74] Almantariotis, Gefflaut, Pádua, Coxam, Costa Gomes. Effect of Fluorination and Size of the Alkyl Side-Chain on the Solubility of Carbon Dioxide in 1-Alkyl-3-Methylimidazolium Bis(Trifluoromethylsulfonyl)Amide Ionic Liquids. *J. Phys. Chem. B* **2010**, *114*, 3608–3617.

[75] Anderson, Dixon, Brennecke. Solubility of CO_2, CH_4, C_2H_6, C_2H_4, O_2, and N_2 in 1-Hexyl-3-Methylpyridinium Bis(Trifluoromethylsulfonyl)Imide: Comparison to Other Ionic Liquids. *Acc. Chem. Res.* **2007**, *40*, 1208–1216.

[76] Hu, Liu, Xu, Zhang. The Molecular Characteristics Dominating the Solubility of Gases in Ionic Liquids. *Chem. Soc. Rev.* **2011**, *40*, 3802–3823.

[77] Safavi, Ghotbi, Taghikhani, Jalili, Mehdizadeh. Study of the Solubility of CO_2, H_2S and Their Mixture in the Ionic Liquid 1-Octyl-3-Methylimidazolium Hexafluorophosphate:

Experimental and Modelling. *J. Chem. Thermodyn.* **2013**, *65*, 220–232.

[78] Shaahmadi, Hashemi Shahraki, Farhadi. The Solubility of Carbon Dioxide and Density for Binary Mixtures of 1-Butyl-3-Methylimidazolium Acetate and 1-Butyl-3-Methylimidazolium Tetrafluoroborate. *J. Chem. Eng. Data* **2019**, *64*, 584–593.

[79] Damanafshan, Mokhtarani, Mirzaei, Mafi, Sharifi, Jalili. Experimental Study of Carbon Dioxide Solubility in Aqueous N -Methyldiethanolamine Solution with 1-Butylpyridinium Tetrafluoroborate Ionic Liquid. *J. Chem. Eng. Data* **2018**, *63*, 2135–2150.

[80] Muldoon, Aki, Anderson, Dixon, Brennecke. Improving Carbon Dioxide Solubility in Ionic Liquids. *J. Phys. Chem. B* **2007**, *111*, 9001–9009.

[81] Pensado, Pádua, Costa Gomes. Influence of Ester Functional Groups on the Liquid-Phase Structure and Solvation Properties of Imidazolium-Based Ionic Liquids. *J. Phys. Chem. B* **2011**, *115*, 3942–3948.

[82] Deng, Husson, Delort, Besse-Hoggan, Sancelme, Costa Gomes. Influence of an Oxygen Functionalization on the Physicochemical Properties of Ionic Liquids: Density, Viscosity, and Carbon Dioxide Solubility as a Function of Temperature. *J. Chem. Eng. Data.* **2011**, *56*, 4194–4202.

[83] Mota-Martinez, Althuluth, Kroon, Peters. Solubility of Carbon Dioxide in the Low-Viscosity Ionic Liquid 1-Hexyl-3-Methylimidazolium Tetracyanoborate. *Fluid Phase Equilib.* **2012**, *332*, 35–39.

[84] Makino, Kanakubo, Masuda, Mukaiyama. Physical and CO_2-Absorption Properties of Imidazolium Ionic Liquids with Tetracyanoborate and Bis(Trifluoromethanesulfonyl)Amide Anions. *J. Solution Chem.* **2014**, *43*, 1601–1613.

[85] Mahurin, Hillesheim, Yeary, Jiang, Dai. High CO_2 Solubility, Permeability and Selectivity in Ionic Liquids with the Tetracyanoborate Anion. *RSC Adv.* **2012**, *2*, 11813–11819.

[86] Kazarian, Welton. Combining Ionic Liquids and Supercritical Fluids: In Situ ATR-IR Study of CO_2 Dissolved in Two Ionic Liquids at High Pressures. *Chem. Commun.* **2000**, *20*, 2047–2048.

[87] Aki, Mellein, Saurer, Brennecke. High-Pressure Phase Behavior of Carbon Dioxide with Imidazolium-Based Ionic Liquids. *J. Phys. Chem. B* **2004**, *108*, 20355–20365.

[88] Bogel-Łukasik, Matkowska, Bogel-Łukasik, Hofman. Isothermal Vapour–Liquid Equilibria in the Binary and Ternary Systems Consisting of an Ionic Liquid, 1-Propanol and CO_2. *Fluid Phase Equilib.* **2010**, *293*, 168–174.

[89] Bogel-Łukasik, Lourenço, Zakrzewska, Bogel-Łukasik. Insight into the Phase Equilibrium Phenomena of Systems Containing Dienes and Dicyanamide Ionic Liquids as a New Potential Application. *J. Phys. Chem. B* **2010**, *114*, 15605–15609.

[90] Seki, Grunwaldt, Baiker. In Situ Attenuated Total Reflection Infrared Spectroscopy of Imidazolium-Based Room-Temperature Ionic Liquids under "Supercritical" CO_2. *J. Phys. Chem. B* **2009**, *113*, 114–122.

[91] Andanson, Jutz, Baiker. Supercritical CO_2 /Ionic Liquid Systems: What Can We Extract from Infrared and Raman Spectra *J. Phys. Chem. B.* **2009**, *113*, 10249–10254.

[92] Anthony, Anderson, Maginn, Brennecke. Anion Effects on Gas Solubility in Ionic Liquids. *J. Phys. Chem. B* **2005**, *109*, 6366–6374.

[93] Carvalho, Coutinho. On the Nonideality of CO_2 Solutions in Ionic Liquids and Other Low Volatile Solvents. *J. Phys. Chem. Lett.* **2010**, *1*, 774–780.

[94] Babarao, Dai, Jiang. Understanding the High Solubility of CO_2 in an Ionic Liquid with the Tetracyanoborate Anion. *J. Phys. Chem. B.* **2011**, *115*, 9789–9794.

[95] Gupta. Tetracyanoborate Based Ionic Liquids for CO2 Capture: From Ab Initio Calculations to Molecular Simulations. *Fluid Phase Equilib.* **2016**, *415*, 34–41.

[96] Peric, Sierra, Martí, Cruañas, Garau, Arning, Bottin-Weber, Stolte. (Eco)Toxicity and Biodegradability of Selected Protic and Aprotic IonicLiquids. *J. Hazard. Mater.* **2013**, *261*, 99–105.

[97] Inês P. E. Macário, Pereira, Coutinho. Potential Threats of Ionic Liquids to the Environment and Ecosphere. In *Encyclopedia of Ionic Liquids*; Springer Singapore:Singapore, 2020.

[98] Jin, Hou, Wu, Ren, Tian, Xiao, Lei. Solubilities and Thermodynamic Properties of SO_2 in Ionic Liquids. *J. Phys. Chem. B* **2011**, *115*, 6585–6591.

[99] Zhao, Zhang, Zeng, Zhou, Dong, Tian, Zhang. Density, Viscosity, and Performances of Carbon Dioxide Capture in 16 Absorbents of Amine + Ionic Liquid + H_2O, Ionic Liquid + H_2O, and Amine + H_2O Systems. *J. Chem. Eng. Data* **2010**, *55*, 3513–3519.

[100] Wang, Luo, Luo, Jiang, Li, Dai. Tuning the Basicity of Ionic Liquids for Equimolar CO_2 Capture. *Angew. Chemie* **2011**, *123*, 5020–5024.

[101] Xu. CO_2 Absorption Behavior of Azole-Based Protic Ionic Liquids: Influence of the Alkalinity and Physicochemical Properties. *J. CO_2 Util.* **2017**, *19*, 1–8.

[102] Kilaru, Scovazzo. Correlations of Low-Pressure Carbon Dioxide and Hydrocarbon Solubilities in Imidazolium-, Phosphonium-, and Ammonium-Based Room-Temperature Ionic Liquids. *Ind. Eng. Chem. Res.* **2008**, *47*, 910–919.

[103] Alcantara, de Carvalho, Álvarez, Ferreira, Paredes, Cardozo-Filho, Silva, Lião, Pires, Mattedi. High Pressure Vapor-Liquid Equilibria for Binary Carbon Dioxide and Protic Ionic Liquid Based on Ethanolamines + Butanoic Acid. *Fluid Phase Equilib.* **2018**, *460*, 162–174.

[104] Fumino, Wulf, Ludwig. The Potential Role of Hydrogen Bonding in Aprotic and Protic Ionic Liquids. *Phys. Chem. Chem. Phys.* **2009**, *11*, 8790–8794.

[105] Ramdin, Amplianitis, Bazhenov, Volkov, Volkov, Vlugt, de Loos. Solubility of CO_2 and CH_4 in Ionic Liquids: Ideal CO_2/CH_4 Selectivity. *Ind. Eng. Chem. Res.* **2014**, *53*, 15427–15435.

[106] Jiang, Zhou, Jiao, Li, Wu, Zhang. SO_2 Gas Separation Using Supported Ionic Liquid Membranes. *J. Phys. Chem. B.* **2007**, *111*, 5058–5061.

[107] Shimoyama, Ito. Predictions of Cation and Anion Effects on Solubilities, Selectivities and Permeabilities for CO2 in Ionic Liquid Using COSMO Based Activity Coefficient Model. *Fluid Phase Equilib.* **2010**, *297*, 178–182.

[108] Lei, Han, Zhang, Li, Zhu, Chen. Solubility of CO_2 in Binary Mixtures of Room-Temperature Ionic Liquids at High Pressures. *J. Chem. Eng. Data* **2012**, *57*, 2153–2159.

[109] Martins, Sharma, Pinho, Gardas, Coutinho, Carvalho. Selection and Characterization of Non-Ideal Ionic Liquids Mixtures to Be Used in CO_2 Capture. *Fluid Phase Equilib.* **2020**, *518*, 112621–112634.

[110] Zhang, Tu, Li, Huang, Hu, Wu, MacFarlane. Selective Separation of H_2S and CO_2 from CH_4 by Supported Ionic Liquid Membranes. *J. Memb. Sci.* **2017**, *543*, 282–287.

[111] Voss, Bara, Gin, Noble. Physically Gelled Ionic Liquids: Solid Membrane Materials with Liquidlike CO_2 Gas Transport. *Chemistry of Materials*. July 28, 2009.

[112] Albo, Santos, Neves, Simeonov, Afonso, Crespo, Irabien. Separation Performance of CO_2 through Supported Magnetic Ionic Liquid Membranes. *Sep. Purif. Technol.* **2012**, *97*, 26–33.

[113] Bednár, Nemestóthy, Bakonyi, Fülöp, Zhen, Lu, Kobayashi, Kumar, Xu, Bélafi-Bakó. Enzymatically-Boosted Ionic Liquid Gas Separation Membranes Using Carbonic Anhydrase of Biomass Origin. *Chem. Eng. J.* **2016**, *303*, 621–626.

[114] Hanioka, Maruyama, Sotani, Teramoto, Matsuyama, Nakashima, Hanaki, Kubota, Goto. CO_2 Separation Facilitated by Task-Specific Ionic Liquids Using a Supported Liquid Membrane. *J. Memb. Sci.* **2008**, *314*, 1–4.

[115] Kasahara, Kamio, Ishigami, Matsuyama. Amino Acid Ionic Liquid-Based Facilitated Transport Membranes for CO_2 Separation. *Chem. Commun.* **2012**, *48*, 6903–6905.

[116] Huang, Zhang, Li, Wu, Hu. Facilitated Separation of CO_2 and SO_2 through Supported Liquid Membranes Using Carboxylate-Based Ionic Liquids. *J. Memb. Sci.* **2014**, *471*, 227–236.

[117] Zhang, Tu, Li, Li, Wu, Hu. Supported Protic-Ionic-Liquid Membranes with Facilitated Transport Mechanism for the Selective Separation of CO_2. *J. Memb. Sci.* **2017**, *527*, 60–67.

[118] Mota-Martinez, Brandl, Hallett, Mac Dowell. Challenges and Opportunities for the Utilisation of Ionic Liquids as Solvents for CO_2 Capture. *Mol. Syst. Des. Eng.* **2018**, *3*, 560–571.

[119] Pereira, Oliveira, Llovell, Vega, Coutinho. Assessing the N_2O/CO_2 High Pressure Separation Using Ionic Liquids with the soft-SAFT EoS. *J. Supercrit. Fluids* **2014**, *92*, 231–241.

[120] Sharma, Singh, Rajamani, Gardas. Influence of Alkyl Substituent on Optical Properties of Carboxylate-Based Protic Ionic Liquids. *ChemistrySelect* **2017**, *2*, 10091–10096.

[121] Chennuri, Losetty, Gardas. Apparent Molar Properties of Hydroxyethyl Ammonium Based Ionic Liquids with Water and Ethanol at Various Temperatures. *J. Mol. Liq.* **2015**, *212*, 444–450.

[122] Earle, Esperança, Gilea, Lopes, Rebelo, Magee, Seddon, Widegren. The Distillation and Volatility of Ionic Liquids. *Nature* **2006**, *439*, 831–834.

[123] Greaves, Drummond. Protic Ionic Liquids: Properties and Applications. *Chem. Rev.* **2008**, *108*, 206–237.

[124] Yoshizawa, Xu, Angell. Ionic Liquids by Proton Transfer: Vapor Pressure, Conductivity, and the Relevance of ΔpKa from Aqueous Solutions. *J. Am. Chem. Soc.* **2003**, *125*, 15411–15419.

[125] Ribeiro, Lima, Silva, Santos. Experimental Evidence for Azeotrope Formation from Protic Ionic Liquids. *ChemPhysChem* **2018**, *19*, 2364–2369.

[126] Crespo, Costa, Hanafiah, Kurnia, Oliveira, Llovell, Vega, Carvalho, Coutinho. New Measurements and Modeling of High Pressure Thermodynamic Properties of Glycols. *Fluid Phase Equilib.* **2017**, *436*, 113–123.

[127] Navarro, Crespo, Costa, Llovell, García, Rodríguez, Carvalho, Vega, Coutinho. New Experimental Data and Modeling of Glymes: Toward the Development of a Predictive Model for Polyethers. *Ind. Eng. Chem. Res.* **2017**, *56*, 7830–7844.

[128] Navarro, Palma, García, Rodríguez, Coutinho, Carvalho. High-Pressure Density of Bis(1-Alkyl-3-Methylimidazolium) Tetraisothiocyanatocobaltate Ionic Liquids: Experimental and PC-SAFT with Volume-Shift Modeling. *J. Chem. Eng. Data* **2019**, *64*, 4827–4833.

[129] Crespo, Costa, Palma, Soares, Martín, Segovia, Carvalho, Coutinho. Thermodynamic Characterization of Deep Eutectic Solvents at High Pressures. *Fluid Phase Equilib.* **2019**, *500*.

[130] Belkadi, Hadj-Kali, Llovell, Gerbaud, Vega. Soft-SAFT Modeling of Vapor-Liquid Equilibria of Nitriles and Their Mixtures. *Fluid Phase Equilib.* **2010**, *289*, 191–200.

[131] Chapman, Gubbins, Jackson, Radosz. SAFT: Equation-of-State Solution Model for

Associating Fluids. *Fluid Phase Equilib.* **1989**, *52*, 31–38.

[132] Chapman, Gubbins, Jackson, Radosz. New Reference Equation of State for Associating Liquids. *Ind. Eng. Chem. Res.* **1990**, *29*, 1709–1721.

[133] Kleiner, Tumakaka, Sadowski. Thermodynamic Modeling of Complex Systems. In *Molecular Thermodynamics of Complex Systems*; Xiaohua Lu, Y. H., Ed.; Springer, Berlin, Heidelberg: Berlin, Heidelberg, 2008.

[134] Belkadi, Hadj-Kali, Llovell, Gerbaud, Vega. Soft-SAFT Modeling of Vapor–Liquid Equilibria of Nitriles and Their Mixtures. *Fluid Phase Equilib.* **2010**, *289*, 191–200.

[135] Crespo, Coutinho. A Statistical Associating Fluid Theory Perspective of the Modeling of Compounds Containing Ethylene Oxide Groups. *Ind. Eng. Chem. Res.* **2019**, *58*, 3562–3582.

[136] Vilas-Boas, Abranches, Crespo, Ferreira, Coutinho, Pinho. Experimental Solubility and Density Studies on Aqueous Solutions of Quaternary Ammonium Halides, and Thermodynamic Modelling for Melting Enthalpy Estimations. *J. Mol. Liq.* **2020**, *300*, 112281–112294.

[137] Crespo, Carvalho, Coutinho, Vega. Exploring Alternative Solvents for Gas Processing Using the Soft-SAFT EoS. In *RDPETRO 2018: Research and Development Petroleum Conference and Exhibition, Abu Dhabi, UAE, 9-10 May 2018*; American Association of Petroleum Geologists, Society of Exploration Geophysicists, European Association of Geoscientists and Engineers, and Society of Petroleum Engineers, 2018.

[138] Gross, Sadowski. Perturbed-Chain SAFT: An Equation of State Based on a Perturbation Theory for Chain Molecules. *Ind. Eng. Chem. Res.* **2001**, *40*, 1244–1260.

[139] Gross, Sadowski. Application of the Perturbed-Chain SAFT Equation of State to Associating Systems. *Ind. Eng. Chem. Res.* **2002**, *41*, 5510–5515.

[140] Paduszyński, Chiyen, Ramjugernath, Letcher, Domańska. Liquid–Liquid Phase Equilibrium of (Piperidinium-Based Ionic Liquid+an Alcohol) Binary Systems and Modelling with NRHB and PCP-SAFT. *Fluid Phase Equilib.* **2011**, *305*, 43–52.

[141] Gross, Sadowski. Application of the Perturbed-Chain SAFT Equation of State to Associating Systems. *Ind. Eng. Chem. Res.* **2002**, *41*, 5510–5515.

[142] Pontes, Crespo, Martins, Silva, Neves, Maximo, Hubinger, Batista, Pinho, Coutinho, Sadowski, Held. Measurement and PC-SAFT Modeling of Solid-Liquid Equilibrium of Deep Eutectic Solvents of Quaternary Ammonium Chlorides and Carboxylic Acids. *Fluid Phase Equilib.* **2017**, *448*, 69–80.

[143] Crespo, Costa, Palma, Soares, Martín, Segovia, Carvalho, Coutinho. Thermodynamic Characterization of Deep Eutectic Solvents at High Pressures. *Fluid Phase Equilib.* **2019**, *500*, 112249–112252.

[144] Palma, Queimada, Coutinho. Modeling of Hydrate Dissociation Curves with a Modified Cubic-Plus-Association Equation of State. *Ind. Eng. Chem. Res.* **2019**, *58*, 14476–14487.

[145] Vilas-Boas, Abranches, Crespo, Ferreira, Coutinho, Pinho. Experimental Solubility and Density Studies on Aqueous Solutions of Quaternary Ammonium Halides, and Thermodynamic Modelling for Melting Enthalpy Estimations. *J. Mol. Liq.* **2020**, *300*, 112281.

[146] Nann, Mündges, Held, Verevkin, Sadowski. Molecular Interactions in 1-Butanol + IL Solution by MeasuringandModelingActivityCoefficients.*J.Phys.Chem.B.* **2013**,*117*,3173–3185.

[147] Paduszyński, Domańska. Solubility of Aliphatic Hydrocarbons in Piperidinium Ionic Liquids: Measurements and Modeling in Terms of Perturbed-Chain Statistical Associating Fluid Theory and Nonrandom Hydrogen-Bonding Theory. *J. Phys. Chem. B.* **2011**, *115*, 12537–12548.

[148] Paduszyński, Lukoshko, Królikowski, Domańska, Szydłowski. Thermodynamic Study of Binary Mixtures of 1-Butyl-1-Methylpyrrolidinium Dicyanamide Ionic Liquid with Molecular Solvents: New Experimental Data and Modeling with PC-SAFT Equation of State. *J. Phys. Chem. B*. **2015**, *119*, 543–551.

[149] Ji, Held, Sadowski. Modeling Imidazolium-Based Ionic Liquids with EPC-SAFT. Part II. Application to H_2S and Synthesis-Gas Components. *Fluid Phase Equilib.* **2014**, *363*, 59–65.

[150] Chen, Mutelet, Jaubert. Modeling the Solubility of Carbon Dioxide in Imidazolium-Based Ionic Liquids with the PC-SAFT Equation of State. *J. Phys. Chem. B*. **2012**, *116*, 14375–14388.

[151] Canales, Held, Lubben, Brennecke, Sadowski. Predicting the Solubility of CO_2 in Toluene + Ionic Liquid Mixtures with PC-SAFT. *Ind. Eng. Chem. Res.* **2017**, *56*, 9885–9894.

[152] Paduszyński. Thermodynamic Modeling of Multicomponent Liquid–Liquid Equilibria in Ionic Liquid Systems with PC-SAFT Equation of State. *Ind. Eng Chem. Res.* **2018**, *57*, 5413–5432.

[153] Felipe J.Blas. Thermodynamic Behaviour of Homonuclear and Heteronuclear Lennard-Jones Chains with Association Sites from Simulation and Theory.*Mol. Phys.* **1997**, *92*, 135–150.

[154] Amaral, Crespo, Dariva, Vega, Carvalho, Coutinho. High-Pressure Solubility of CO_2 in Glymes. *Fuel* **2018**, *219*, 120–125.

[155] Losetty, Sivapragasam. Recent Advances and Thermophysical Properties of Acetate-Based Protic Ionic Liquids. *Chem. Sci. J.* **2016**, *7*, 1000128–1000135.

[156] Gardas, Freire, Carvalho, Marrucho, Fonseca, Ferreira, Coutinho. High-Pressure Densities and Derived Thermodynamic Properties of Imidazolium-Based Ionic Liquids. *J. Chem. Eng. Data* **2007**, *52*, 80–88.

[157] Chhotaray, Gardas. Thermophysical Properties of Ammonium and Hydroxylammonium Protic Ionic Liquids. *J. Chem. Thermodyn.* **2014**, *72*, 117–124.

[158] Machanová, Boisset, Sedláková, Anouti, Bendová, Jacquemin. Thermophysical Properties of Ammonium-Based Bis{(Trifluoromethyl)Sulfonyl}imide Ionic Liquids: Volumetric and Transport Properties. *J. Chem. Eng. Data.* **2012**, *57*, 2227–2235.

[159] Bhattacharjee, Carvalho, Coutinho. The Effect of the Cation Aromaticity upon the Thermophysical Properties of Piperidinium- and Pyridinium-Based Ionic Liquids. *Fluid Phase Equilib.* **2014**, *375*, 80–88.

[160] Navarro, Palma, García, Rodríguez, Coutinho, Carvalho. High Pressure Density of Tricyanomethanide-Based Ionic Liquids: Experimental and PC-SAFT Modelling. *Fluid Phase Equilib.* **2020**, *520*, 112652–112660.

[161] Sarabando, Magano, Ferreira, Santos, Carvalho, Mattedi, Fonseca, Santos. Influence of Temperature and Pressure on the Density and Speed of Sound of N-Ethyl-2-Hydroxyethylammonium Propionate Ionic Liquid. *J. Chem. Thermodyn.* **2019**, *131*, 303–313.

[162] Navarro, Palma, García, Rodríguez, Coutinho, Carvalho. High-Pressure Density of Bis(1-Alkyl-3-Methylimidazolium) Tetraisothiocyanatocobaltate Ionic Liquids: Experimental and PC-SAFT with Volume-Shift Modeling. *J. Chem. Eng. Data.* **2019**, *64*, 4827–4833.

[163] Jacquemin, Husson, Mayer, Cibulka. High-Pressure Volumetric Properties of Imidazolium-Based Ionic Liquids: Effect of the Anion. *J. Chem. Eng. Data.* **2007**, *52*, 2204–2211.

[164] Neves, Kurnia, Coutinho, Marrucho, Lopes, Freire, Rebelo. Systematic Study of the Thermophysical Properties of Imidazolium-Based Ionic Liquids with Cyano-Functionalized

Anions. *J. Phys. Chem. B.* **2013**, *117*, 10271–10283.

[165] Oliveira, Llovell, Coutinho, Vega. New Procedure for Enhancing the Transferability of Statistical Associating Fluid Theory (SAFT) Molecular Parameters: The Role of Derivative Properties. *Ind. Eng. Chem. Res.* **2016**, *55*, 10011–10024.

[166] NguyenHuynh, Falaix, Passarello, Tobaly, de Hemptinne. Predicting VLE of Heavy Esters and Their Mixtures Using PC-SAFT. *Fluid Phase Equilib.* **2008**, *264*, 184–200.

[167] NguyenHuynh, Passarello, Tobaly, de Hemptinne. Application of PC-SAFT EOS to Polar Systems Using a Segment Approach. *Fluid Phase Equilib.* **2008**, *264*, 62–75.

[168] Pedrosa, Pàmies, Coutinho, Marrucho, Vega. Phase Equilibria of Ethylene Glycol Oligomers and Their Mixtures. *Ind. Eng. Chem. Res.* **2005**, *44*, 7027–7037.

[169] Llovell, Vega. Global Fluid Phase Equilibria and Critical Phenomena of Selected Mixtures Using the Crossover Soft-SAFT Equation. *J. Phys. Chem. B* **2006**, *110*, 1350–1362.

[170] Almeida Crespo. Modelling the Solid-Liquid Equilibria of Deep Eutectic Solvents, Master's thesis, Aveiro University, 2016.

[171] Carvalho, Álvarez, Schröder, Gil, Marrucho, Aznar, Santos, Coutinho. Specific Solvation Interactions of CO_2 on Acetate and Trifluoroacetate Imidazolium Based Ionic Liquids at High Pressures. *J. Phys. Chem. B.* **2009**, *113*, 6803–6812.

[172] Carvalho, Álvarez, Marrucho, Aznar, Coutinho. High Pressure Phase Behavior of Carbon Dioxide in 1-Butyl-3-Methylimidazolium Bis(Trifluoromethylsulfonyl)Imide and 1-Butyl-3-Methylimidazolium Dicyanamide Ionic Liquids. *J. Supercrit. Fluids* **2009**, *50*, 105–111.

[173] Carvalho, Álvarez, Marrucho, Aznar, Coutinho. High Carbon Dioxide Solubilities in Trihexyltetradecylphosphonium-Based Ionic Liquids. *J. Supercrit. Fluids* **2010**, *52*, 258–265.

[174] Pérez-Salado Kamps, Tuma, Xia, Maurer. Solubility of CO_2 in the Ionic Liquid [Bmim][PF_6]. *J. Chem. Eng. Data* **2003**, *48*, 746–749.

[175] Yunus, Mutalib, Man, Bustam, Murugesan. Solubility of CO_2 in Pyridinium Based Ionic Liquids. *Chem. Eng. J.* **2012**, *189–190*, 94–100.

[176] Blanchard, Gu, Brennecke. High-Pressure Phase Behavior of Ionic Liquid/CO_2 Systems. *J. Phys. Chem. B* **2001**, *105*, 2437–2444.

[177] Shariati, Peters. High-Pressure Phase Behavior of Systems with Ionic Liquids: II. The Binary System Carbon Dioxide+1-Ethyl-3-Methylimidazolium Hexafluorophosphate. *J. Supercrit. Fluids* **2004**, *29*, 43–48.

[178] Cadena, Anthony, Shah, Morrow, Brennecke, Maginn. Why Is CO_2 so Soluble in Imidazolium-Based Ionic Liquids? *J. Am. Chem. Soc.* **2004**, *126*, 5300–5308.

[179] Gutkowski, Shariati, Peters. High-Pressure Phase Behavior of the Binary Ionic Liquid System 1-Octyl-3-Methylimidazolium Tetrafluoroborate+CO_2. *J. Supercrit. Fluids.* **2006**, *39*, 187–191.

[180] Anthony, Maginn, Brennecke. Solubilities and Thermodynamic Properties of Gases in the Ionic Liquid 1- n -Butyl-3-Methylimidazolium Hexafluorophosphate. *J. Phys. Chem. B.* **2002**, *106*, 7315–7320.

[181] Huang, Zhang, Xu, Wu, Hu, Xu. Protic Ionic Liquids for the Selective Absorption of H_2S from CO_2: Thermodynamic Analysis. *AIChE J.* **2014**, *60*, 4232–4240.

[182] Yuan, Zhang, Liu, Lu. Solubilities of CO_2 in Hydroxyl Ammonium Ionic Liquids at Elevated Pressures. *Fluid Phase Equilib.* **2007**, *257*, 195–200.

[183] Gonzalez-Miquel, Bedia, Palomar, Rodriguez. Solubility and Diffusivity of CO_2 in

[Hxmim][NTf$_2$], [Omim][NTf$_2$], and [Dcmim][NTf$_2$] at T=(298.15, 308.15, and 323.15) K and Pressures up to 20 Bar. *J. Chem. Eng. Data.* **2014**, *59*, 212–217.

[184] Moya, Palomar, Gonzalez-Miquel, Bedia, Rodriguez. Diffusion Coefficients of CO$_2$ in Ionic Liquids Estimated by Gravimetry. *Ind. Eng. Chem. Res.* **2014**, *53*, 13782–13789.

[185] de Riva, Ferro, del Olmo, Ruiz, Lopez, Palomar. Statistical Refinement and Fitting of Experimental Viscosity-to-Temperature Data in Ionic Liquids. *Ind. Eng. Chem. Res.* **2014**, *53*, 10475–10484.

[186] Gonzalez-Miquel, Bedia, Abrusci, Palomar, Rodriguez. Anion Effects on Kinetics and Thermodynamics of CO$_2$ Absorption in Ionic Liquids. *J. Phys. Chem. B* **2013**, *117*, 3398–3406.

[187] Krupiczka, Rotkegel, Ziobrowski. Comparative Study of CO$_2$ Absorption in Packed Column Using Imidazolium Based Ionic Liquids and MEA Solution. *Sep. Purif. Technol.* **2015**, *149*, 228–236.

[188] de Riva, Suarez-Reyes, Moreno, Díaz, Ferro, Palomar. Ionic Liquids for Post-Combustion CO 2 Capture by Physical Absorption: Thermodynamic, Kinetic and Process Analysis. *Int. J. Greenh. Gas Control* **2017**, *61*, 61–70.

[189] Silva, Moya, Sousa, Santiago, Sintra, Carreira, Palomar, Coutinho, Carvalho. Encapsulated Amino-Acid-Based Ionic Liquids for CO$_2$ Capture. *Eur. J. Inorg. Chem.* **2020**, *2020*, 3158–3166.

[190] Song, Avelar Bonilla, Morales-Collazo, Lubben, Brennecke. Recyclabilityof Encapsulated Ionic Liquids for Post-Combustion CO$_2$ Capture. *Ind. Eng. Chem. Res.* **2019**, *58*, 4997–5007.

[191] Lemus, Bedia, Moya, Alonso-Morales, Gilarranz, Palomar, Rodriguez. Ammonia Capture from the Gas Phase by Encapsulated Ionic Liquids (ENILs). *RSC Adv.* **2016**, *6*, 61650–61660.

[192] Supasitmongkol, Styring. High CO$_2$ Solubility in Ionic Liquids and a Tetraalkylammonium-Based Poly(Ionic Liquid). *Energy Environ. Sci.* **2010**, *3*, 1961–1972.

Appendixes

Appendix A. Ionic Liquids NMR Analysis

^{1}H

N,N-diethylethanolammonium acetate [DEEA][Ace] | 1.5:1

^{13}C
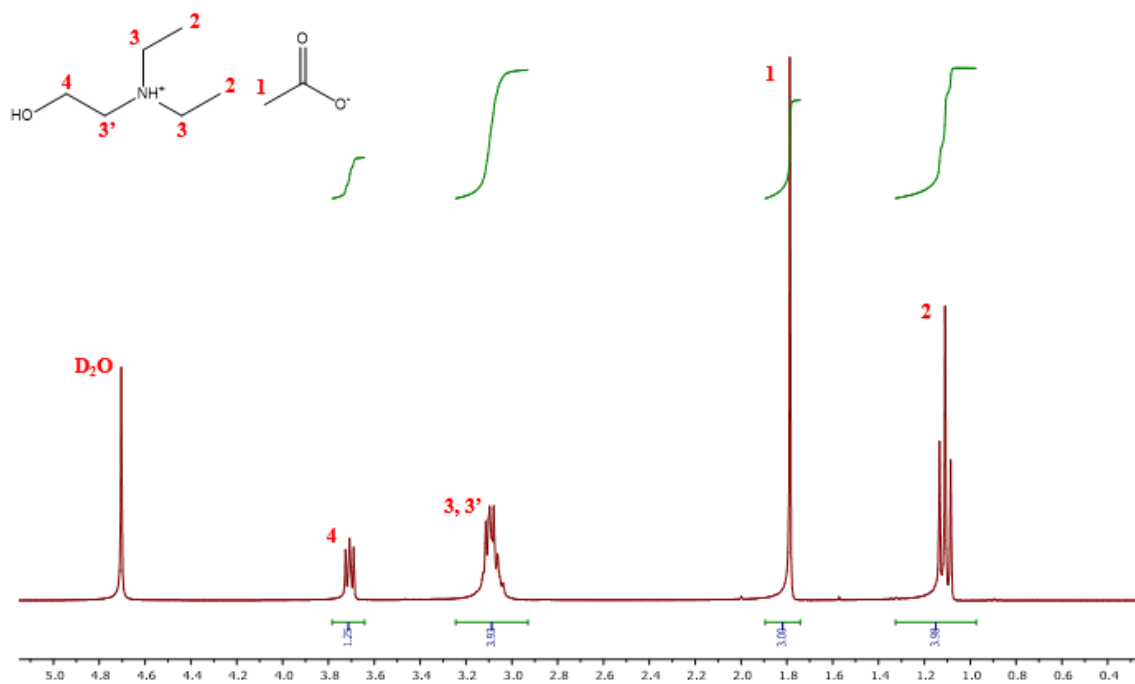
N,N-diethylethanolammonium acetate [DEEA][Ace] | 1.5:1

Solvent: D$_2$O

¹H
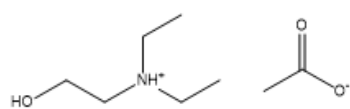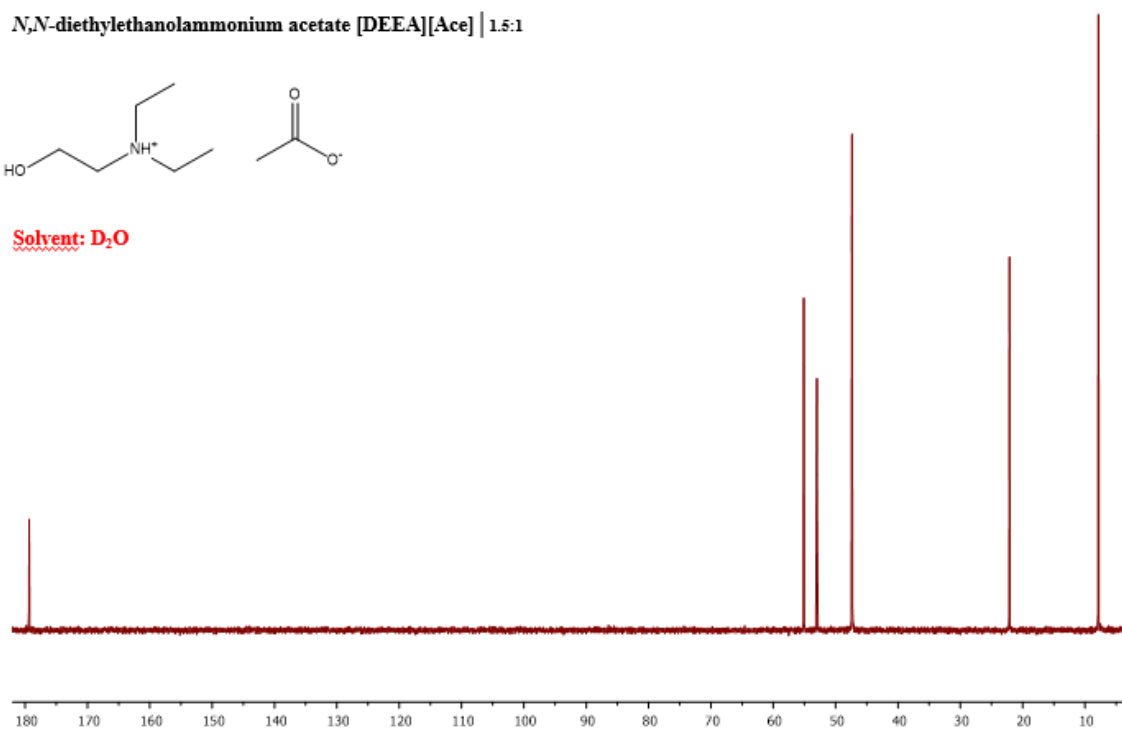
N,N-diethylethanolammonium propanoate [DEEA][Prop] | 1.5:1
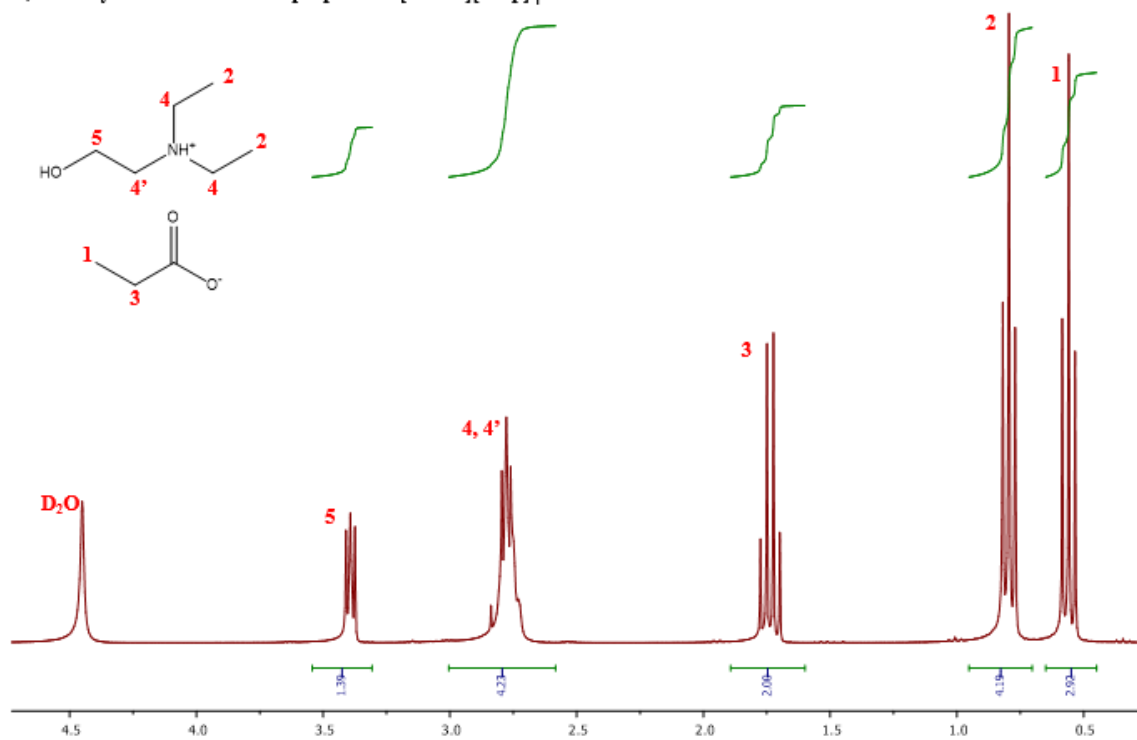
¹³C

N,N-diethylethanolammonium propanoate [DEEA][Prop] | 1.5:1

Solvent: D₂O
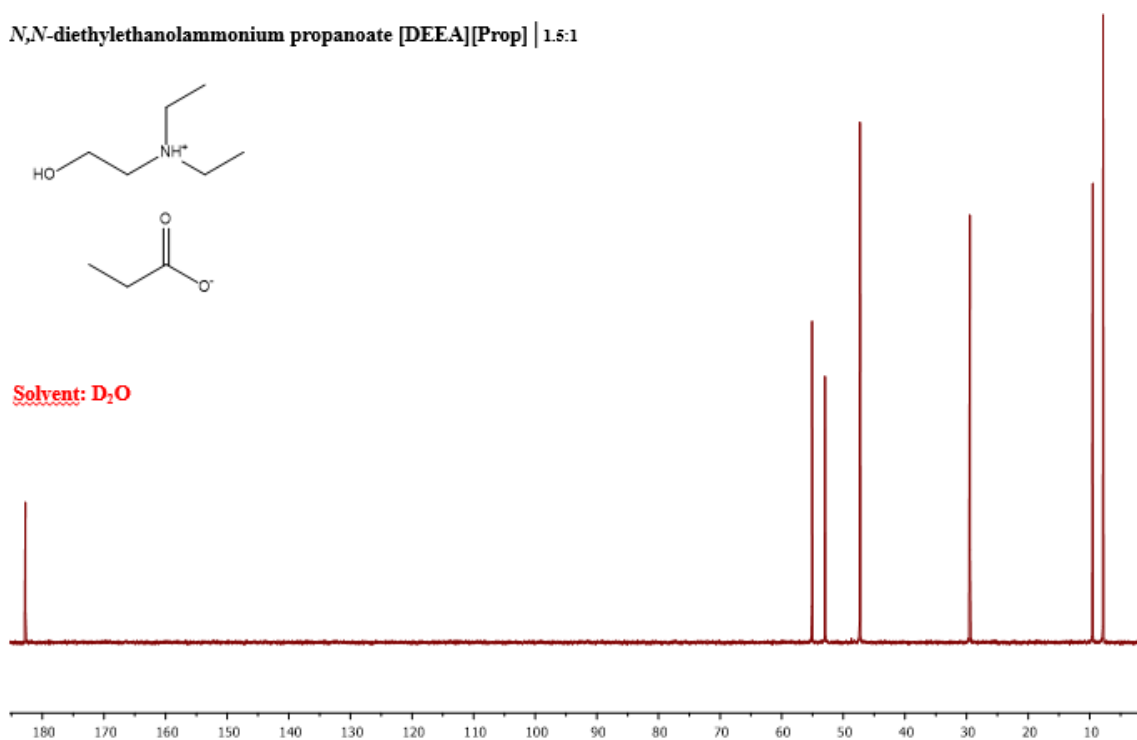
N,N-diethylethanolammonium butanoate [DEEA][But] │ 1:1

¹³C

N,N-diethylethanolammonium butanoate [DEEA][But] │ 1:1

Solvent: D₂O

64

¹H
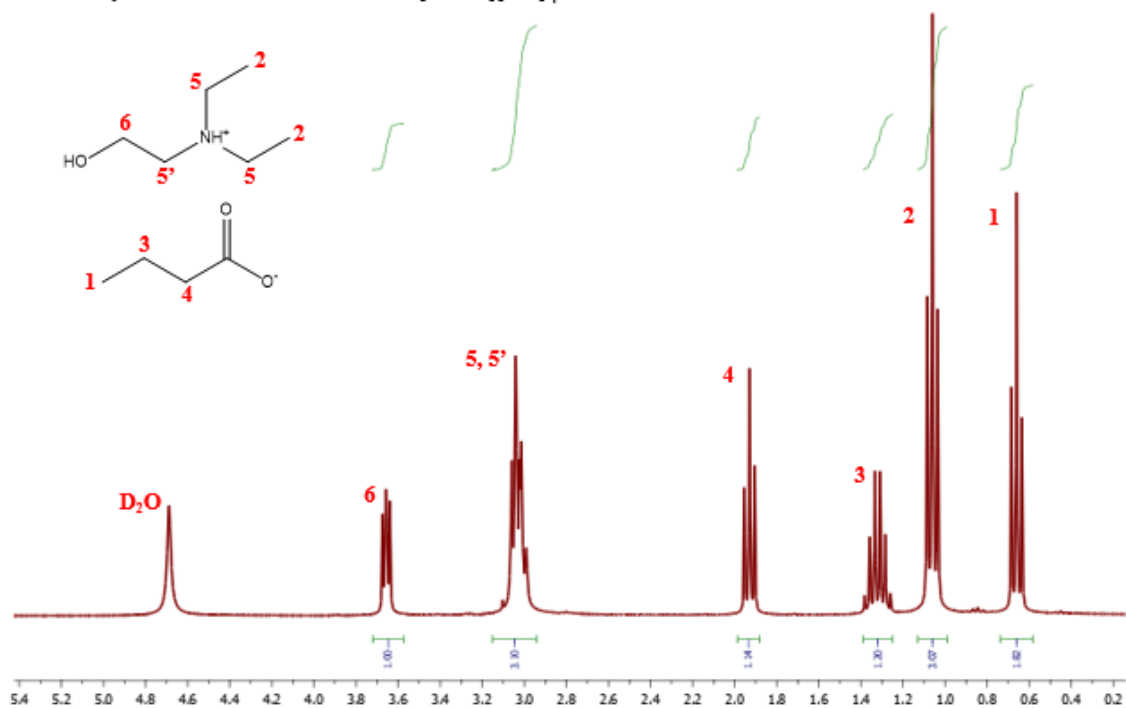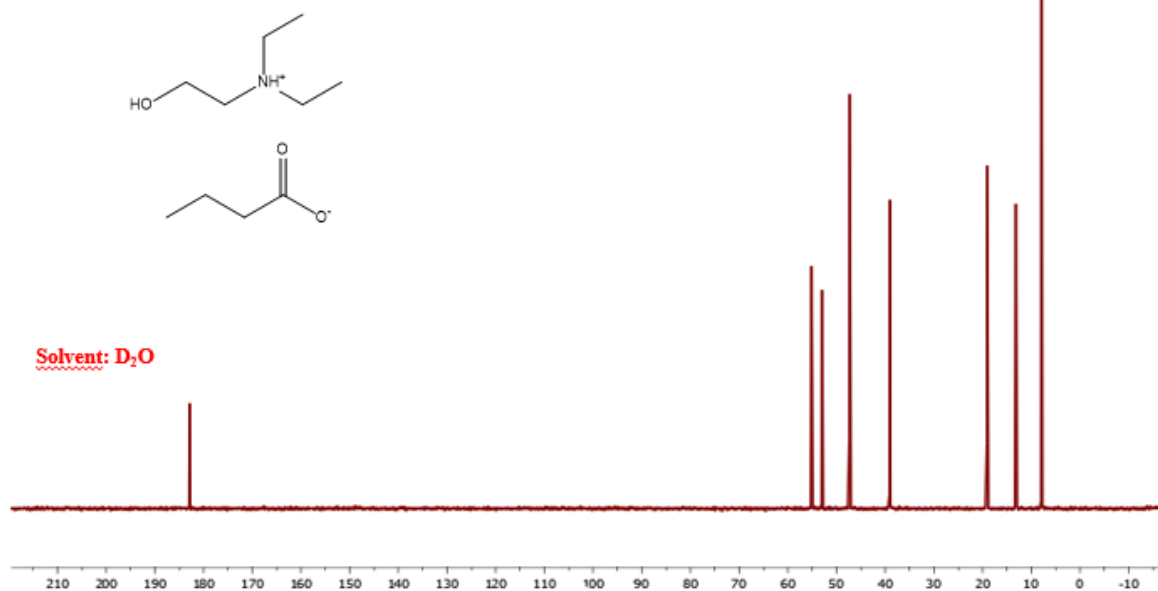
N,N-diethylethanolammonium butanoate [DEEA][But] │2:1

¹³C

N,N-diethylethanolammonium butanoate [DEEA][But] │2:1

Solvent: D₂O

¹H
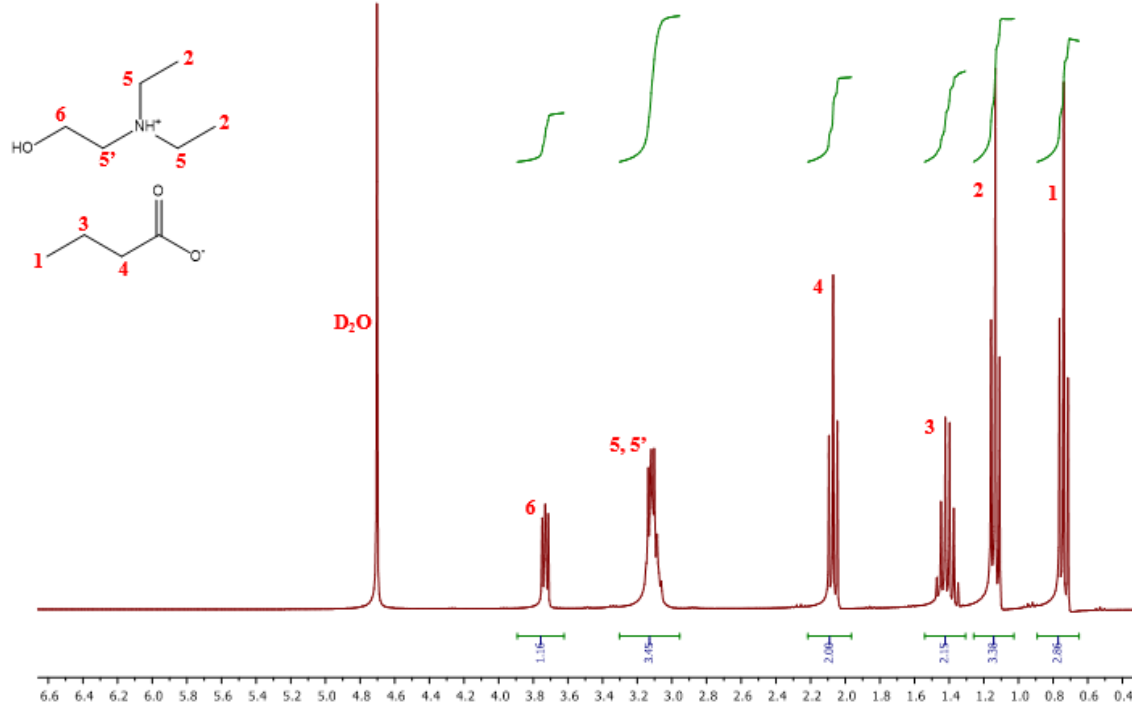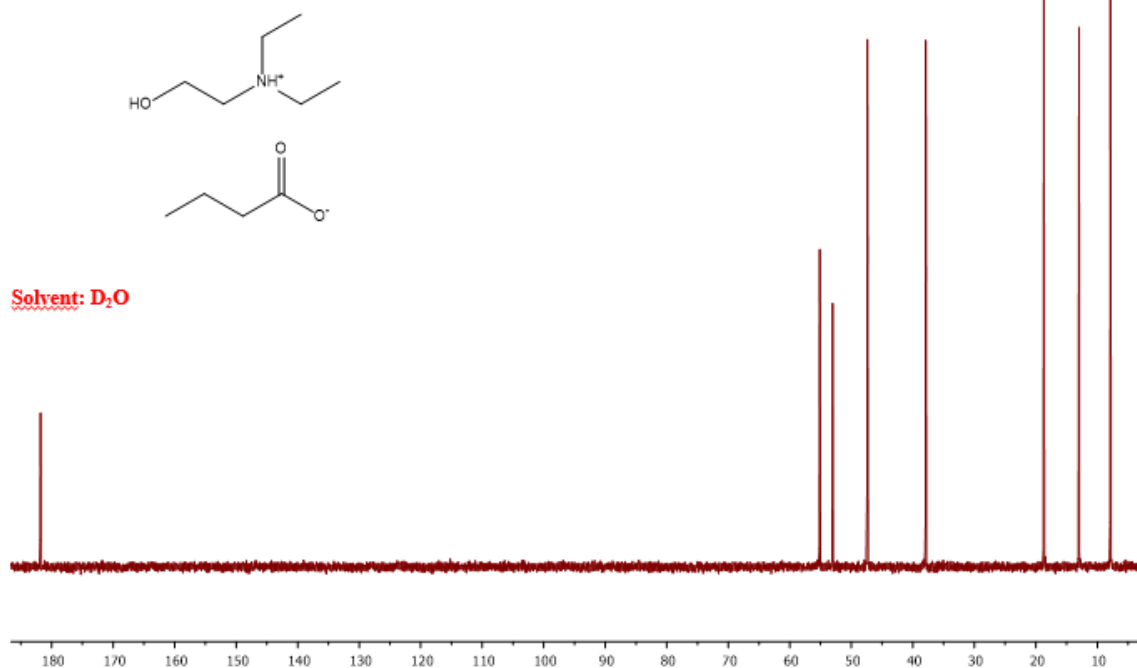
N,N-diethylethanolammonium pentanoate [DEEA][Pent] │ 1:1

¹³C

N,N-diethylethanolammonium pentanoate [DEEA][Pent] │ 1:1

Solvent: D₂O

66

¹H
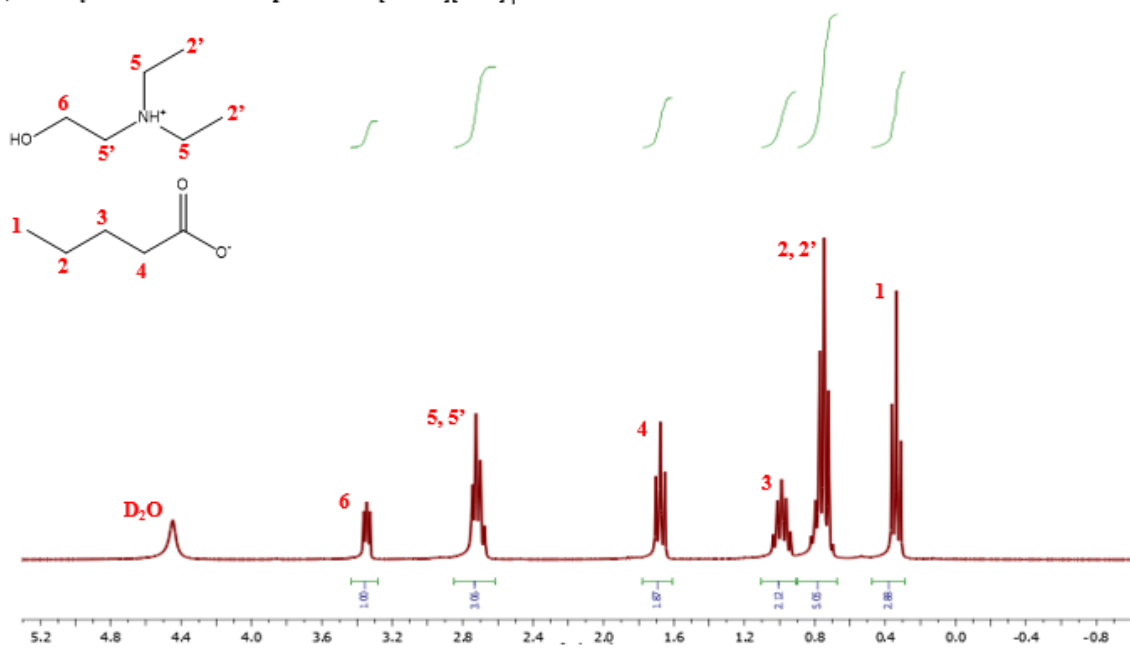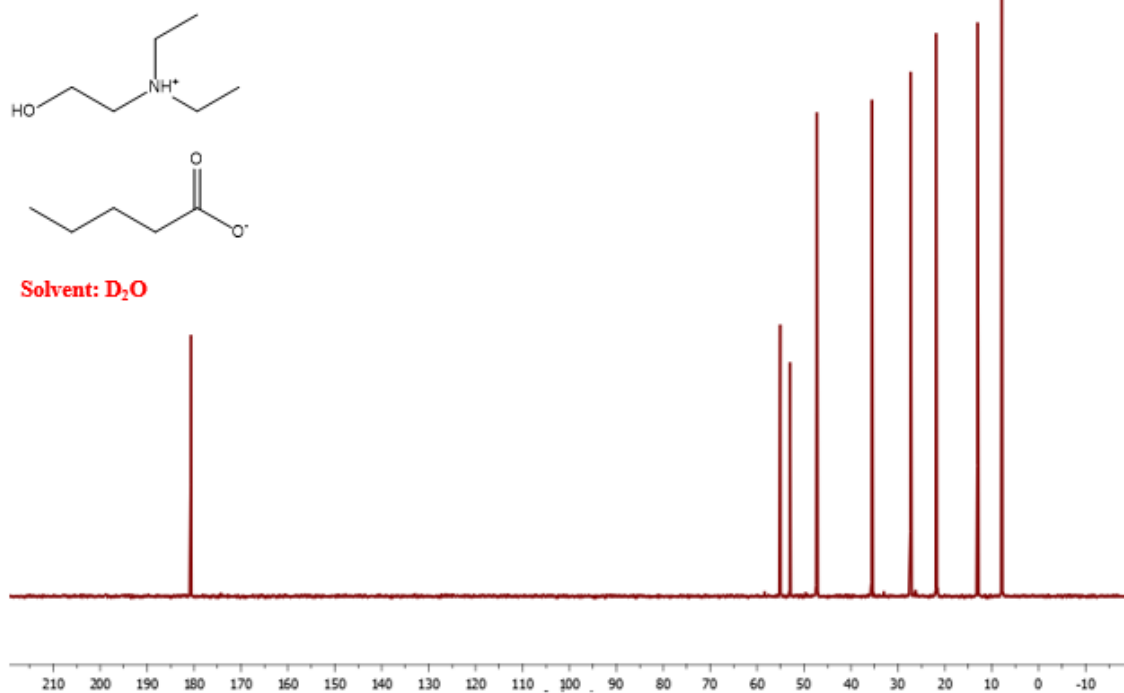
N,N-diethylethanolammonium pentanoate [DEEA][Pent] │ 2:1

¹³C

N,N-diethylethanolammonium pentanoate [DEEA][Pent] │ 2:1

Solvent: D₂O

¹H

¹H
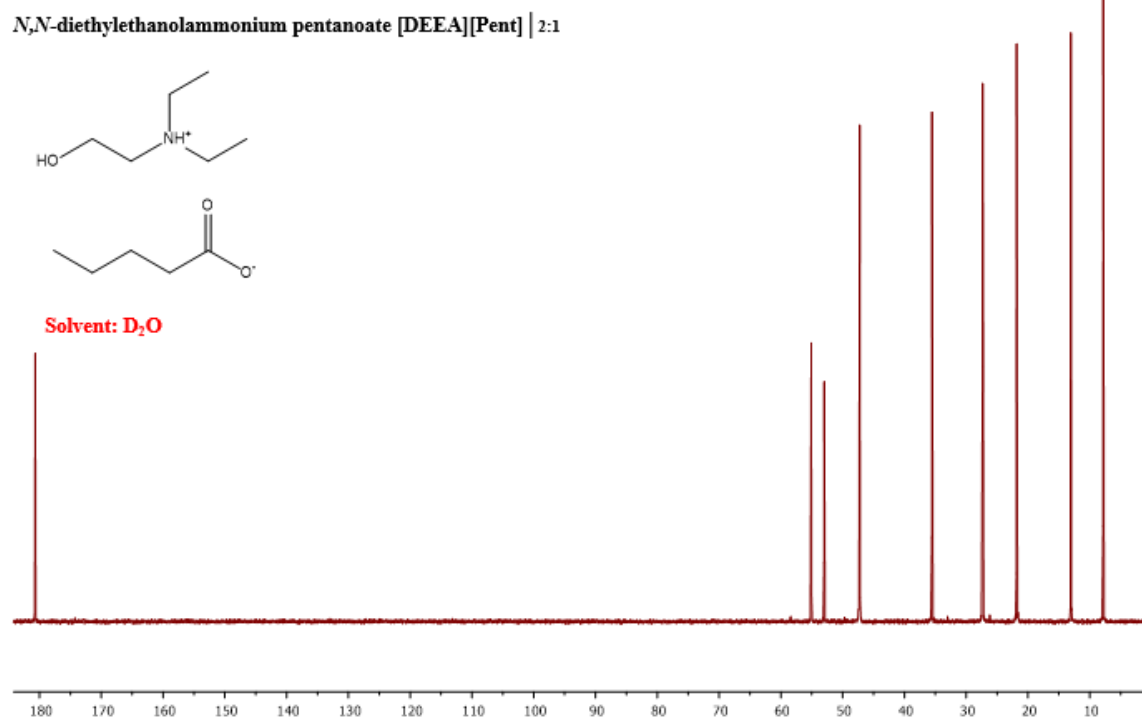
N,N-diethylethanolammonium hexanoate │ 2:1

¹³C

¹³C
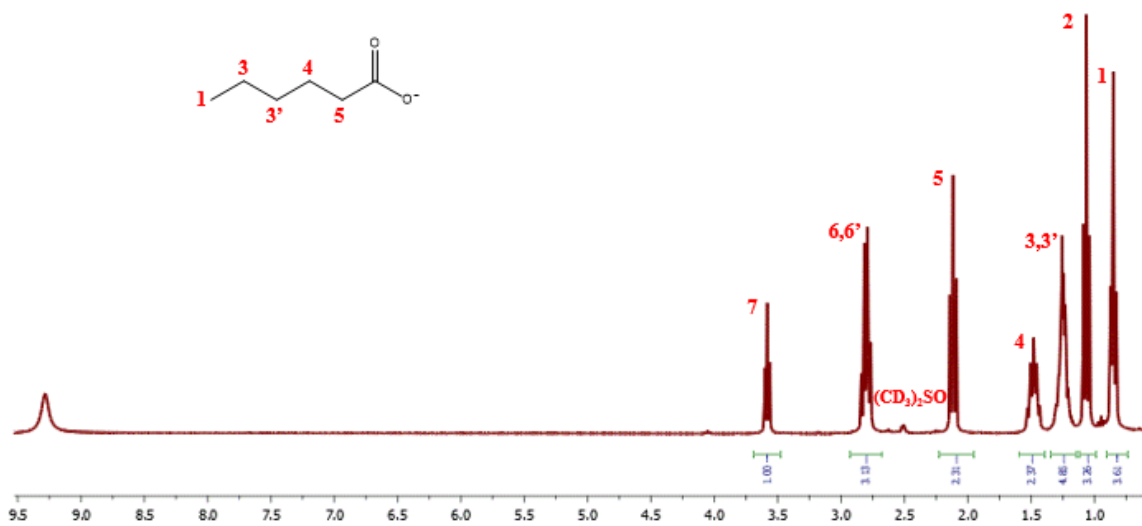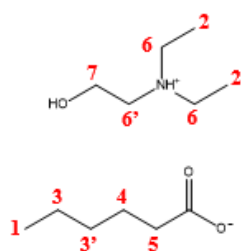
N,N-diethylethanolammonium hexanoate [DEEA][Hex] │ 2:1
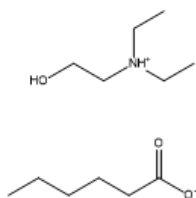
Solvent: (CD₃)₂SO
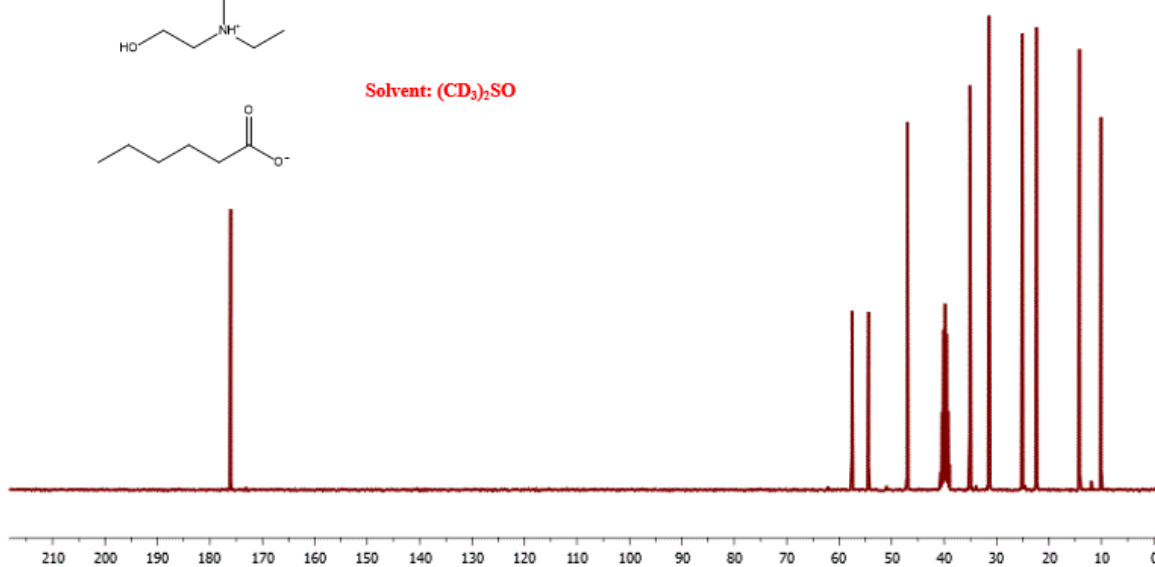
Appendix B. **High pressure density**

Pressure transducer Calibration

Table B.1. Data points used in the calibration of the pressure transducer.

Electric Tension /mV	Pressure /bar
3.0020	2.05
2.8900	2.92
2.7613	3.97
2.6490	4.90
2.5340	5.85
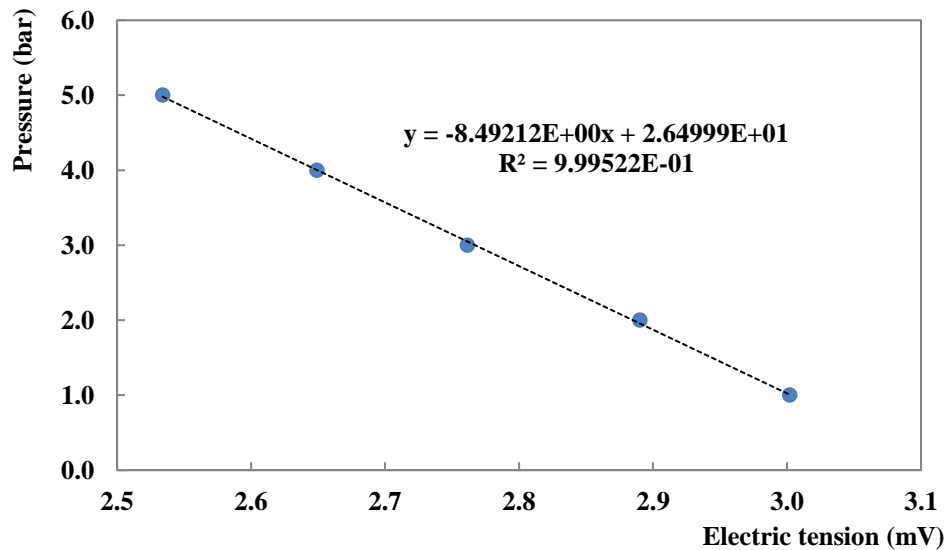
Figure B.1. Linear regression of the pressure vs electric tension used in the calibration of the pressure transducer.

High pressure densimeter calibration

Table B.2. Polynomial coefficients of Equation (1), used to calculate density.

A_1	-8.4624070E+00
A_2	3.5541749E-03
A_3	-3.1724892E-05
A_4	1.7615723E-06
A_5	4.1575518E-08
A_6	2.6022002E-07
A_7	-1.1449866E-09
A_8	3.8043060E-12
A_9	-3.0416313E-13
A_{10}	-6.1389498E-15
A_{11}	1.5751972E-13

High-pressure density data

Table B.3. Density and molar volume of [DEEA][Ace] │ 1.5:1 as a function of temperature and pressure.

283 K			293 K			303 K			313 K			323 K		
p (MPa)	ρ (g·cm⁻³)	Vm (cm³·mol⁻¹)	p (MPa)	ρ (g·cm⁻³)	Vm (cm³·mol⁻¹)	p (MPa)	ρ (g·cm⁻³)	Vm (cm³·mol⁻¹)	p (MPa)	ρ (g·cm⁻³)	Vm (cm³·mol⁻¹)	p (MPa)	ρ (g·cm⁻³)	Vm (cm³·mol⁻¹)
0.14	1.0500	197.87	0.14	1.0411	199.55	0.16	1.0326	201.21	0.14	1.0238	202.93	0.12	1.0152	204.65
1.052	1.0502	197.83	1.00	1.0416	199.47	1.07	1.0330	201.12	1.05	1.0243	202.82	1.03	1.0158	204.54
2.017	1.0506	197.75	2.07	1.0421	199.36	2.01	1.0335	201.02	1.99	1.0248	202.74	2.03	1.0163	204.43
5.058	1.0522	197.46	5.03	1.0438	199.05	5.02	1.0352	200.69	5.07	1.0265	202.39	5.03	1.0180	204.08
7.029	1.0532	197.27	7.07	1.0447	198.86	7.12	1.0363	200.48	7.07	1.0277	202.16	7.09	1.0193	203.83
10.079	1.0544	197.04	10.01	1.0462	198.59	10.06	1.0379	200.17	10.06	1.0293	201.84	9.99	1.0209	203.50
15.077	1.0567	196.61	15.05	1.0486	198.13	15.03	1.0403	199.71	15.03	1.0320	201.32	15.00	1.0236	202.96
20.044	1.0591	196.17	20.04	1.0509	197.69	20.05	1.0427	199.25	20.06	1.0346	200.82	19.96	1.0262	202.46
25.101	1.0612	195.77	25.08	1.0533	197.25	25.12	1.0452	198.78	25.12	1.0370	200.36	25.02	1.0290	201.91
30.006	1.0633	195.40	30.04	1.0554	196.85	30.07	1.0474	198.36	30.17	1.0394	199.88	30.06	1.0316	201.40
35.027	1.0654	195.00	35.07	1.0576	196.44	35.04	1.0496	197.94	35.08	1.0417	199.44	35.10	1.0339	200.96
40.028	1.0674	194.64	40.05	1.0597	196.05	40.07	1.0519	197.50	40.01	1.0441	198.99	40.00	1.0363	200.47
45.019	1.0694	194.29	45.07	1.0618	195.67	45.03	1.0542	197.08	45.08	1.0464	198.55	45.04	1.0387	200.02
50.023	1.0712	193.95	50.04	1.0636	195.34	50.07	1.0563	196.69	50.01	1.0485	198.15	50.05	1.0411	199.56
55.025	1.0730	193.62	55.07	1.0658	194.93	55.05	1.0583	196.31	55.06	1.0507	197.73	55.16	1.0433	199.13
60.084	1.0750	193.26	60.08	1.0677	194.58	60.09	1.0601	195.98	60.09	1.0528	197.33	60.17	1.0454	198.75
65.132	1.0769	192.92	65.02	1.0697	194.23	65.12	1.0622	195.60	65.06	1.0548	196.97	65.04	1.0476	198.33
70.024	1.0787	192.60	70.02	1.0714	193.91	70.02	1.0641	195.25	70.08	1.0569	196.58	70.07	1.0497	197.93
75.139	1.0803	192.31	75.08	1.0732	193.59	75.10	1.0661	194.87	75.00	1.0587	196.24	75.07	1.0516	197.56
80.035	1.0821	192.00	80.18	1.0750	193.27	79.99	1.0680	194.53	80.01	1.0608	195.85	80.06	1.0536	197.18
85.065	1.0838	191.69	85.03	1.0768	192.94	85.09	1.0697	194.23	85.07	1.0625	195.54	85.08	1.0557	196.80
90.125	1.0855	191.40	90.02	1.0785	192.64	90.04	1.0715	193.90	90.09	1.0645	195.17	90.18	1.0577	196.43
95.147	1.0862	191.27	95.05	1.0801	192.35	95.18	1.0735	193.54	95.00	1.0664	194.83	95.07	1.0595	196.09

Table B.3. Density and molar volume of [DEEA][Ace] │ 1.5:1 as a function of temperature and pressure (Cont.).

333 K			343 K			353 K			363 K		
p (MPa)	ρ (g·cm⁻³)	Vm (cm³·mol⁻¹)	p (MPa)	ρ (g·cm⁻³)	Vm (cm³·mol⁻¹)	p (MPa)	ρ (g·cm⁻³)	Vm (cm³·mol⁻¹)	p (MPa)	ρ (g·cm⁻³)	Vm (cm³·mol⁻¹)
0.12	1.0065	206.42	0.11	0.9976	208.26	0.16	0.9879	210.31	0.16	0.9777	212.51
1.02	1.0070	206.32	1.04	0.9977	208.23	1.03	0.9885	210.18	1.04	0.9783	212.36
2.12	1.0076	206.20	2.11	0.9984	208.08	2.06	0.9892	210.03	2.05	0.9790	212.22
4.93	1.0093	205.84	5.06	1.0005	207.66	5.14	0.9912	209.61	5.08	0.9812	211.75
7.13	1.0106	205.58	7.03	1.0017	207.42	7.15	0.9923	209.36	7.12	0.9827	211.42
10.14	1.0124	205.21	10.14	1.0037	206.99	10.05	0.9943	208.95	10.13	0.9848	210.98
15.05	1.0152	204.64	15.05	1.0067	206.39	15.14	0.9976	208.26	15.03	0.9881	210.27
20.12	1.0180	204.09	20.13	1.0096	205.79	20.00	1.0005	207.66	20.07	0.9913	209.59
25.02	1.0207	203.55	25.06	1.0125	205.20	25.00	1.0034	207.05	25.07	0.9944	208.93
30.07	1.0235	202.99	30.10	1.0153	204.64	29.95	1.0063	206.46	30.01	0.9973	208.33
35.12	1.0261	202.48	35.02	1.0180	204.09	35.06	1.0092	205.86	35.04	1.0003	207.70
40.05	1.0286	201.98	40.04	1.0206	203.57	40.04	1.0118	205.34	40.05	1.0031	207.12
45.02	1.0310	201.50	45.05	1.0230	203.10	45.16	1.0145	204.79	45.10	1.0058	206.56
50.09	1.0334	201.05	50.01	1.0255	202.59	50.03	1.0171	204.26	50.13	1.0085	206.00
55.06	1.0357	200.60	55.03	1.0280	202.10	55.05	1.0196	203.76	55.02	1.0125	205.20
60.15	1.0380	200.16	60.08	1.0300	201.70	60.11	1.0222	203.26	60.09	1.0137	204.96
65.06	1.0402	199.73	65.08	1.0324	201.23	65.13	1.0245	202.79	65.09	1.0161	204.47
70.08	1.0424	199.31	70.01	1.0347	200.79	70.07	1.0268	202.33	70.08	1.0176	204.17
75.05	1.0444	198.92	75.04	1.0370	200.34	75.05	1.0292	201.87	75.07	1.0202	203.65
80.05	1.0464	198.55	80.02	1.0390	199.96	80.06	1.0313	201.44	80.17	1.0236	202.97
85.02	1.0486	198.14	85.04	1.0413	199.52	85.00	1.0334	201.05	85.12	1.0268	202.34
90.01	1.0504	197.80	89.93	1.0431	199.17	90.07	1.0355	200.63	90.09	1.0290	201.90
95.05	1.0524	197.42	95.10	1.0452	198.77	95.12	1.0374	200.26	95.07	1.0296	201.79

Table B.4. Density and molar volume of [DEEA][Prop] │1.5:1 as a function of temperature and pressure.

283 K			293 K			303 K			313 K			323 K		
p (MPa)	ρ (g·cm⁻³)	Vm (cm³·mol⁻¹)	p (MPa)	ρ (g·cm⁻³)	Vm (cm³·mol⁻¹)	p (MPa)	ρ (g·cm⁻³)	Vm (cm³·mol⁻¹)	p (MPa)	ρ (g·cm⁻³)	Vm (cm³·mol⁻¹)	p (MPa)	ρ (g·cm⁻³)	Vm (cm³·mol⁻¹)
0.10	1.0107	226.39	0.10	1.0019	228.37	0.10	0.9931	230.40	0.10	0.9838	232.57	0.10	0.9751	234.66
1.00	1.0112	226.28	1.00	1.0025	228.25	1.00	0.9936	230.28	1.00	0.9843	232.45	1.00	0.9757	234.51
2.00	1.0116	226.18	2.00	1.0030	228.12	2.00	0.9942	230.16	2.00	0.9849	232.31	2.00	0.9762	234.38
5.00	1.0132	225.84	5.00	1.0046	227.77	5.00	0.9958	229.78	5.00	0.9867	231.90	5.00	0.9780	233.95
7.00	1.0142	225.61	7.00	1.0056	227.54	7.00	0.9969	229.52	7.00	0.9878	231.63	7.00	0.9793	233.65
10.00	1.0156	225.29	10.00	1.0072	227.18	10.00	0.9985	229.16	10.00	0.9895	231.23	10.00	0.9810	233.25
15.00	1.0180	224.77	15.00	1.0096	226.63	15.00	1.0011	228.56	15.00	0.9923	230.60	15.00	0.9839	232.55
20.00	1.0203	224.26	20.00	1.0120	226.10	20.00	1.0037	227.97	20.00	0.9949	229.98	20.00	0.9868	231.88
25.00	1.0226	223.75	25.00	1.0144	225.55	25.00	1.0061	227.43	25.00	0.9975	229.39	25.00	0.9895	231.23
30.00	1.0248	223.27	30.00	1.0166	225.06	30.00	1.0085	226.87	30.00	1.0001	228.80	30.00	0.9921	230.63
35.00	1.0270	222.79	35.00	1.0189	224.56	35.00	1.0108	226.37	35.00	1.0024	228.25	35.00	0.9945	230.08
40.00	1.0290	222.36	40.00	1.0212	224.06	40.00	1.0128	225.91	40.00	1.0048	227.72	40.00	0.9970	229.50
45.00	1.0312	221.89	45.00	1.0234	223.59	45.00	1.0151	225.41	45.00	1.0073	227.15	45.00	0.9995	228.92
50.00	1.0331	221.47	50.00	1.0254	223.14	50.00	1.0172	224.93	50.00	1.0095	226.65	50.00	1.0019	228.37
55.00	1.0352	221.03	55.00	1.0274	222.71	55.00	1.0193	224.48	55.00	1.0118	226.15	55.00	1.0042	227.86
60.00	1.0372	220.61	60.00	1.0295	222.25	60.00	1.0215	224.00	60.00	1.0139	225.67	60.00	1.0065	227.33
65.00	1.0390	220.23	65.00	1.0315	221.83	65.00	1.0237	223.52	65.01	1.0159	225.23	65.00	1.0087	226.83
70.00	1.0409	219.82	70.00	1.0334	221.41	70.00	1.0257	223.08	70.00	1.0181	224.75	70.00	1.0106	226.41
75.00	1.0428	219.42	75.00	1.0353	221.00	75.00	1.0278	222.63	75.00	1.0201	224.30	75.00	1.0129	225.91

Table B.4. Density and molar volume of [DEEA][Prop]│1.5:1 as a function of temperature and pressure (Cont.).

333 K			343 K			353 K		
p	ρ	Vm	p	ρ	Vm	p	ρ	Vm
(MPa)	(g·cm⁻³)	(cm³·mol⁻¹)	(MPa)	(g·cm⁻³)	(cm³·mol⁻¹)	(MPa)	(g·cm⁻³)	(cm³·mol⁻¹)
0.10	0.9656	236.97	0.10	0.9563	239.26	0.10	0.9465	241.75
1.00	0.9662	236.83	1.00	0.9570	239.09	1.00	0.9471	241.58
2.00	0.9668	236.67	2.00	0.9576	238.93	2.00	0.9478	241.40
5.00	0.9687	236.20	5.00	0.9597	238.43	5.00	0.9500	240.86
7.00	0.9700	235.89	7.00	0.9609	238.12	7.00	0.9513	240.52
10.00	0.9718	235.44	10.00	0.9628	237.65	10.00	0.9534	240.00
15.01	0.9748	234.74	15.00	0.9660	236.87	15.00	0.9567	239.16
20.00	0.9777	234.04	20.00	0.9688	236.17	20.00	0.9599	238.37
25.00	0.9805	233.37	25.00	0.9718	235.44	25.00	0.9631	237.59
30.00	0.9833	232.71	30.00	0.9747	234.74	30.00	0.9660	236.88
35.00	0.9859	232.09	35.00	0.9773	234.12	35.00	0.9689	236.15
40.00	0.9883	231.51	40.00	0.9801	233.45	40.00	0.9716	235.50
45.00	0.9909	230.92	45.00	0.9827	232.83	45.00	0.9744	234.83
50.00	0.9934	230.32	50.00	0.9852	232.24	50.00	0.9770	234.20
55.00	0.9958	229.78	55.00	0.9877	231.66	55.00	0.9796	233.57
60.00	0.9982	229.22	60.00	0.9901	231.09	60.00	0.9822	232.97
65.00	1.0004	228.72	65.00	0.9925	230.53	65.00	0.9845	232.41
70.00	1.0026	228.21	70.00	0.9948	230.00	70.00	0.9870	231.83
75.00	1.0048	227.72	75.00	0.9971	229.47	75.00	0.9892	231.31

Table B.5. Density and molar volume of [DEEA][But] │ 2:1 as a function of temperature and pressure.

283 K			293 K			303 K			313 K			323 K		
p (MPa)	ρ (g·cm⁻³)	Vm (cm³·mol⁻¹)	p (MPa)	ρ (g·cm⁻³)	Vm (cm³·mol⁻¹)	p (MPa)	ρ (g·cm⁻³)	Vm (cm³·mol⁻¹)	p (MPa)	ρ (g·cm⁻³)	Vm (cm³·mol⁻¹)	p (MPa)	ρ (g·cm⁻³)	Vm (cm³·mol⁻¹)
0.10	1.0056	291.78	0.10	0.9974	294.16	0.10	0.9894	296.56	0.10	0.9812	299.01	0.10	0.9732	301.48
1.00	1.0060	291.64	1.00	0.9979	294.01	1.00	0.9898	296.42	1.00	0.9818	298.84	1.00	0.9737	301.32
2.00	1.0065	291.50	2.00	0.9985	293.85	2.00	0.9903	296.26	2.00	0.9823	298.68	2.00	0.9744	301.12
5.00	1.0081	291.04	5.00	1.0001	293.37	5.00	0.9919	295.79	5.00	0.9841	298.13	5.00	0.9761	300.57
7.00	1.0090	290.79	7.00	1.0011	293.07	7.00	0.9931	295.45	7.00	0.9852	297.80	7.00	0.9773	300.20
10.00	1.0104	290.37	10.00	1.0026	292.65	10.00	0.9948	294.95	10.00	0.9869	297.28	10.00	0.9791	299.66
15.00	1.0128	289.69	15.00	1.0051	291.90	15.00	0.9974	294.16	15.00	0.9897	296.45	15.00	0.9820	298.79
20.00	1.0152	289.01	20.00	1.0076	291.18	20.00	1.0000	293.41	20.00	0.9922	295.72	20.00	0.9848	297.94
25.00	1.0174	288.39	25.00	1.0100	290.50	25.00	1.0024	292.71	25.00	0.9948	294.93	25.00	0.9874	297.15
30.00	1.0196	287.76	30.00	1.0123	289.83	30.00	1.0048	292.00	30.00	0.9972	294.22	30.00	0.9899	296.40
35.00	1.0217	287.16	35.00	1.0145	289.20	35.00	1.0071	291.33	35.00	0.9998	293.47	35.00	0.9925	295.61
40.00	1.0238	286.57	40.00	1.0166	288.62	40.00	1.0094	290.67	40.00	1.0021	292.80	40.00	0.9949	294.89
45.00	1.0259	285.99	45.00	1.0188	287.99	45.00	1.0116	290.04	45.00	1.0043	292.13	45.00	0.9973	294.19
50.00	1.0279	285.44	50.00	1.0207	287.46	50.00	1.0137	289.45	50.00	1.0067	291.46	50.00	0.9997	293.48
55.00	1.0299	284.88	55.00	1.0228	286.87	55.00	1.0158	288.85	55.00	1.0088	290.83	55.00	1.0020	292.81
60.00	1.0318	284.35	60.00	1.0248	286.29	60.00	1.0178	288.26	60.00	1.0110	290.20	60.00	1.0043	292.15
65.00	1.0337	283.84	65.00	1.0268	285.75	65.00	1.0199	287.68	65.00	1.0131	289.61	65.00	1.0064	291.54
70.00	1.0356	283.33	70.00	1.0286	285.24	70.00	1.0219	287.10	70.00	1.0152	289.00	70.00	1.0086	290.91
75.00	1.0373	282.84	75.00	1.0307	284.67	75.00	1.0239	286.56	75.00	1.0172	288.43	75.00	1.0105	290.35
80.00	1.0391	282.35	80.00	1.0325	284.15	80.00	1.0257	286.04	80.00	1.0191	287.89	80.00	1.0125	289.77
85.00	1.0410	281.86	85.00	1.0343	283.68	85.00	1.0276	285.53	85.00	1.0210	287.37	85.00	1.0145	289.21
90.00	1.0426	281.41	90.00	1.0360	283.20	90.00	1.0294	285.03	90.00	1.0230	286.82	90.00	1.0164	288.67
95.00	1.0443	280.97	95.00	1.0378	282.71	95.00	1.0313	284.50	95.00	1.0248	286.30	95.00	1.0185	288.08

Table B.5. Density and molar volume of [DEEA][But] │ 2:1 as a function of temperature and pressure (Cont.).

333 K			343 K			353 K			363 K		
p (MPa)	ρ (g·cm⁻³)	Vm (cm³·mol⁻¹)	p (MPa)	ρ (g·cm⁻³)	Vm (cm³·mol⁻¹)	p (MPa)	ρ (g·cm⁻³)	Vm (cm³·mol⁻¹)	p (MPa)	ρ (g·cm⁻³)	Vm (cm³·mol⁻¹)
0.10	0.9650	304.05	0.10	0.9548	307.28	0.10	0.9455	310.32	0.10	0.9354	313.68
1.00	0.9655	303.87	1.00	0.9555	307.07	1.00	0.9461	310.11	1.00	0.9360	313.45
2.00	0.9662	303.67	2.00	0.9561	306.87	2.00	0.9468	309.88	2.00	0.9367	313.23
5.00	0.9682	303.05	5.00	0.9581	306.23	5.00	0.9489	309.20	5.00	0.9389	312.49
7.00	0.9694	302.68	7.00	0.9594	305.82	7.00	0.9503	308.75	7.00	0.9404	311.99
10.00	0.9712	302.10	10.00	0.9613	305.21	10.00	0.9522	308.12	10.00	0.9424	311.34
15.00	0.9743	301.15	15.00	0.9646	304.17	15.00	0.9555	307.06	15.00	0.9459	310.17
20.00	0.9771	300.27	20.00	0.9675	303.24	20.00	0.9587	306.05	20.00	0.9493	309.08
25.00	0.9799	299.42	25.00	0.9707	302.27	25.00	0.9617	305.08	25.00	0.9524	308.06
30.00	0.9826	298.59	30.00	0.9734	301.40	30.00	0.9646	304.15	30.00	0.9556	307.04
35.00	0.9852	297.79	35.00	0.9762	300.54	35.00	0.9677	303.20	35.00	0.9587	306.04
40.00	0.9878	297.03	40.00	0.9789	299.73	40.00	0.9704	302.34	40.00	0.9617	305.09
45.00	0.9903	296.27	45.00	0.9815	298.94	45.00	0.9731	301.52	45.00	0.9643	304.28
50.00	0.9927	295.57	50.00	0.9839	298.20	50.00	0.9756	300.73	50.00	0.9671	303.40
55.00	0.9950	294.87	55.00	0.9864	297.46	55.00	0.9782	299.93	55.00	0.9696	302.60
60.00	0.9973	294.20	60.00	0.9888	296.72	60.00	0.9820	298.77	60.00	0.9723	301.77
65.00	0.9996	293.53	65.00	0.9911	296.03	65.00	0.9831	298.43	65.00	0.9748	300.99
70.00	1.0018	292.88	70.00	0.9934	295.36	70.00	0.9855	297.71	70.00	0.9772	300.23
75.00	1.0039	292.27	75.00	0.9956	294.70	75.00	0.9878	297.03	75.00	0.9796	299.49
80.00	1.0060	291.65	80.00	0.9979	294.02	80.00	0.9901	296.34	80.00	0.9820	298.79
85.00	1.0080	291.06	85.00	1.0000	293.41	85.00	0.9923	295.68	85.00	0.9844	298.06
90.00	1.0100	290.50	90.00	1.0019	292.83	90.00	0.9944	295.04	90.00	0.9865	297.42
95.00	1.0120	289.93	95.00	1.0040	292.23	95.00	0.9966	294.41	95.00	0.9887	296.75

Table B.6. Density and molar volume of [DEEA][Pent] │2:1 as a function of temperature and pressure.

283 K			293 K			303 K			313 K			323 K		
p	ρ	Vm	p	ρ	Vm	p	ρ	Vm	p	ρ	Vm	p	ρ	Vm
(MPa)	(g·cm^{-3})	(cm^3·mol^{-1})	(MPa)	(g·cm^{-3})	(cm^3·mol^{-1})	(MPa)	(g·cm^{-3})	(cm^3·mol^{-1})	(MPa)	(g·cm^{-3})	(cm^3·mol^{-1})	(MPa)	(g·cm^{-3})	(cm^3·mol^{-1})
0.12	0.9850	326.35	0.13	0.9769	329.06	0.14	0.9692	332.34	0.14	0.9611	334.47	0.15	0.9532	337.23
1.01	0.9855	326.19	1.02	0.9773	328.91	1.02	0.9696	331.83	1.08	0.9617	334.25	1.02	0.9538	337.04
2.02	0.9860	326.00	2.01	0.9785	328.52	2.04	0.9703	331.27	2.07	0.9623	334.03	2.03	0.9544	336.82
5.00	0.9876	325.47	5.02	0.9792	328.29	5.00	0.9720	330.70	5.04	0.9643	333.35	5.05	0.9565	336.08
7.01	0.9887	325.13	7.02	0.9806	327.81	7.01	0.9731	330.35	7.03	0.9654	332.97	7.02	0.9577	335.64
10.03	0.9903	324.59	10.05	0.9824	327.20	10.02	0.9749	329.73	10.04	0.9672	332.35	10.04	0.9595	335.00
15.02	0.9929	323.75	15.02	0.9852	326.28	15.06	0.9776	328.81	15.02	0.9701	331.35	15.03	0.9626	333.94
20.01	0.9954	322.95	20.02	0.9878	325.43	20.03	0.9804	327.89	20.04	0.9732	330.32	20.00	0.9655	332.93
25.01	0.9978	322.17	25.01	0.9903	324.60	25.05	0.9826	327.15	25.02	0.9756	329.50	25.03	0.9684	331.94
30.00	1.0002	321.38	30.00	0.9927	323.80	30.01	0.9850	326.34	30.05	0.9784	328.55	30.08	0.9712	330.99
35.00	1.0025	320.64	35.08	0.9951	323.02	35.06	0.9875	325.53	35.07	0.9810	327.68	35.04	0.9738	330.08
40.00	1.0048	319.92	40.00	0.9974	322.29	40.07	0.9899	324.71	40.08	0.9835	326.84	40.11	0.9765	329.18
45.03	1.0068	319.27	45.02	0.9998	321.53	45.04	0.9923	323.94	45.04	0.9860	326.03	45.09	0.9791	328.30
50.00	1.0091	318.56	50.02	1.0019	320.85	50.08	0.9945	323.22	50.01	0.9883	325.25	50.11	0.9816	327.46
55.00	1.0113	317.86	55.05	1.0042	320.09	55.02	0.9968	322.48	55.06	0.9907	324.47	55.07	0.9841	326.64
60.03	1.0131	317.36	60.02	1.0064	319.41	60.03	0.9990	321.77	60.07	0.9930	323.71	60.05	0.9864	325.89
65.00	1.0152	316.72	65.01	1.0085	318.75	65.03	1.0013	321.02	65.07	0.9952	323.00	65.07	0.9888	325.10
70.02	1.0172	316.09	70.02	1.0105	318.11	70.04	1.0033	320.41	70.02	0.9973	322.31	70.05	0.9910	324.38
75.03	1.0192	315.51	75.02	1.0125	317.47	75.09	1.0055	319.68	75.05	0.9995	321.60	75.03	0.9932	323.67
80.01	1.0212	314.77	80.00	1.0145	316.87	80.01	1.0075	319.05	80.04	1.0017	320.92	80.04	0.9952	322.99
85.01	1.0230	314.23	85.00	1.0165	316.22	85.04	1.0095	318.41	85.05	1.0037	320.26	85.01	0.9973	322.29
90.01	1.0248	313.88	90.01	1.0185	316.03	90.03	1.0113	317.86	90.08	1.0057	319.68	90.01	0.9994	321.64
95.00	1.0267	313.67	95.01	1.0203	315.50	95.04	1.0134	317.60	95.02	1.0077	319.30	95.06	1.0014	321.16

Table B.6. Density and molar volume of [DEEA][Pent] │ 2:1 as a function of temperature and pressure (Cont.).

333 K			343 K			353 K			363 K		
p (MPa)	*ρ* (g·cm⁻³)	*Vm* (cm³·mol⁻¹)	*p* (MPa)	*ρ* (g·cm⁻³)	*Vm* (cm³·mol⁻¹)	*p* (MPa)	*ρ* (g·cm⁻³)	*Vm* (cm³·mol⁻¹)	*p* (MPa)	*ρ* (g·cm⁻³)	*Vm* (cm³·mol⁻¹)
0.16	0.9451	340.14	0.15	0.9368	342.90	0.15	0.9274	345.74	0.12	0.9189	349.53
1.06	0.9456	339.95	1.01	0.9374	342.78	1.04	0.9283	345.70	1.02	0.9195	349.29
2.05	0.9464	339.67	2.06	0.9381	342.67	2.16	0.9292	345.65	2.09	0.9203	348.98
5.06	0.9486	338.88	5.04	0.9404	341.84	5.06	0.9316	344.91	5.05	0.9227	348.09
7.03	0.9498	338.42	7.02	0.9417	341.34	7.09	0.9331	344.37	7.03	0.9242	347.51
10.09	0.9519	337.69	10.05	0.9438	340.60	10.08	0.9352	343.57	10.04	0.9266	346.63
15.02	0.9551	336.56	15.16	0.9465	339.63	15.03	0.9388	342.25	15.08	0.9301	345.49
20.05	0.9582	335.47	20.01	0.9499	338.41	20.11	0.9423	341.13	20.11	0.9338	344.28
25.05	0.9612	334.44	25.10	0.9531	337.25	25.11	0.9456	339.95	25.07	0.9375	342.92
30.03	0.9639	333.48	30.10	0.9565	336.08	30.07	0.9486	338.88	30.07	0.9404	341.89
35.06	0.9668	332.48	35.06	0.9591	335.17	35.03	0.9517	337.78	35.06	0.9436	340.74
40.02	0.9696	331.53	40.05	0.9620	334.16	40.04	0.9546	336.76	40.05	0.9465	339.66
45.04	0.9722	330.63	45.06	0.9646	333.23	45.06	0.9574	335.78	45.05	0.9495	338.61
50.07	0.9748	329.77	50.00	0.9674	332.29	50.07	0.9603	334.75	50.04	0.9523	337.61
55.02	0.9772	328.93	55.15	0.9700	331.38	55.02	0.9631	333.79	55.01	0.9550	336.60
60.03	0.9797	328.10	60.08	0.9725	330.53	60.13	0.9656	332.92	60.14	0.9578	335.56
65.02	0.9821	327.30	65.01	0.9750	329.79	65.03	0.9681	332.05	65.07	0.9604	334.81
70.10	0.9845	326.52	70.01	0.9773	328.97	70.08	0.9704	331.25	70.27	0.9628	334.01
75.04	0.9867	325.77	75.09	0.9798	328.03	75.03	0.9730	330.43	75.08	0.9653	333.04
80.06	0.9889	325.00	80.02	0.9820	327.29	80.07	0.9753	329.68	80.07	0.9677	332.21
85.03	0.9910	324.31	85.04	0.9843	326.63	85.04	0.9777	329.02	85.07	0.9703	331.30
90.04	0.9931	323.56	90.02	0.9864	325.88	90.04	0.9799	328.53	90.01	0.9726	330.76
95.03	0.9951	322.95	95.02	0.9886	325.38	95.04	0.9821	326.93	95.14	0.9749	329.59

Table B.7. Density and molar volume of [DEEA][Hex] │ 2:1 as a function of temperature and pressure.

283 K			293 K			303 K			313 K			323 K		
p (MPa)	ρ (g·cm⁻³)	Vm (cm³·mol⁻¹)	p (MPa)	ρ (g·cm⁻³)	Vm (cm³·mol⁻¹)	p (MPa)	ρ (g·cm⁻³)	Vm (cm³·mol⁻¹)	p (MPa)	ρ (g·cm⁻³)	Vm (cm³·mol⁻¹)	p (MPa)	ρ (g·cm⁻³)	Vm (cm³·mol⁻¹)
0.16	0.9727	359.33	0.17	0.9639	362.60	0.15	0.9574	365.07	0.15	0.9500	367.91	0.14	0.9426	370.78
1.08	0.9733	359.10	1.04	0.9657	361.91	1.06	0.9582	364.77	1.06	0.9506	367.68	1.01	0.9432	370.57
2.00	0.9738	358.93	2.05	0.9663	361.71	2.08	0.9588	364.51	2.02	0.9513	367.41	2.02	0.9439	370.29
5.06	0.9755	358.28	5.04	0.9680	361.06	5.04	0.9607	363.82	5.01	0.9532	366.69	5.04	0.9459	369.49
7.01	0.9766	357.89	7.08	0.9692	360.61	7.09	0.9619	363.36	7.08	0.9545	366.19	7.02	0.9471	369.02
10.10	0.9782	357.30	10.00	0.9708	360.01	10.08	0.9636	362.73	10.07	0.9563	365.50	10.06	0.9491	368.27
15.06	0.9808	356.35	15.04	0.9736	358.99	15.10	0.9663	361.69	15.03	0.9591	364.41	15.03	0.9521	367.10
20.09	0.9833	355.44	20.09	0.9761	358.07	20.02	0.9691	360.66	20.05	0.9619	363.34	20.03	0.9551	365.96
25.04	0.9857	354.60	25.05	0.9785	357.18	25.16	0.9716	359.72	25.07	0.9647	362.31	25.04	0.9578	364.90
30.10	0.9880	353.75	30.02	0.9812	356.21	30.14	0.9741	358.79	30.10	0.9672	361.35	30.09	0.9606	363.83
35.08	0.9904	352.91	35.03	0.9834	355.40	35.01	0.9766	357.90	35.02	0.9698	360.38	35.06	0.9631	362.89
40.03	0.9926	352.13	40.08	0.9857	354.57	40.08	0.9791	356.97	40.08	0.9725	359.41	40.10	0.9658	361.87
45.06	0.9948	351.35	45.06	0.9882	353.69	45.17	0.9813	356.16	45.14	0.9749	358.52	45.01	0.9683	360.95
50.02	0.9971	350.53	50.06	0.9903	352.95	50.14	0.9831	355.53	50.12	0.9773	357.64	50.16	0.9709	360.00
55.05	0.9991	349.84	55.03	0.9922	352.25	55.08	0.9857	354.57	55.06	0.9793	356.90	55.11	0.9731	359.15
60.09	1.0013	349.07	60.03	0.9943	351.50	60.07	0.9880	353.76	60.06	0.9818	355.99	60.08	0.9756	358.27
65.04	1.0029	348.52	65.08	0.9967	350.68	65.02	0.9903	352.94	65.05	0.9840	355.20	65.10	0.9778	357.43
70.09	1.0046	347.90	70.21	0.9987	349.97	70.03	0.9923	352.23	70.08	0.9861	354.42	70.14	0.9802	356.58
75.14	1.0070	347.08	75.29	1.0007	349.26	75.08	0.9942	351.56	75.07	0.9881	353.72	75.04	0.9820	355.90
80.00	1.0080	346.73	80.04	1.0025	348.63	80.05	0.9963	350.80	80.11	0.9902	352.97	80.00	0.9841	355.16
85.04	1.0101	346.00	85.02	1.0045	347.95	85.09	0.9983	350.09	85.02	0.9923	352.21	85.05	0.9864	354.32
90.05	1.0123	345.25	90.05	1.0065	347.27	90.02	1.0002	349.42	90.04	0.9943	351.51	90.04	0.9885	353.58
95.07	1.0132	344.96	95.04	1.0070	347.08	95.05	1.0006	349.29	95.13	0.9955	351.08	95.05	0.9899	353.08

Table B.7. Density and molar volume of [DEEA][Hex] │ 2:1 as a function of temperature and pressure (Cont.).

333 K			343 K			353 K			363 K		
p	*ρ*	*Vm*	*p*	*ρ*	*Vm*	*p*	*ρ*	*Vm*	*p*	*ρ*	*Vm*
(MPa)	(g·cm⁻³)	(cm³·mol⁻¹)	(MPa)	(g·cm⁻³)	(cm³·mol⁻¹)	(MPa)	(g·cm⁻³)	(cm³·mol⁻¹)	(MPa)	(g·cm⁻³)	(cm³·mol⁻¹)
0.16	0.9339	374.23	0.17	0.9261	377.41	0.18	0.9178	380.83	0.19	0.9092	384.41
1.12	0.9346	373.96	1.03	0.9267	377.14	1.08	0.9185	380.51	1.03	0.9098	384.16
2.04	0.9353	373.69	2.06	0.9275	376.84	2.03	0.9192	380.21	2.03	0.9106	383.84
5.02	0.9374	372.84	5.07	0.9298	375.90	5.08	0.9216	379.24	5.06	0.9131	382.77
7.13	0.9388	372.29	7.08	0.9312	375.35	7.22	0.9232	378.58	7.08	0.9146	382.14
10.10	0.9408	371.51	10.02	0.9333	374.50	10.10	0.9252	377.76	10.07	0.9170	381.15
15.09	0.9439	370.26	15.05	0.9366	373.18	15.16	0.9288	376.29	15.05	0.9204	379.72
20.03	0.9470	369.08	20.06	0.9398	371.90	20.09	0.9321	374.99	20.07	0.9241	378.22
25.02	0.9500	367.90	25.02	0.9428	370.71	25.11	0.9353	373.68	25.06	0.9274	376.88
30.05	0.9529	366.80	30.00	0.9457	369.58	30.16	0.9385	372.42	30.06	0.9307	375.54
35.06	0.9556	365.76	35.09	0.9486	368.43	35.11	0.9413	371.32	35.36	0.9336	374.38
40.07	0.9583	364.72	40.06	0.9514	367.36	40.05	0.9444	370.10	40.21	0.9358	373.47
45.12	0.9610	363.69	45.03	0.9540	366.36	45.06	0.9470	369.07	45.06	0.9393	372.09
50.05	0.9634	362.78	50.07	0.9567	365.34	50.11	0.9499	367.95	50.06	0.9423	370.93
55.02	0.9659	361.86	55.10	0.9593	364.33	55.08	0.9525	366.94	55.05	0.9450	369.84
60.11	0.9684	360.90	60.06	0.9617	363.44	60.25	0.9551	365.94	60.13	0.9472	369.01
65.07	0.9708	360.03	65.16	0.9643	362.46	65.07	0.9576	365.00	65.01	0.9488	368.38
70.19	0.9731	359.18	70.10	0.9667	361.56	70.10	0.9602	364.01	70.04	0.9528	366.82
75.06	0.9754	358.33	75.03	0.9689	360.73	75.04	0.9624	363.15	75.08	0.9564	365.45
80.05	0.9775	357.56	80.08	0.9711	359.91	80.10	0.9645	362.37	80.06	0.9583	364.73
85.13	0.9796	356.78	85.03	0.9735	359.04	85.12	0.9667	361.54	85.04	0.9610	363.70
90.10	0.9817	356.02	90.19	0.9756	358.25	89.97	0.9687	360.80	90.10	0.9630	362.95
95.04	0.9838	355.28	95.05	0.9777	357.49	95.12	0.9724	359.44	95.04	0.9638	362.64

Appendix C.

PC-SAFT Results

Table C.1. Comparison between the PC-SAFT results for two associative schemes (2/2 and 2/3) for [DEEA][But]│₂:₁. In this analysis only one restriction was imposed to the system: $k^{HB} \geq 0.001$.

Association scheme 2/2		Association scheme 2/3	
m	**18.115**	m	**17.343**
σ/Å	2.8334	σ/Å	2.8832
ε/K	211.35	ε/K	216.66
ε^{HB}/K	3580.0	ε^{HB}/K	3282.0
k^{HB}	**0.001000**	k^{HB}	**0.001000**
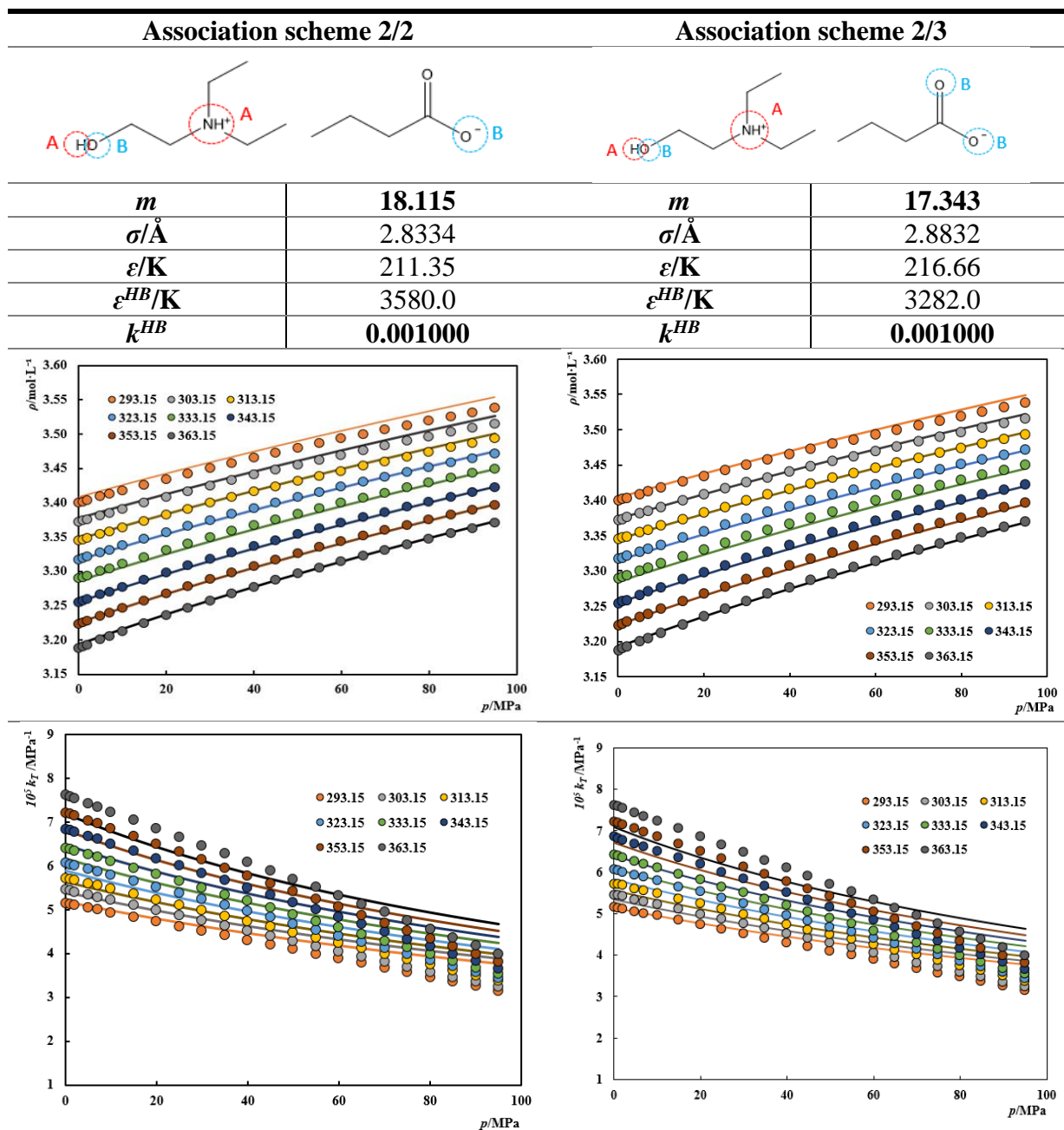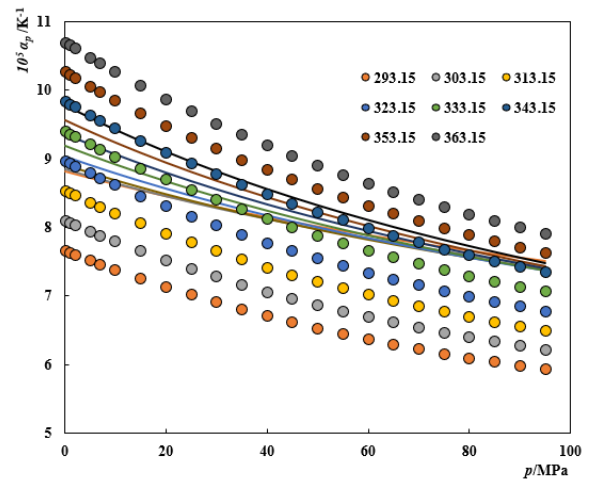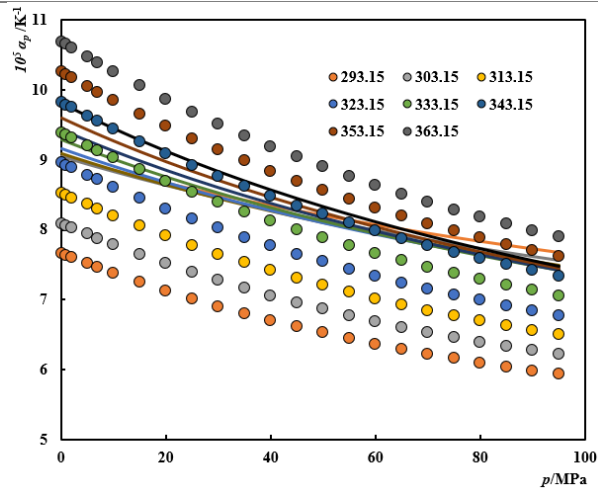
Table C.2. PC-SAFT results applying different types of restrictions to [DEEA][Prop] $|$ 1.5:1, using association scheme 2/3. On the left side of the table the results obtained are shown keeping m fixed and varying four parameters of the model; On the right side of the table, the results obtained are shown keeping m fixed and applying the constraint, $k^{HB} \geq 0.001$, varying the remaining three parameters.

Restrictions used			
m fixed			
• k^{HB} without limitation		• $k^{HB} \geq 0.001$	
m	**12.553**	*m*	**12.553**
σ/Å	3.1212	σ/Å	3.1195
ε/K	233.21	ε/K	229.62
ε^{HB}/K	5773.9	ε^{HB}/K	3196.1
k^{HB}	**2x10^{-07}**	k^{HB}	**0.001**
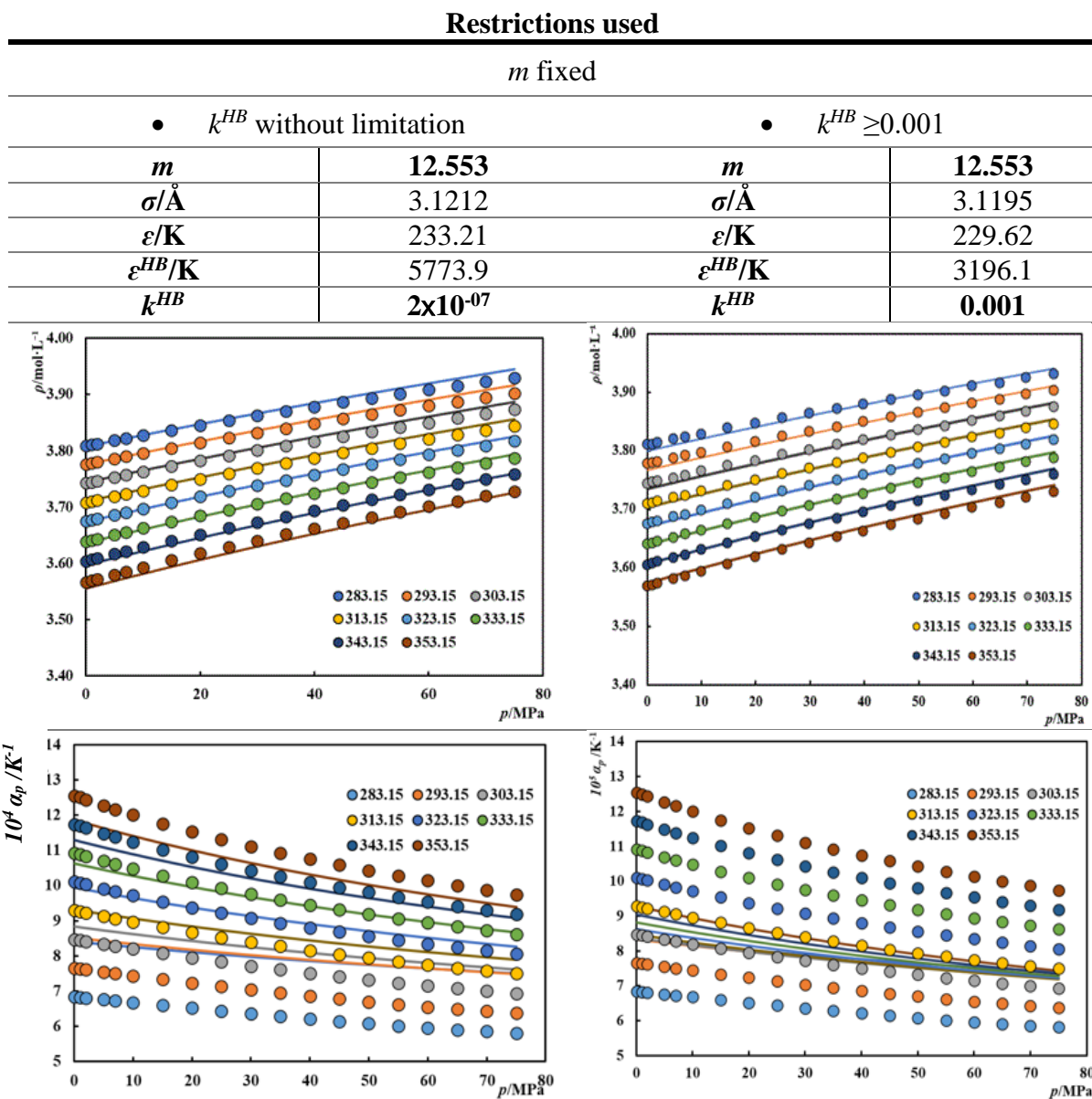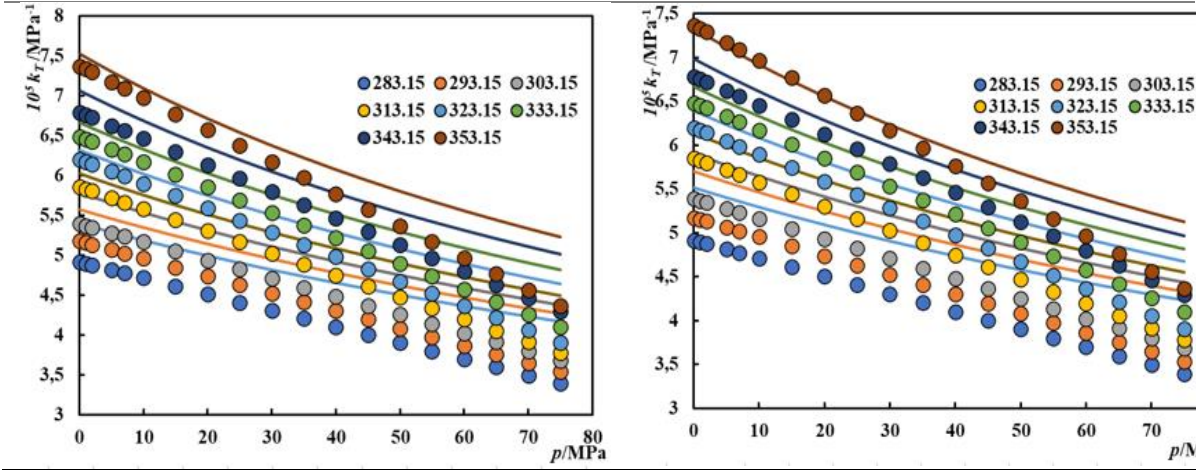
Table C.1. PC-SAFT modeling results for [DEEA][But]│$_{2:1}$ applying only one restriction to the parameters, $k^{HB} \geq 0.001$, varying the remaining four parameters. The associative scheme used is 2/3.

m	**20.774**
σ/Å	2.6908
ε/K	196.25
ε^{HB}/K	3509.8
k^{HB}	**0.001000**
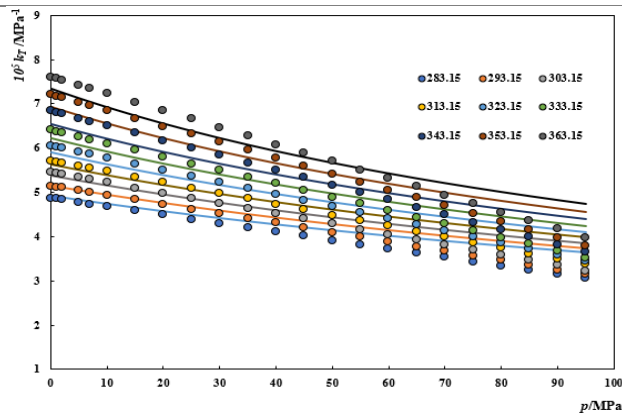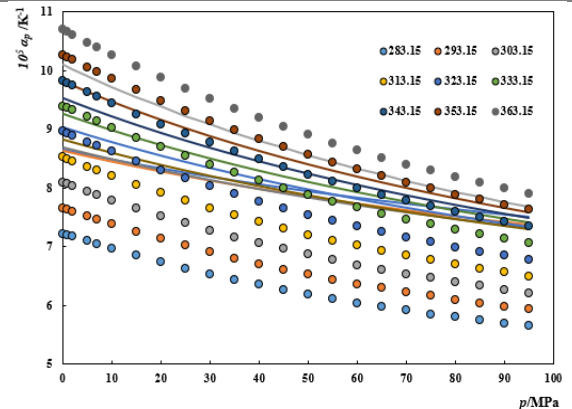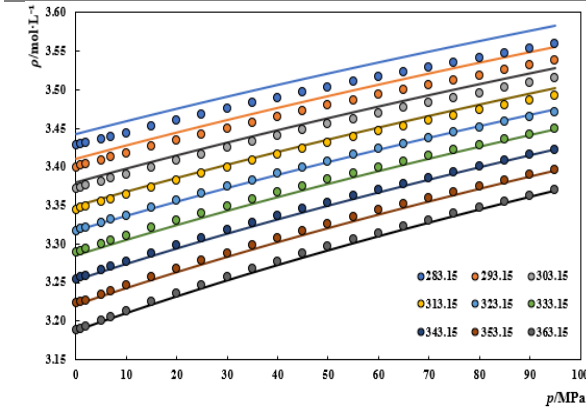
Table C.2. PC-SAFT modeling results for [DEEA][But]│$_{2:1}$ keeping the m fixed by applying a constraint, $k^{HB} \geq 0.01$, varying the remaining three parameters. The associative scheme used is 2/3.

m	**12.636**
$\sigma/\text{Å}$	3.2428
ε/K	250.6
$\varepsilon^{HB}/\text{K}$	2448.5
k^{HB}	**0.01000**
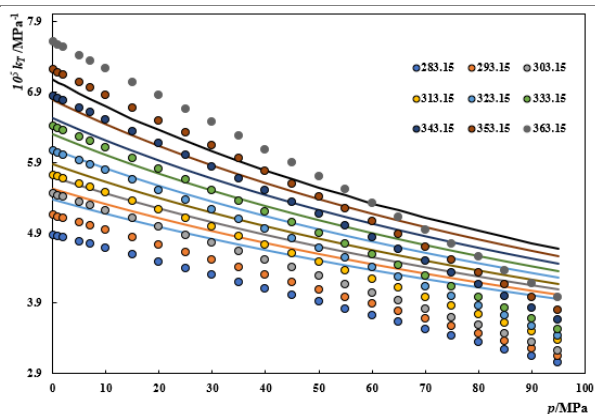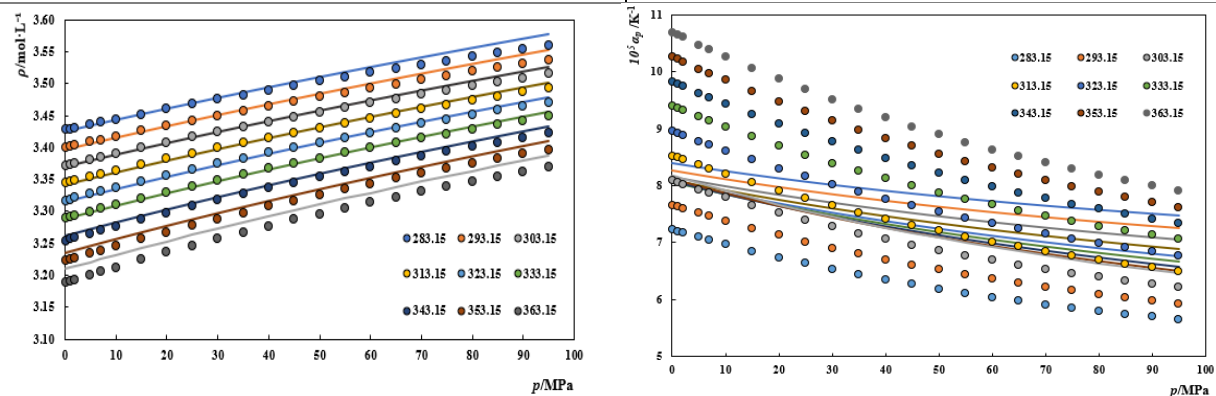
Average absolute deviation values

Table C.5. Percentage values of the average absolute deviation of the analysed properties compared to the experimental data obtained for the four studied PIL systems.

PILs	$\%AAD_\rho$	$\%AAD_{\alpha_P}$	$\%AAD_{k_T}$
[DEEA][Ace] │ 1.5:1	0.09	4.53	3.89
[DEEA][Prop] │ 1.5:1	0.05	2.95	2.78
[DEEA][But] │ 1:1	0.09	5.49	4.67
[DEEA][Pent] │ 1:1	0.05	1.68	4.82

Appendix D.

Vapor-liquid equilibrium data

Table D.1. VLE for the binary system CO_2 + [DEEA][Ace] $\big|$ 1.5:1.

						T/K								
	303			313			323			333			343	
p/MPa	x_{CO2}	$m_{CO2}/$ $mol_{CO2} \cdot kg_{IL}^{-1}$	p/MPa	x_{CO2}	$m_{CO2}/$ $mol_{CO2} \cdot kg_{IL}^{-1}$	p/MPa	x_{CO2}	$m_{CO2}/$ $mol_{CO2} \cdot kg_{IL}^{-1}$	p/MPa	x_{CO2}	$m_{CO2}/$ $mol_{CO2} \cdot kg_{IL}^{-1}$	p/MPa	x_{CO2}	$m_{CO2}/$ $mol_{CO2} \cdot kg_{IL}^{-1}$
0.482	0.082	0.376	0.498	0.079	0.361	0.518	0.075	0.341	0.538	0.072	0.326	0.554	0.068	0.307
0.414	0.072	0.326	0.434	0.070	0.317	0.454	0.067	0.302	0.475	0.064	0.288	0.491	0.060	0.269
0.330	0.060	0.269	0.343	0.057	0.254	0.355	0.054	0.240	0.367	0.050	0.221	0.380	0.046	0.203
0.247	0.048	0.212	0.258	0.045	0.198	0.269	0.042	0.184	0.279	0.038	0.166	0.289	0.034	0.148
0.181	0.037	0.162	0.198	0.036	0.157	0.208	0.034	0.146	0.215	0.030	0.130	0.222	0.026	0.112
0.110	0.024	0.103	0.116	0.023	0.099	0.121	0.021	0.090	0.125	0.018	0.077	0.130	0.015	0.064

Table D.2. VLE for the binary system CO_2 + [DEEA][Prop] | 1.5:1.

							T/K							
	303			313			323			333			343	
p/MPa	x_{CO2}	$m_{CO2}/$ $mol_{CO2} \cdot kg_{IL}$	p/MPa	x_{CO2}	$m_{CO2}/$ $mol_{CO2} \cdot kg_{IL}$	p/MPa	x_{CO2}	$m_{CO2}/$ $mol_{CO2} \cdot kg_{IL}$	p/MPa	x_{CO2}	$m_{CO2}/$ $mol_{CO2} \cdot kg_{IL}$	p/MPa	x_{CO2}	$m_{CO2}/$ $mol_{CO2} \cdot kg_{IL}$
0.504	0.104	0.529	0.513	0.100	0.513	0.534	0.097	0.490	0.552	0.093	0.468	0.570	0.089	0.413
0.421	0.088	0.440	0.437	0.085	0.437	0.451	0.082	0407	0.468	0.079	0.391	0.484	0.075	0.343
0.350	0.074	0.364	0.362	0.071	0.362	0.375	0.067	0.327	0.387	0.064	0.312	0.400	0.060	0.270
0.277	0.061	0.296	0.285	0.057	0.285	0.295	0.053	0.255	0.304	0.049	0.235	0.314	0.046	0.204
0.215	0.049	0.235	0.221	0.045	0.221	0.229	0.041	0.195	0.237	0.038	0.180	0.244	0.035	0.153
0.110	0.026	0.122	0.114	0.024	0.114	0.118	0.021	0.098	0.122	0.019	0.088	0.126	0.017	0.073

Table D.3. VLE for the binary system CO_2 + [DEEA][But] | 1:1.

							T/K							
	303			313			323			333			343	
p/MPa	x_{CO2}	$m_{CO2}/$ $mol_{CO2} \cdot kg_{IL}$	p/MPa	x_{CO2}	$m_{CO2}/$ $mol_{CO2} \cdot kg_{IL}$	p/MPa	x_{CO2}	$m_{CO2}/$ $mol_{CO2} \cdot kg_{IL}$	p/MPa	x_{CO2}	$m_{CO2}/$ $mol_{CO2} \cdot kg_{IL}$	p/MPa	x_{CO2}	$m_{CO2}/$ $mol_{CO2} \cdot kg_{IL}$
0.482	0.064	0.333	0.502	0.062	0.322	0.519	0.059	0.305	0.533	0.056	0.289	0.555	0.053	0.273
0.376	0.051	0.262	0.381	0.048	0.246	0.390	0.045	0.230	0.403	0.042	0.214	0.416	0.039	0.198
0.301	0.042	0.214	0.312	0.040	0.203	0.321	0.037	0.187	0.332	0.034	0.171	0.346	0.032	0.161
0.248	0.036	0.182	0.257	0.034	0.171	0.265	0.031	0.156	0.274	0.028	0.140	0.282	0.026	0.127
0.159	0.024	0.120	0.172	0.023	0.115	0.186	0.022	0.110	0.203	0.020	0.099	0.206	0.018	0.087
0.111	0.017	0.084	0.115	0.015	0.074	0.121	0.014	0.069	0.125	0.012	0.059	0.129	0.011	0.052

Table D.4. VLE for the binary system CO_2 + [DEEA][Pent] $\big|$ 1:1.

							T/K							
	303			313			323			333			343	
p/MPa	x_{CO2}	$m_{CO2}/$ $mol_{CO2}\cdot kg_{IL}$	p/MPa	x_{CO2}	$m_{CO2}/$ $mol_{CO2}\cdot kg_{IL}$	p/MPa	x_{CO2}	$m_{CO2}/$ $mol_{CO2}\cdot kg_{IL}$	p/MPa	x_{CO2}	$m_{CO2}/$ $mol_{CO2}\cdot kg_{IL}$	p/MPa	x_{CO2}	$m_{CO2}/$ $mol_{CO2}\cdot kg_{IL}$
0.504	0.104	0.440	0.513	0.100	0.418	0.534	0.097	0.396	0.552	0.093	0.370	0.570	0.089	0.354
0.421	0.088	0.386	0.437	0.085	0.364	0.451	0.082	0.343	0.468	0.079	0.322	0.484	0.075	0.301
0.350	0.074	0.322	0.362	0.071	0.301	0.375	0.067	0.281	0.387	0.064	0.260	0.400	0.060	0.240
0.277	0.061	0.220	0.285	0.057	0.205	0.295	0.053	0.185	0.304	0.049	0.165	0.314	0.046	0.151
0.215	0.049	0.112	0.221	0.045	0.098	0.229	0.041	0.084	0.237	0.038	0.074	0.244	0.035	0.065
0.110	0.026	0.440	0.114	0.024	0.418	0.118	0.021	0.396	0.122	0.019	0.370	0.126	0.017	0.354

Appendix E.

Modelling the VLE data

Table E.1. soft-SAFT EoS modelling of the system CO_2 + [DEEA][Ace]$\big|_{1.5:1}$, with interaction parameter constant ($\xi_{ij}=1.085$).

	T/K									
	303		**313**		**323**		**333**		**343**	
	p/MPa									
x_{CO2}	$\xi_{ij}=1$	$\xi_{ij}=1.085$	$\xi_{ij}=1$	$\xi_{ij}=1.085$	$\xi_{ij}=1$	$\xi_{ij}=1.085$	$\xi_{ij}=1$	$\xi_{ij}=1.085$	$\xi_{ij}=1$	$\xi_{ij}=1.085$
0.000	0.000	0.000	0.000	0.000	0.000	0.000	0.000	0.000	0.000	0.000
0.010	0.105	0.047	0.119	0.055	0.132	0.063	0.145	0.071	0.158	0.080
0.015	0.159	0.070	0.179	0.082	0.199	0.094	0.218	0.107	0.238	0.120
0.020	0.212	0.094	0.239	0.110	0.266	0.126	0.292	0.143	0.318	0.161
0.025	0.266	0.118	0.300	0.138	0.333	0.159	0.367	0.180	0.399	0.202
0.030	0.321	0.142	0.361	0.166	0.402	0.191	0.442	0.217	0.481	0.243
0.035	0.375	0.167	0.423	0.194	0.470	0.224	0.518	0.254	0.563	0.284
0.040	0.430	0.191	0.485	0.223	0.540	0.257	0.594	0.291	0.647	0.326
0.045	0.486	0.216	0.548	0.252	0.610	0.290	0.671	0.329	0.730	0.368
0.050	0.542	0.240	0.611	0.281	0.680	0.323	0.748	0.367	0.815	0.411
0.055	0.598	0.265	0.674	0.310	0.751	0.357	0.827	0.405	0.900	0.454
0.060	0.655	0.291	0.738	0.339	0.822	0.390	0.905	0.443	0.986	0.497
0.065	0.712	0.316	0.803	0.369	0.894	0.424	0.985	0.482	1.073	0.540
0.070	0.769	0.341	0.868	0.399	0.967	0.459	1.065	0.521	1.160	0.584
0.075	0.827	0.367	0.933	0.429	1.040	0.493	1.146	0.560	1.248	0.628
0.080	0.885	0.393	0.999	0.459	1.114	0.528	1.227	0.600	1.337	0.673
0.085	0.944	0.419	1.066	0.489	1.188	0.563	1.309	0.640	1.427	0.718
0.090	1.003	0.445	1.133	0.520	1.263	0.599	1.392	0.680	1.518	0.763
0.095	1.063	0.471	1.200	0.551	1.339	0.634	1.476	0.721	1.609	0.808
0.100	1.123	0.498	1.268	0.582	1.415	0.670	1.560	0.761	1.701	0.854

Table E.2. soft-SAFT EoS modelling of the system CO_2 + [DEEA][Prop] $|$ 1.5:1, with interaction parameter constant (ξ_{ij}=1.080).

	T/K									
	303		**313**		**323**		**333**		**343**	
	p/MPa									
x_{CO2}	ξ_{ij}=1	ξ_{ij}= 1.080	ξ_{ij}=1	ξ_{ij}= 1.080	ξ_{ij}=1	ξ_{ij}= 1.080	ξ_{ij}=1	ξ_{ij}= 1.080	ξ_{ij}=1	ξ_{ij}= 1.080
0.000	0.000	0.000	0.000	0.000	0.000	0.000	0.000	0.000	0.000	0.000
0.010	0.082	0.039	0.093	0.046	0.104	0.053	0.115	0.060	0.125	0.067
0.015	0.124	0.059	0.140	0.069	0.156	0.080	0.173	0.090	0.189	0.102
0.020	0.166	0.079	0.187	0.093	0.209	0.107	0.231	0.121	0.253	0.136
0.025	0.208	0.099	0.235	0.116	0.263	0.134	0.290	0.152	0.318	0.171
0.030	0.250	0.120	0.283	0.140	0.316	0.161	0.350	0.183	0.383	0.205
0.035	0.293	0.140	0.331	0.164	0.371	0.189	0.410	0.214	0.448	0.241
0.040	0.336	0.161	0.380	0.188	0.425	0.216	0.470	0.246	0.514	0.276
0.045	0.379	0.181	0.429	0.212	0.480	0.244	0.531	0.278	0.581	0.312
0.050	0.423	0.202	0.479	0.236	0.536	0.272	0.592	0.310	0.648	0.348
0.055	0.467	0.223	0.529	0.261	0.592	0.301	0.654	0.342	0.716	0.384
0.060	0.511	0.244	0.579	0.286	0.648	0.329	0.717	0.375	0.784	0.421
0.065	0.555	0.266	0.629	0.311	0.705	0.358	0.779	0.407	0.853	0.458
0.070	0.600	0.287	0.680	0.336	0.762	0.387	0.843	0.440	0.922	0.495
0.075	0.646	0.309	0.732	0.361	0.819	0.417	0.907	0.474	0.992	0.532
0.080	0.691	0.331	0.784	0.387	0.877	0.446	0.971	0.507	1.063	0.570
0.085	0.737	0.353	0.836	0.413	0.936	0.476	1.036	0.541	1.134	0.608
0.090	0.783	0.375	0.888	0.438	0.995	0.506	1.102	0.575	1.206	0.646
0.095	0.830	0.397	0.941	0.465	1.055	0.536	1.168	0.610	1.279	0.685
0.100	0.876	0.419	0.995	0.491	1.115	0.566	1.234	0.644	1.352	0.724
0.105	0.924	0.442	1.048	0.517	1.175	0.597	1.301	0.679	1.425	0.764
0.110	0.971	0.465	1.103	0.544	1.236	0.628	1.369	0.715	1.500	0.803

Table E.3. soft-SAFT EoS modelling of the system CO_2 + [DEEA][But]$|$ 1:1, with interaction parameter constant (ξ_{ij}=0.970).

x_{CO2}	T/K									
	303		313		323		333		343	
	p/MPa									
	ξ_{ij}=1	ξ_{ij}=0.970	ξ_{ij}=1	ξ_{ij}=0.970	ξ_{ij}=1	ξ_{ij}=0.970	ξ_{ij}=1	ξ_{ij}=0.970	ξ_{ij}=1	ξ_{ij}=0.970
0.000	0.000	0.000	0.000	0.000	0.000	0.000	0.000	0.000	0.000	0.000
0.010	0.050	0.066	0.057	0.075	0.065	0.084	0.073	0.093	0.081	0.102
0.015	0.075	0.099	0.086	0.113	0.098	0.126	0.110	0.140	0.122	0.153
0.020	0.101	0.133	0.116	0.151	0.131	0.169	0.147	0.187	0.163	0.205
0.025	0.127	0.167	0.145	0.189	0.165	0.212	0.184	0.235	0.204	0.258
0.030	0.153	0.201	0.175	0.228	0.198	0.255	0.222	0.283	0.246	0.311
0.035	0.179	0.235	0.205	0.267	0.232	0.299	0.260	0.332	0.289	0.364
0.040	0.205	0.270	0.235	0.306	0.267	0.343	0.299	0.381	0.331	0.418
0.045	0.232	0.305	0.266	0.346	0.301	0.388	0.338	0.430	0.374	0.473
0.050	0.259	0.341	0.297	0.386	0.336	0.433	0.377	0.480	0.418	0.528
0.055	0.286	0.376	0.328	0.427	0.371	0.478	0.416	0.531	0.461	0.583
0.060	0.313	0.412	0.359	0.467	0.407	0.524	0.456	0.582	0.506	0.639
0.065	0.340	0.448	0.390	0.509	0.443	0.570	0.496	0.633	0.550	0.695
0.070	0.368	0.485	0.422	0.550	0.479	0.617	0.537	0.685	0.595	0.752
0.075	0.396	0.521	0.454	0.592	0.515	0.664	0.578	0.737	0.641	0.810
0.080	0.424	0.559	0.487	0.634	0.552	0.711	0.619	0.790	0.686	0.868
0.085	0.452	0.596	0.519	0.677	0.589	0.759	0.660	0.843	0.733	0.926
0.090	0.481	0.634	0.552	0.720	0.626	0.808	0.702	0.897	0.779	0.985
0.095	0.510	0.672	0.585	0.763	0.664	0.856	0.745	0.951	0.826	1.045
0.100	0.539	0.710	0.619	0.807	0.702	0.905	0.787	1.005	0.874	1.105

Table E.4. soft-SAFT EoS modelling of the system CO_2 + [DEEA][Pent] $|_{1:1}$, with interaction parameter constant (ξ_{ij}=0.980).

x_{CO_2}	T/K									
	303		**313**		**323**		**333**		**343**	
	p/MPa									
	ξ_{ij}=1	ξ_{ij}=0.980	ξ_{ij}=1	ξ_{ij}=0.980	ξ_{ij}=1	ξ_{ij}=0.980	ξ_{ij}=1	ξ_{ij}=0.980	ξ_{ij}=1	ξ_{ij}=0.980
0.000	0.000	0.000	0.000	0.000	0.000	0.000	0.000	0.000	0.000	0.000
0.010	0.040	0.048	0.046	0.055	0.053	0.062	0.059	0.070	0.066	0.077
0.015	0.061	0.073	0.070	0.083	0.080	0.094	0.089	0.105	0.100	0.116
0.020	0.081	0.097	0.094	0.111	0.107	0.126	0.120	0.140	0.133	0.155
0.025	0.102	0.122	0.117	0.140	0.134	0.158	0.150	0.176	0.168	0.195
0.030	0.123	0.147	0.142	0.168	0.161	0.190	0.181	0.213	0.202	0.235
0.035	0.144	0.172	0.166	0.197	0.189	0.223	0.212	0.249	0.237	0.276
0.040	0.165	0.198	0.190	0.226	0.217	0.256	0.244	0.286	0.272	0.316
0.045	0.187	0.223	0.215	0.256	0.245	0.289	0.276	0.323	0.307	0.358
0.050	0.208	0.249	0.240	0.285	0.273	0.322	0.308	0.361	0.343	0.399
0.055	0.230	0.275	0.265	0.315	0.302	0.356	0.340	0.398	0.379	0.441
0.060	0.252	0.302	0.290	0.345	0.331	0.390	0.372	0.437	0.415	0.483
0.065	0.274	0.328	0.316	0.376	0.360	0.425	0.405	0.475	0.451	0.526
0.070	0.296	0.355	0.342	0.406	0.389	0.460	0.438	0.514	0.488	0.569
0.075	0.319	0.382	0.368	0.437	0.419	0.495	0.472	0.553	0.526	0.613
0.080	0.342	0.409	0.394	0.468	0.449	0.530	0.506	0.593	0.563	0.657
0.085	0.365	0.437	0.421	0.500	0.479	0.566	0.540	0.633	0.601	0.701
0.090	0.388	0.464	0.447	0.532	0.510	0.602	0.574	0.673	0.640	0.746
0.095	0.411	0.492	0.474	0.564	0.540	0.638	0.609	0.714	0.678	0.791
0.100	0.434	0.520	0.501	0.596	0.571	0.675	0.644	0.755	0.717	0.836